UNIVERSITÀ DI PARMA

UNIVERSITÀ DEGLI STUDI DI PARMA
RESEARCH DOCTORATE IN
CIVIL ENGINEERING AND ARCHITECTURE
XXXI CYCLE

Modeling and simulation of stimuli-responsive viscoelastic polymers

Coordinator: Prof. ANDREA CARPINTERI

Tutor: Prof. ROBERTO BRIGHENTI

Ph.D. candidate
FEDERICO ARTONI

ACADEMIC YEARS 2015/2018

Abstract

The development of a physics-based approach and of a numerical model for the study of the mechanical behavior of advanced polymeric materials is motivated by several real-world applications. The description of the energy state of polymeric materials through their network's chains configuration allows to model the problem, by accounting for the main involved mechanisms (such as rate-dependence, damage, swelling, etc.) and is suitable for developing a continuous approach, readily usable for the Finite Element implementation. The models proposed in the literature already present singularly some of the above mentioned features, nevertheless a comprehensive and physics-based approach is particularly desired for the development of new polymer-like materials and for the so-called advanced «responsive polymers».

The aim of this thesis is to develop a comprehensive theoretical formulation, deeply rooted in the physics of the involved phenomena, and also its Finite Element implementation, for the simulation of real problems requiring to determine quantitatively the mechanical response of such a class of materials. Particular attention has been paid to the rate-dependent response of polymers, as well as to the chains failure (damage mechanism); the mixing with a fluid phase inducing the swelling of the material and the presence of the so-called mechanophore molecules - inducing mechanical effects to the network - has also been taken into account. For each of the above listed features, a detailed explanation is provided and the proposed theoretical model is illustrated; moreover, numerical examples are provided in order to underline the effects of the involved physical parameters and to prove the reliability of the proposed solution. Subsequently, the Finite Element implementation of the proposed theoretical model is illustrated and some numerical parametric tests are illustrated. Finally, some real experimental cases are presented and the mechanical response is numerically simulated through the developed theory, implemented in a nonlinear Finite Element code.

Sommario

Lo sviluppo di una formulazione teorica basata su concetti fisici e di un idoneo modello numerico risulta particolarmente necessaria per lo studio della risposta meccanica di materiali polimerici avanzati, utilizzati oggigiorno in un gran numero di applicazioni pratiche. La valutazione dello stato energetico dei polimeri - ottenuta mediante la descrizione della configurazione delle catene polimeriche - consente di modellare il materiale tenendo conto dei principali fenomeni coinvolti (dipendenza dal tempo, danno, rigonfiamento, ecc.). Tale approccio risulta particolarmente adatto per lo sviluppo di un modello continuo, facilmente implementabile in una formulazione agli Elementi Finiti. In letteratura sono disponibili diversi modelli che tengono conto di alcuni dei predetti fenomeni; tuttavia un approccio globale basato sulla fisica dei fenomeni coinvolti non risulta ancora disponibile, nonostante risulti assolutamente necessario per lo sviluppo di materiali polimerici innovativi, come i cosiddetti polimeri «responsivi».

Scopo della presente tesi è quello di sviluppare una formulazione teorica, fondata sulla fisica dei meccanismi alla microscala, e la sua implementazione in un codice agli Elementi Finiti, finalizzato alla simulazione di problemi reali che richiedano lo studio quantitativo della risposta meccanica di tali materiali. Una particolare attenzione è stata posta alla modellazione del comportamento viscoelastico dei polimeri ed ai meccanismi di danneggiamento derivanti dalla rottura delle catene polimeriche. La formulazione proposta tiene inoltre conto della possibile presenza di un fluido che interagisce col polimero e ne provoca il rigonfiamento, così come della presenza di molecole sensibili a stimoli esterni che provocano effetti meccanici rilevabili sul polimero stesso. Per ciascuno dei predetti fenomeni viene fornita un'illustrazione dettagliata del modello teorico proposto. Sono inoltre riportati alcuni esempi numerici finalizzati ad evidenziare gli effetti sulla risposta meccanica dei principali parametri fisici coinvolti e dimostrare l'efficacia del modello proposto. Viene inoltre illustrata l'implementazione agli Elementi Finiti del modello teorico sviluppato e vengono riportati i risultati di alcuni esempi parametrici significativi. Vengono infine presentati i risultati di alcuni test sperimentali condotti su materiali viscoelastici e su materiali responsivi; i risultati sperimentali sono confrontati con quanto ottenuto mediante le simulazioni numeriche ottenute tramite la teoria sviluppata, implementata in un codice non lineare agli Elementi Finiti.

NOMENCLATURE

$\mathscr{B}_0$, $\mathscr{B}$	reference and current configuration of a body, respectively
$\mathbf{b}$, b_{ij}	left Cauchy-Green deformation tensor
b	length of a Kuhn's segment
$\mathbf{C}$, C_{ij}	right Cauchy-Green deformation tensor
C_s, c_s	solvent concentration in the reference and current configuration, respectively
C_A, C_D	frequency factors for the mechanophores activation and deactivation, respectively
$\mathbf{D}$	global nodal displacement vector
$\mathscr{D}$	damage
D	dissipated power
$\mathbf{E}$, E_{ij}	Green-Lagrange strain tensor
E_b	stiffness of the chemical bond between two Kuhn's segments
$\mathbf{e}$, e_{ij}	Euler-Almansi strain tensor
$\mathbf{F}$, F_{ij}	deformation gradient tensor
$\mathbf{f}$, f_i	force vector in a polymer chain
$\mathscr{G}$	functional
$\mathbf{G}$, G_i	body force vector in the reference configuration
$\mathbf{g}$, g_i	body force vector in the current configuration
h, $\overline{h}$	fraction of active mechanophores and network's average value, respectively
$\mathbf{I}$	identity tensor
J	volume ratio
J_{sw}	volume ratio related to the mechanophores activation
$\mathbf{K}$	global stiffness matrix
k_a, k_d	dynamic cross-links activation and deactivation rate, respectively
k_A, k_D	mechanophores activation and deactivation rate, respectively
k_B	Boltzmann constant, $k_B = 1.38 \cdot 10^{-23}$ J/K
$\mathbf{L}$, L_{ij}	velocity gradient tensor
$\mathscr{L}$, $\mathscr{L}^{-1}$	Langevin function and its inverse, respectively
N	number of Kuhn's segment in a polymer chain
n	number of polymer chains per unit volume
n_a	number of active polymer chains per unit volume
n_μ	number of polymeric chains per unit volume evaluated from the shear modulus
p	hydrostatic pressure
$\mathbf{P}$, P_{ij}	first Piola-Kirchhoff stress tensor

$\mathscr{R}$	Rayleigh dissipation function
$\mathbf{R}$	global unbalanced nodal forces vector
$\mathbf{r}_0$, r_{0i}	mean square end-to-end vector
$\mathbf{r}$, r_i	end-to-end vector in the current configuration
$\mathscr{R}$	dissipated power due to the polymer-solvent interaction
$\mathbf{S}$, S_{ij}	second Piola-Kirchhoff stress tensor
t	time
T	absolute temperature
$\mathbf{U}$, U_{ij}	stretch tensor
$\mathbf{u}$, u_i	displacement vector
V_s	molar volume of solvent
W	work
$\overline{w}$	bond strength
$\mathbf{X}$, X_i	position vector in the reference configuration
$\mathbf{x}$, x_i	position vector in the current configuration
α_{sw}	volume fraction of mechanophores
ΔG_A, ΔG_D	Gibbs energy barriers for activation and deactivation reactions, respectively
ΔS	entropy variation
δ_{ij}	Kronecker's delta
δs_{sw}	mechanophore size change
$\boldsymbol{\varepsilon}$, ε_{ij}	Hencky strain tensor
ζ	friction-like parameter of the polymer-solvent interaction
η	viscous-like unfolding parameter
λ	stretch
λ_b	stretch of a Kuhn's segment
μ	shear modulus
Π	potential energy
ρ, ρ_0, $\overline{\rho}_0$	current, reference and initial Chain Configuration Density Function (CCDF), respectively
$\boldsymbol{\sigma}$, σ_{ij}	Cauchy stress tensor
φ, φ_0, $\overline{\varphi}_0$	current, reference and initial normalized Chain Configuration Density Function (CCDF), respectively
χ	Flory-Huggins mixing parameter
ψ	free energy of a single polymer chain
ψ_b	free energy related to the stretch of a Kuhn's segment
ψ_{sw}	free energy related to the mechanophore activation
Ψ	free energy density of a polymer network
Ψ_{mix}	mixing free energy density
ω_f	failure rate
Ω, Ω_0	current and reference configuration space, respectively

TABLE OF CONTENTS

List of Figures

CHAPTER 1

INTRODUCTION

Polymers and polymer-like materials have known a huge diffusion in the last decades in many advanced and every-days application fields. Since their mechanical behavior can be usefully employed to describe the response of quite different materials - such as soft tissues and biological matters - the development of a comprehensive mechanical model, enabling to quantify their response under mechanical loading is quite desirable. A physics-based model, accounting for the main involved phenomena (entropic-governed response, damage, chains unentanglement, dynamic bond and bond exchange, swelling, etc.), allows to model and predict the response of existing polymer-like materials and to design new ones, according to the desired properties or performances.

Motivation of the work

The aim of the present work is to develop a model capable of capturing the mechanical response of polymers and polymer-like materials, by accounting for the main physical involved phenomena.

We consider the basic entropic nature of this class of materials, as well as the main aspects that enter into the scene when a real material is stretched: rate-dependent phenomena, damage mechanisms and failure of chains, disentanglement effects and

fluid uptake (swelling), typically occurring in polymers having a good affinity with a fluid (gels). Moreover, dealing with advanced materials – typically identified as «functional» or «stimuli-responsive» polymers – we account for the presence of stimuli-responsive molecules inserted into the polymer network; such molecules provide a mechanical detectable effect at the mesoscale level, leading to a so-called responsive material.

A physics-based model – based on the general idea to describe the polymer's mechanical response through the evolution of its chains network configuration – is proposed. It has the ability to consider all the above mentioned phenomena, whose effects are accounted for through their influence on the network configuration and chains force. Finally, the theoretical model has been implemented in a finite element (FE) code and some numerical simulations have been performed.

Outline of the thesis

The thesis is organized as follows.

Chapter 2 presents a short introduction on the mechanics of polymeric materials, illustrating the main physical aspects involved and the most diffused literature models.

Chapter 3 deals with the illustration of the basic concept of the proposed model: the idea of updating the state of the material through the update of the network's chains configuration is presented in various cases, from the purely elastic network deformation to the case of polymers with physical bonds, which enables the so-called dynamic crosslinking (i.e. the spontaneous material re-arrangement at the microscale), up to the unfolding and the chains failure phenomena.

Chapter 4 considers the mechanics of polymers with embedded switchable molecules (also known as *mechanophores*), whose activation can be triggered by both chemical or mechanical actions; since the case of a chemical stimulus is typically associated to the presence of a fluid phase carrying the chemical agent, the swelling mechanism has also been accounted for. At the end of each chapter, some representative examples are presented and discussed.

Chapter 5 discusses the main aspects of the numerical implementation of the above proposed physics-based model into a FE code. Starting from the strong form of the

governing equations, the weak form is derived and the matrix-based formulation of the resulting FE is obtained; finally, some parametric examples are presented and illustrated.

Chapter 6 presents some numerical tests performed on real elements and the comparison with experimental results is discussed.

CHAPTER 2

INTRODUCTION TO THE MECHANICS OF POLYMERIC MATERIALS

Polymers are one of the most diffused kind of substances in modern world. Several billions of tons of industrial goods made of materials which share a single chemical property - the high molecular weight obtained through repeating structural units - have been produced since 1950s [60]. Artificial materials such as plastics are basically made by polymers and proper additives. This simple and effective structure is widespread in Nature: examples are DNA and proteins, which are made of large size chains formed by the covalent union of various monomer units.

The ubiquitous use of plastic changed the costumes and the economy in the second half of the 20th century. On the other hand, plastics represent a great part of the waste produced in the world, which uncontrolled release in the environment causes huge pollution problems, such as the marine garbage patches [42].

Elastomers (or rubber) were firstly mentioned in 1516 in the book «De Orbe Nuovo» by Pietro Martire d'Anghiera and were a natural rubber obtained from the tree *Heveea Brasiliensis*. The word «polymer» was firstly used in 1833 by Jons Jacob Berzelius. In his studies, he discovered that two substances may have the same chemical composition and different molecular weight. In the late XIX century, August Kekulé, suggested that natural organic substances, like proteins, starch and cellulose, may consist of very long chains, and also derive their special properties from this structure. A great

progress in polymer science was due to Hermann Staudinger, that demonstrated that polymerization process lead to long chains of covalently bonded monomers [135]. The large-scale industrial production of plastics, fibers and elastomers for low-cost goods, and also for engineering applications, dramatically increased after World War II [51].

Polymer science boasts seven Nobel prizes, six of them in Chemistry and one in Physics. The chemists were: Staudinger (1953), Natta and Ziegler (1963), Flory (1974), MacDiarmid, Heeger and Shirakawa (2000), Fenn, Tanaka and Wüthrich (2002), Grubbs, Schrock, Chauvin (2005); the physician was de Gennes in 1991.

The great interest in the field of polymer chemistry is confirmed by the number of international journals devoted to this issue, such as: *Progress in Polymer Science, Polymer Reviews, Macromolecules, Polymer Chemistry, Polymer, European Polymer Journal, Polymer Degradation and Stability, Journal of Polymer Science, Reactive and Functional Polymers, Polymer Testing, Polymer Journal*.

Papers about polymer physics, and in particular related to the mechanical aspects, can be found in journals devoted to mechanics of materials, such as: *Nature Materials, Materials Science and Engineering, Advanced Materials, Materials Today, Materials Horizons, International Journal of Plasticity, International Materials Reviews, Journal of the Mechanics and Physics of Solids*.

On the other hand, journals traditionally devoted to the mechanics of material often report researches dealing with such a class of materials.

2.1 Literature review on engineering applications of polymeric materials

Polymeric materials are widely used in our everyday life, but applications in new fields are constantly explored by researchers: for example, polymer-based biomaterials are used for implants and medical devices [8]; polymer membranes are used to separate gases, such as hydrogen and carbon dioxide from natural gas, or to desalinize seawater and to clean dirty water [116]; electroactive polymers are promising materials for actuators, sensors or soft robots [127]; polymers can be also used for manifacturing deformable solid batteries [159]. Futhermore, polymeric materials have also noticeable properties in the fields of fracture and contact mechanics, because of the large deformations that they can reach [27] and the high fracture toughness that, often, exhibit [25]. The stress field near to a geometrical discontinuity, e.g. due to a crack or to a

contact surface, is deeply different to the stress field observed in more stiff materials, like metals or ceramics [98]. This peculiar stress field is the key to understand the effectiveness of an elastomeric sealant [18], as well as the high defect resistance of elastomeric thin plates in presence of defects [24, 28, 29] and to study the fracture behavior occurring during cutting processes [133, 134].

Polymers can be classified in several ways. A common classification divides polymers into three main groups: thermoplastics, thermosets and elastomers.

Thermoplastics. The main property of a thermoplastic polymer is to become malleable above a certain temperature and to solidify upon cooling. Thermoplastics have long linear or branched chains, jointed together by intermolecular bonds without cross-links. The plasticity of these materials increases with temperature because heat promotes the rupture of the weak intermolecular bonds. Thermoplastics are normally fabricated by the simultaneous application of heat and pressure; the processes are totally reversible and may be repeated, so thermoplasts can be easily recycled.

Among the thermoplastics we can mention: Polyacetals, used for manifacturing of mechanical components because of their good strenght and stiffness; Acrylics, used for lenses and displays because of their tunable optical properties; Fluoroplastics, which have unique non-adhesive and low friction properties; Aramids, used as reinforcing fibers and bulletproof vests; Polycarbonate, used for helmets and wind shields; Polyethylene, ubiquitously used because of its low cost; Polystyrene, Polyvinyl Chloride, etc.

Thermosets. Thermosetting plastics are polymeric materials obtained through irreversibly curing from a soft state to a stronger form. They are composed of long chains strongly cross-linked to one another to form a rigid 3D network structure. Heat is required, during the curing process, to permanently set the plastic. Thermosets cannot be recycled and are, usually, more brittle than thermoplastics but they often possess better mechanical, thermal, chemical and electrical resistance and better dimensional stability than thermoplastics.

Examples of thermosets are: Epoxies, which posses excellent mechanical and adhesive properties and are widely used as sealants or as matrix for fiber reinforced structural components; Polyesters, used in car chassis, often with the addition of reinforcing fibers; Polyurethanes, one of the largest classes of polymers, with mechanical properties that can be tailored over a wide range; Silicones, Phenolics, Polyimides, etc.

Elastomers. Also known as rubbers, these polymers, at room temperature, can undergo large elongations under load and return to their original shape when the load is released. As the termosets, elastomers usually require a curing process (vulcanization) to form crosslinks, but the low linking degree lets high freedom of motion to the chains, so these materials can withstand elastically high deformations.

Examples of elastomers are: Polybutadiene rubber, which is the main component of tires; Chloroprene rubber, used for gaskets, hoses, etc.; Cloroprene, commercially known as Neoprene; Silicone rubber, Polyisoprene, Nitrile rubber, etc.

2.2 Literature review on mechanical models for polymers

2.2.1 Nonlinear solid mechanics

In this section, we briefly recall some basis of the nonlinear theory of continuum mechanics. A comprehensive review of these topics can be found in [70].

Configurations. Let us consider a body which, at a reference time t_0, occupies a region $\mathscr{B}_0$ of the space; thereafter, some deformations occur on the body, so that, at current time t, it occupies a region $\mathscr{B}$. A material point of the body has coordinates $\mathbf{X}$ in the *reference configuration*, while in the *current configuration* it occupies the spatial point identified by the position vector $\mathbf{x}$.

Adopting the *Lagrangian* (or *material*) *description*, the kinematic and static quantities are referred to the reference configuration, while in the *Eulerian* (or *spatial*) *description*, all these quantities are referred to the current deformed configuration.

Kinematics. The deformation gradient $\mathbf{F}$ is a second-order tensor which linearly transforms a material distance vector $\mathrm{d}\mathbf{X}$ into the corresponding spatial distance vector, $\mathrm{d}\mathbf{x} = \mathbf{F}\,\mathrm{d}\mathbf{X}$. Using this definition, it can be expressed as

$$F_{ij} = \frac{\partial x_i}{\partial X_j} = x_{i,j} = u_{i,j} + \delta_{ij} \qquad \text{or} \qquad \mathbf{F} = \operatorname{Grad}\mathbf{u} + \mathbf{I} \tag{2.1}$$

where the displacement field $\mathbf{u}$ is defined, in the Lagrangian framework, as $\mathbf{u} : \mathscr{B}_0 \times \mathscr{T} \to \mathbb{R}^3 \mid \mathbf{u}(\mathbf{X},t) = \mathbf{x}(\mathbf{X},t) - \mathbf{X}(t_0)$, being $\mathscr{T}$ the time domain. The determinant of the deformation gradient tensor, $J = \det\mathbf{F} > 0$, indicates the volume change associated

to the deformation $\mathbf{F}$ of an infinitesimal material element, i.e. it represents the ratio between the current and the reference volume of the element. The deformation gradient can be decomposed into its volumetric part $\mathbf{F}_{vol}$ and its deviatoric part $\mathbf{F}_{dev}$ using the *multiplicative decomposition*, $\mathbf{F} = \mathbf{F}_{vol}\,\mathbf{F}_{dev}$, being $\mathbf{F}_{vol} = J^{1/3}\,\mathbf{I}$ and $\mathbf{F}_{dev} = J^{-1/3}\,\mathbf{F}$, where $\mathbf{I}$ is the identity tensor.

The material time derivative of the deformation gradient is

$$\dot{F}_{ij} = \frac{\partial \dot{x}_i}{\partial X_j} = \frac{\partial \dot{x}_i}{\partial x_k}\frac{\partial x_k}{\partial X_j} = L_{ik}F_{kj} \qquad \text{or} \qquad \dot{\mathbf{F}} = \mathbf{L}\mathbf{F} \tag{2.2}$$

where the tensor $\mathbf{L}$ is the spatial velocity gradient, namely $L_{ij} = \partial \dot{x}_i/\partial x_j$. It is worth mentioning that the trace of $\mathbf{L}$ is the divergence of the velocity field; recalling the continuity equation, if the material is incompressible the divergence of the velocity vanishes, i.e. $\mathrm{tr}\,\mathbf{L} = L_{ii} = \dot{x}_{i,i} = 0$.

The deformation gradient can be also decomposed into the product of the stretch tensor $\mathbf{U}$ and the rotation tensor $\mathbf{R}$ by the so-called *polar decomposition*, $\mathbf{F} = \mathbf{R}\,\mathbf{U}$. The principal components of the material tensor $\mathbf{U}$ are the eigenvalues $\lambda_1, \lambda_2, \lambda_3$ (called *principal stretches*) that satisfy $\mathbf{U}\mathbf{N} = \lambda\mathbf{N}$ for the set of eigenvectors $\mathbf{N}^{(1)}, \mathbf{N}^{(2)}, \mathbf{N}^{(3)}$, which form the principal reference system.

The right Cauchy-Green deformation tensor $\mathbf{C} = \mathbf{F}^T\mathbf{F}$ represents a simpler way to compute the pure stretching part of $\mathbf{F}$; in fact, using the polar decomposition, it results $\mathbf{C} = \mathbf{F}^T\mathbf{F} = \mathbf{U}^T\mathbf{R}^T\mathbf{R}\,\mathbf{U} = \mathbf{U}^2$, because $\mathbf{R}^T = \mathbf{R}^{-1}$ and $\mathbf{U}^T = \mathbf{U}$. The *spectral decomposition* of the right Cauchy-Green tensor is [38]

$$\mathbf{C} = \mathbf{U}^2 = \sum_{k=1}^{3} \lambda_k^2\,\mathbf{N}^{(k)} \otimes \mathbf{N}^{(k)} \tag{2.3}$$

The principal stretches λ_1, λ_2 and λ_3 are the square roots of the eigenvalues of $\mathbf{C}$. Useful quantities are the three invariants of the right Cauchy-Green tensor, namely

$$\begin{aligned} I_1 &= \mathrm{tr}\,\mathbf{C} = C_{ii} = \lambda_1^2 + \lambda_2^2 + \lambda_3^2 \\ I_2 &= \frac{1}{2}\left[(\mathrm{tr}\,\mathbf{C})^2 - \mathrm{tr}(\mathbf{C}^2)\right] = \frac{1}{2}\left(C_{ii}^2 - C_{ij}C_{ij}\right) = \lambda_1^2\lambda_2^2 + \lambda_1^2\lambda_3^2 + \lambda_2^2\lambda_3^2 \\ I_3 &= J^2 = \det\mathbf{C} = \lambda_1^2\lambda_2^2\lambda_3^2 \end{aligned} \tag{2.4}$$

Strain measures. The definition of strain is not unique, so that different measures could be defined. A family of strain measures is [69, 129]

$$\boldsymbol{\epsilon} = \begin{cases} \dfrac{1}{n}\left(\mathbf{U}^n - \mathbf{I}\right) & \text{if } n \neq 0 \\ \ln\mathbf{U} & \text{if } n = 0 \end{cases} \tag{2.5}$$

setting $n = -2$ we obtain the *Euler-Almansi* strain tensor, $\mathbf{e} = (\mathbf{I} - \mathbf{U}^{-2})/2$, with $n = 2$ we have the *Green-Lagrange* strain tensor $\mathbf{E} = (\mathbf{C} - \mathbf{I})/2$, while with $n = 0$ we have the Hencky true strain tensor $\boldsymbol{\varepsilon} = \ln \mathbf{U}$.

Stress measures. In the following discussion we mainly use three measures of stress: the *Cauchy* stress tensor $\boldsymbol{\sigma}$ (also called *true stress*), the *first Piola-Kirchhoff* stress tensor $\mathbf{P}$ (also called *nominal stress*) and the *second Piola-Kirchhoff* stress tensor $\mathbf{S}$. These three quantities are related each other through [70, cap. 3]

$$\boldsymbol{\sigma} = J^{-1}\mathbf{P}\mathbf{F}^T = J^{-1}\mathbf{F}\mathbf{S}\mathbf{F}^T\,, \qquad \mathbf{P} = J\boldsymbol{\sigma}\mathbf{F}^{-T} = \mathbf{F}\mathbf{S}\,, \qquad \mathbf{S} = J\mathbf{F}^{-1}\boldsymbol{\sigma}\mathbf{F}^{-T} = \mathbf{F}^{-1}\mathbf{P} \tag{2.6}$$

The Cauchy stress is referred to the current deformed configuration, while the first and second Piola-Kirchhoff stresses are referred to the initial undeformed configuration. Among them, the first Piola-Kirchhoff stress tensor results to be not-symmetric.

Hyperelastic material. A material is defined *Cauchy-elastic* if there exists a biunique correspondence between the stress and the deformation state, i.e. if the stress field depends only on the state of deformation and not on the deformation history. As a subclass of elastic materials, a material is called *hyperelastic* if a scalar-valued function of the deformations, $\Psi = \Psi(\mathbf{F})$, whose derivatives are the stresses, exists. Such a function is called *free energy*, or *strain energy density*; physically it represents the elastic energy per unit volume stored in the material. The existence of solutions of the mechanical problem is based on the condition of convexity of the strain-energy function, which requires, beyond others, $\Psi(\mathbf{F}) \geq 0$ and $\Psi(\mathbf{I}) = 0$ [6, 37].

For an hyperelastic material, the stress tensors can be obtained in terms of derivatives of the free energy function as

$$\mathbf{P} = \frac{\partial \Psi(\mathbf{F})}{\partial \mathbf{F}}\,, \qquad \mathbf{S} = 2\frac{\partial \Psi(\mathbf{C})}{\partial \mathbf{C}}\,, \qquad \boldsymbol{\sigma} = 2J^{-1}\frac{\partial \Psi(\mathbf{b})}{\partial \mathbf{b}}\mathbf{b} \tag{2.7}$$

where $\mathbf{b} = \mathbf{F}\mathbf{F}^T$ is the left Cauchy-Green deformation tensor. For an isotropic material, the stress can be also written in terms of the strain invariants. Expressing the free energy as $\Psi = \Psi(I_1, I_2, I_3)$ we have [70, §6.2], [125]

$$\mathbf{S} = 2\left[\left(\frac{\partial \Psi}{\partial I_1} + I_1\frac{\partial \Psi}{\partial I_2}\right)\mathbf{I} - \frac{\partial \Psi}{\partial I_2}\mathbf{C} + I_3\frac{\partial \Psi}{\partial I_3}\mathbf{C}^{-1}\right] \tag{2.8}$$

$$\boldsymbol{\sigma} = 2J^{-1}\left[\left(I_2\frac{\partial \Psi}{\partial I_2} + I_3\frac{\partial \Psi}{\partial I_3}\right)\mathbf{I} + \frac{\partial \Psi}{\partial I_1}\mathbf{b} - I_3\frac{\partial \Psi}{\partial I_2}\mathbf{b}^{-1}\right] \tag{2.9}$$

The stress can be also written in terms of principal stretches; expressing $\Psi = \Psi(\lambda_1, \lambda_2, \lambda_3)$ we have

$$P_i = \frac{\partial \Psi}{\partial \lambda_i}, \qquad S_i = \frac{1}{\lambda_i}\frac{\partial \Psi}{\partial \lambda_i}, \qquad \sigma_i = J^{-1}\lambda_i \frac{\partial \Psi}{\partial \lambda_i} \tag{2.10}$$

The spectral decomposition of the stress tensors shows that their principal directions are coaxial with the principal directions of the deformation gradient.

Incompressible Hyperelastic Materials. The incompressibility condition, $J = \det\mathbf{F} = 1$, may be forced by introducing a Lagrange multiplier p into the strain energy; the amended form becomes $\Psi = \Psi(\mathbf{F}) - p(J-1)$. Physically p represents an hydrostatic pressure acting on the material point. The constitutive relations (2.7), in this case becomes

$$\mathbf{P} = \frac{\partial \Psi(\mathbf{F})}{\partial \mathbf{F}} - p\mathbf{F}^{-T}, \qquad \mathbf{S} = 2\frac{\partial \Psi(\mathbf{C})}{\partial \mathbf{C}} - p\mathbf{C}^{-1}, \qquad \boldsymbol{\sigma} = \frac{\partial \Psi(\mathbf{F})}{\partial \mathbf{F}}\mathbf{F}^{T} - p\mathbf{I} \tag{2.11}$$

Furthermore, the relations (2.8) become

$$\mathbf{S} = 2\left(\frac{\partial \Psi}{\partial I_1} + I_1\frac{\partial \Psi}{\partial I_2}\right)\mathbf{I} - 2\frac{\partial \Psi}{\partial I_2}\mathbf{C} - p\mathbf{C}^{-1}, \qquad \boldsymbol{\sigma} = -p\mathbf{I} + 2\frac{\partial \Psi}{\partial I_1}\mathbf{b} - 2\frac{\partial \Psi}{\partial I_2}\mathbf{b}^{-1} \tag{2.12}$$

and the (2.10) become

$$P_i = \frac{\partial \Psi}{\partial \lambda_i} - \lambda_i^{-1}p, \qquad S_i = \lambda_i^{-1}\frac{\partial \Psi}{\partial \lambda_i} - \lambda_i^{-2}p, \qquad \sigma_i = \lambda_i\frac{\partial \Psi}{\partial \lambda_i} - p \tag{2.13}$$

Such a hydrostatic pressure can be determined from the equilibrium equation.

Mechanical problem. The mechanical problem to be solved has three independent unknown fields: displacement, stretch (or strain) and stress. The three equations required to find the solution are: the equilibrium equation, a proper constitutive relation and the compatibility equation, beyond the essential and natural boundary condition.

In the Lagrangian framework there relations are

$$\operatorname{Div}\mathbf{P} + \mathbf{G} = \mathbf{0}, \qquad \mathbf{P} = \frac{\partial \Psi}{\partial \mathbf{F}}, \qquad \mathbf{F} = \operatorname{Grad}\mathbf{u} + \mathbf{I}, \qquad \text{in} \quad \mathscr{B}_0 \tag{2.14}$$

$$\mathbf{u} = \overline{\mathbf{u}} \quad \text{in} \quad \partial\mathscr{B}_{0u}, \qquad \mathbf{P}\,\mathbf{N} = \mathbf{T}_{ext} \quad \text{in} \quad \partial\mathscr{B}_{0\sigma}, \qquad \text{with} \qquad \partial\mathscr{B}_0 = \partial\mathscr{B}_{0u} \cup \partial\mathscr{B}_{0\sigma} \tag{2.15}$$

where $\mathbf{G}$ are the body force, $\overline{\mathbf{u}}$ are the displacements applied to the boundary region $\partial\mathscr{B}_{0u}$, $\mathbf{N}$ are the unit vectors normal to the surface and $\mathbf{T}_{ext}$ are the stresses applied to the boundary region $\partial\mathscr{B}_{0\sigma}$.

On the other hand, in the Eulerian framework the above equations become

$$\operatorname{div}\boldsymbol{\sigma} + \mathbf{g} = \mathbf{0}\,, \qquad \boldsymbol{\sigma} = 2J^{-1}\frac{\partial \Psi}{\partial \mathbf{b}}\mathbf{b}\,, \qquad \mathbf{b} = \mathbf{F}\mathbf{F}^T \qquad \text{in} \quad \mathscr{B} \tag{2.16}$$

$$\mathbf{u} = \overline{\mathbf{u}} \quad \text{in} \quad \partial\mathscr{B}_u\,, \qquad \boldsymbol{\sigma}\,\mathbf{n} = \mathbf{t}_{ext} \quad \text{in} \quad \partial\mathscr{B}_\sigma\,, \qquad \text{with} \qquad \partial\mathscr{B} = \partial\mathscr{B}_u \cup \partial\mathscr{B}_\sigma \tag{2.17}$$

2.3 Hyperelastic constitutive models

Many hyperelastic constitutive models, based on different expressions of the free energy, are available in literaure [1, 16, 67, 103, 122]. These model can be divided into three classes: phenomenologicals, experimentals and physics-based.

Phenomenological models. In this class of models the strain energy Ψ is established *a priori* using arbitrary mathematical functions. Many models adopt functions based on series expansion; a good example is the Rivlin's power series of the strain invariants [124]

$$\Psi = \sum_{i,j=0}^{\infty} C_{ij}(I_1 - 3)^i (I_2 - 3)^j\,, \qquad C_{00} = 0 \tag{2.18}$$

where C_{ij} are material parameters. Examples of phenomenologial models can be found in Mooney [108], Biderman [12], Carmichael et al. [34], Ogden [113], James et al. [75], Tobisch [139], Shariff [131]. These models require the knowledge of various parameters, often difficult to be determined and not always with a clear physical meaning.

Experimentally motivated models. In this class of models the strain energy function is determined by fitting experimental data with proper functions. An example is the Gent's model [58]

$$\Psi = -\frac{E}{6} J_m \ln\left(1 - \frac{J_1}{J_m}\right) \tag{2.19}$$

where E is the elastic modulus for small deformations, $J_1 = I_1 - 3$ is a stretch invariant and J_m is the experimentally measured limit value of J_1. Such a model implies the existence of a limit stretch due to a singularity of the stress for $J_1 = J_m$.

Models developed to fit experimental data can be found in Rivlin and Saunders [126], Gent and Thomas [59], Klingbell and Shield [84], Hart-Smith [67], Valanis and Landel [147], Yeoh and Fleming [157, 158].

Physics-based models. In this class of models the strain energy arises from the statistical thermodynamic of the polymer chains network. Some authors focuse on the geometric pattern of an elementary network cell, such as the neo-Hookean [143], the 3-chains [76], the 4-chains [55, 151], the 8-chains [3] or the full-network models [107, 138, 146, 156]. Other models attempt to reproduce the chemo-physical properties of real chains, like in Isihara et al. [73], or the Slip-Link [7], the van der Waals [81] and the constrained junctions [54] model. Other models are based on topological constraints which limit the chain's freedom, such as the tube [50] and the extended-tube models [79].

2.3.1 Polymer chain mechanics

Several relations are available in literature to model the force vs. extension of a single polymer chain. A widely adopted model is the freely jointed chain [65, 86], in which the chain is replaced by a sequence of rigid segments of constant length; each segment can rotate freely around the junction point with respect to the subsequent segment.

Other Authors limit the chain's degrees of freedom by considering the internal constraints arising from the chemical properties of the molecular's bond, such as in the freely-rotating model [5], or in the rotational isomeric state model [4]. Other models consider the «excluded volume» in order to avoid self-intersections of the chain [49, 52], for instance by using the random-walk theory [33].

Chains with non-negligible bending stiffness, such as DNA or proteins, are often studied with the worm-like chain model [35, 85], in which the chain is seen as a continuously flexible rod.

In the middle 1980s, the development of experimental techniques based on atomic force microscopy [13] opened the opportunity to directly measure the force vs. extension curve of a single polymer chain. For instance, the experimental campaign carried out by Ortiz [114] pointed out that many biological polymers can be described by the freely jointed chain model or by the worm-like chain model for strains smaller than the full stretch limit. When the molecule's conformation approaches its contour length, the elastic contribution to the mechanical behavior becomes important and must be considered. The experiments carried out by Bemis et al. [10], Cocco et al. [41], Rief et al. [123], Marszalek et al. [106], Liphardt et al. [97] showed the J-shaped form of the force vs. extension relation for many polymers. Furthermore, they observed that biological polymers are often in a folded state when they are stress free. The presence

of an external force induces the unfolding of the molecule, highlighted by sharp drops of the measured force during the experiments carried out by controlling the applied displacement.

2.3.2 Thermodynamic definition of the free energy

The *free energy* Ψ is a thermodynamic quantity defined as

$$\Psi \doteq U - TS \tag{2.20}$$

where U is the internal energy, T is the absolute temperature and S is the entropy. From this definition, the variation of the free energy is $d\Psi = dU - TdS - SdT$. If the deformation process takes place at constant temperature (*isothermal process*) this relation reduces to $d\Psi = dU - TdS$.

The first law of thermodynamics states that the variation of internal energy dU during a process is $dU = dQ + dW$, where dQ is the heat flux and dW the infinitesimal work done by the external forces. Furthermore, the second law of thermodynamics defines the exchange of heat dQ for a reversible process as $dQ = TdS$. Using these two founding laws, for an elastic deformation taking place at constant temperature, it results $d\Psi = dW$, which implies that the variation of the free energy is equal to the work done by the applied forces.

Furthermore, if the system is closed, its internal energy is constant, namely $dU = 0$, from which the free energy variation is [144, §1.2.1]

$$d\Psi = dW = -TdS \tag{2.21}$$

By integrating both sides of the above relation from the initial and final thermodynamic states, it results $\Psi = -TS$.

Let us consider a polymeric chain whose ends are at the distance r. We indicate the free energy of a single polymer chain with the lowercase symbol ψ. If we apply a force f to that chain, which modifies the distance between the chain's ends by the quantity dr, we produce a work $dW = f\,dr$; thus, that force can be related with the free energy through

$$f = \frac{\partial \psi}{\partial r} = -T\frac{\partial S}{\partial r} \tag{2.22}$$

The above expression states that a linear relation between mechanical force and the entropy variation exists. The role of entropy marks an essential difference between

rubber elasticity and the mechanical behavior of other materials, like metals, ceramics, rocks, etc. In fact, materials with crystalline structure are characterized by an *enthalpic elasticity*, which means that external work increases the enthalpy of the crystal because it moves the atoms from their position of minimum energy. On the other hand, rubbers are characterized by an *entropic elasticity*, because the external work produces mainly a reduction of the entropy of the network.

According to the statistical theory developed by Boltzmann, the variation of entropy ΔS of a thermodynamic system is given by [53]

$$\Delta S = k_B \ln \frac{\Omega}{\Omega_0} \tag{2.23}$$

where, in our case, Ω_0 is the number of possible conformations of the chain in the reference configuration, while Ω is the same number in the current configuration. We consider, as reference configuration, a free chain without restraints or applied forces, and as current configuration a chain whose extremities are forced, by some external actions, to have a fixed distance. The presence of external actions reduces the freedom of the chain, so it results $\Omega < \Omega_0$ for any deformation process. It means that the reference configuration is the state of maximum entropy and any deformation reduces the entropy of the chain up to the lower (theoretical) limit of fully stretched chain, in which $\Omega = 1$. Furthermore, the ratio Ω/Ω_0 can be viewed as the probability distribution of the chain's conformations.

2.3.3 Freely Jointed Chain (FJC)

The polymer chain is modeled as a sequence of N rigid segments with length b [88, 145]. The orientation of each segment is assumed to be independent from the orientation of the others. The shape of the chain can be assumed to be described by a *random walk* of constant length b. The 3D vector between the initial and final point of the chain is denoted by $\mathbf{r}$ and it is called *end-to-end distance*. The end-to-end distance is the only parameter that characterizes a molecular conformation (i.e. the shapes, or arrangements) of a chain.

2.3.3.1 Gaussian statistic

Let us consider a single Kuhn's segment of length b, which can rotate freely in the space. The projection of the end-to-end vector $\mathbf{b}$ of the segment along a given direction

has uniform probability distribution with expected value 0 and variance $b^2/3$, with $b = \|\mathbf{b}\|$. The end-to-end vector $\mathbf{r}$ of a freely jointed chain with N Kuhn's segments can be obtained as $\mathbf{r} = \sum_{i=1}^{N} \mathbf{b}_i$. If all vectors $\mathbf{b}_i$ are independent, the Central Limit Theorem states that, for $N \to \infty$, the distribution of $\mathbf{r}$ is normal with expected value 0 and standard deviation $b\sqrt{N/3}$. More specifically, if the initial point of the chain is fixed in the origin, the probability density that the final point is in the infinitesimal volume around the point of coordinates $\mathbf{r} = (r_x, r_y, r_z)$ is

$$\varphi(\mathbf{r}) = \frac{1}{b^3}\left(\frac{3}{2\pi N}\right)^{3/2} \exp\left(-\frac{3\,r^2}{2Nb^2}\right) \tag{2.24}$$

where $r = \|\mathbf{r}\|$. It can be noted that the probability density has spherical symmetry and it can be expressed as the product of three independent normal distributions; this implies that the distribution is isotropic. The probability that the final point of the chain is on the surface of a sphere of radius r is

$$\varphi_s(r) = \frac{1}{b^3}\left(\frac{3}{2\pi N}\right)^{3/2} \exp\left(-\frac{3\,r^2}{2Nb^2}\right) \cdot 4\pi r^2 \tag{2.25}$$

where $4\pi r^2$ is the surface of the sphere. The expected value of this distribution is

$$r_0^2 = \frac{\int_0^\infty r\,\varphi_s(r)\,dr}{\int_0^\infty \varphi_s(r)\,dr} = Nb^2 \tag{2.26}$$

This is a crucial result of the statistical theory, because it means that in the force-free state, the most probable conformations of a freely jointed chain are those characterized by the end-to-end distance $r_0 = b\sqrt{N}$, which is also called *mean-square distance*. All the possible values of the end-to-end distance can be referred to the mean-square value as $r = \lambda r_0$, where λ represents the chain's stretch. When the chain is fully-stretched, the end-to-end distance reaches the value $r = Nb$, that is to say $\lambda = \sqrt{N}$, which is the limit stretch of the chain, assuming that the Kuhn segments are rigid.

Replacing the distribution (2.24) in the definition (2.23), the entropy and the free energy become

$$\Delta S(r) = k_B \ln\frac{\varphi(r)}{\varphi(0)} = -\frac{3k_B r^2}{2Nb^2}\,, \qquad \psi(r) = -T\Delta S = \frac{3k_B T}{2Nb^2} r^2 \tag{2.27}$$

where $\varphi(0)$ is the probability density evaluated in $r = 0$, i.e. in the reference state Ω_0. Finally, the force acting on the chain can be obtained from (2.22) as follows

$$f = \frac{\partial \psi}{\partial r} = -\frac{k_B T}{\varphi(r)}\frac{\partial \varphi(r)}{\partial r} = \frac{3k_B T}{Nb^2} r = \frac{3k_B T}{b} \cdot \frac{\lambda}{\sqrt{N}} \tag{2.28}$$

where $\lambda = r/r_0$ is the chain's stretch w.r.t. the mean-square end-to-end distance $r_0 = b\sqrt{N}$.

This simple linear relationship between stretch and force allows us to make some observations: 1) in the Gaussian regime, the chain behaves as a linear elastic spring governed by Hooke's law; 2) when the chain is *unstretched*, that is to say when $\lambda = 1$, the force *is not zero*; 3) the chain's force is equal to zero if and only if $\lambda = 0$. The last condition is physically impossible for a bulk material, while it has a clearly meaning in the light of the statistical thermodynamic. The condition $\lambda = 0$, or $r = 0$, corresponds to the situation in which all the configurations are equally probable, namely for an isolated chain, such as a chain immersed in a large amount of neutral solvent. 4) The stretch is always $\lambda \geq 0$ and so also the force is always $f \geq 0$, thus the chain is always elongated and it can bear only tensile forces.

2.3.3.2 Non-Gaussian statistic

The use of the Gaussian probability distribution is valid only under the restrictive assumption of «not too large» extension of the chain, i.e. for stretch up to about 150% [103]. To overcome this restriction it is necessary to use a different distribution of the end-to-end distance. The founders of the non-Gaussian theory were Kuhn and Grün in the early 1940s. In their pioneeristic work [87], they proposed the use of the Langevin function as the probability distribution. The Langevin function $\mathscr{L}(x)$ is defined as

$$\mathscr{L}(x) \doteq \coth(x) - \frac{1}{x} \tag{2.29}$$

In the statistical formulation it is necessary to use the inverse of the above function, $\mathscr{L}^{-1}(x)$, which does not have an explicit mathematical expression. Several approximate expressions of the function $\mathscr{L}^{-1}(x)$ have been proposed [44], such as the Taylor series expansion

$$\mathscr{L}^{-1}(x) \approx 3x + \frac{9}{5}x^3 + \frac{297}{175}x^5 + \frac{1539}{875}x^7 + \dots \tag{2.30}$$

or the one suggested by Jedynak [77], which is more efficient for numerical approximations

$$\mathscr{L}^{-1}(x) \approx x\frac{3 - 2.6x + 0.7x^2}{(1-x)(1+0.1x)} \tag{2.31}$$

$\mathscr{L}^{-1}(x)$ is defined in the interval $-1 < x < 1$ and it is a continuous, smooth and monotonically increasing function. In the interval of interest for our problems, i.e. $0 \leq x < 1$,

it is always non-negative. The values at the extremities of the interval are $\mathscr{L}^{-1}(0) = 0$ and $\lim_{x\to 1} \mathscr{L}^{-1}(x) = \infty$.

Adopting the Langevin statistic distribution implies that the orientation of each Kuhn segment is influenced by the orientation of the whole chain. The resulting free energy is [156]

$$\psi = k_B T N \left(\frac{\lambda}{\sqrt{N}} \beta + \ln \frac{\beta}{\sinh \beta} \right), \qquad \beta = \mathscr{L}^{-1}\left(\frac{\lambda}{\sqrt{N}} \right) \tag{2.32}$$

and the force in the chain is

$$f = \frac{k_B T}{b} \beta \tag{2.33}$$

It can be noticed that the above expression of the force can be linearised by adopting the Taylor series expansion (2.30) arrested to the first term as $\mathscr{L}^{-1}(x) \approx 3x$; in this way, the expression (2.28) previously obtained using the Gaussian distribution, can be recovered.

The force vs. stretch plot of (2.33) is illustrated in fig. 2.1 together with the linear expression (2.28) and with the outcome of the so-called Extended Freely Jointed Chain model (EFJC, see §2.3.3.3). It can be observed that the non-Gaussian theory leads to a finite deformability of the chain, because the chain's stiffness tends to infinity when the stretch approaches the limit deformation $\lambda = \sqrt{N}$. Furthermore, the model does not consider the rupture of the chain, which can thus sustain any tensile load value.

2.3.3.3 Extended Freely Jointed Chain (EFJC)

An interesting improvement of the Freely Jointed Chain model can be obtained by removing the assumption of rigidity of the Kuhn segments and assuming, instead, that each segment behaves as an elastic element [102]. The segment's length is b in the undeformed configuration and $\lambda_b b$ in the current, deformed, configuration, where λ_b represents the segment's stretch. Let us define the enthalpic energy related to the stretch of a single segment as a function of λ_b, namely $\psi_b = \psi_b(\lambda_b)$. Then, the free energy of a chain made of N elastic segments is

$$\Psi = N\psi_b + k_B T N \left(\frac{\lambda}{\lambda_b \sqrt{N}} \beta_b + \ln \frac{\beta_b}{\sinh \beta_b} \right), \qquad \beta_b = \mathscr{L}^{-1}\left(\frac{\lambda}{\lambda_b \sqrt{N}} \right) \tag{2.34}$$

where $\lambda = r/r_0$ is the chain's stretch. The chain's force is given by

$$f = \frac{k_B T}{b \lambda_b} \beta_b \tag{2.35}$$

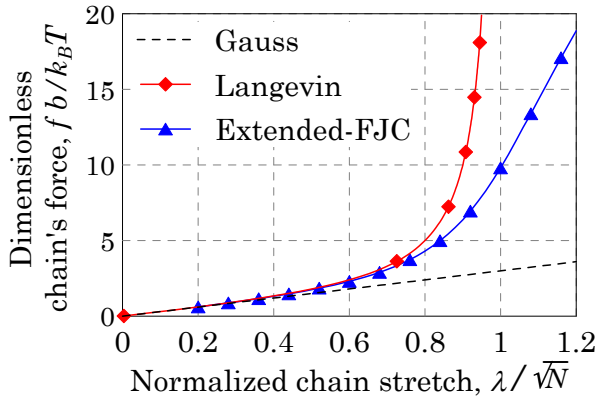

Figure 2.1: *Chain force vs. chain stretch curves obtained by using the Gaussian and the Langevin distribution and the Extended Freely Jointed Chain model.*

In this way, the free energy of the chain is decomposed inTO an enthalpic and an entropic part. For a given chain stretch λ, the enthalpic contribution increases with λ_b, while the entropic contribution decreases. The solution value of λ_b is the one that fulfills the condition of minimum of the free energy $\partial\Psi/\partial\lambda_b = 0$. This condition provides the supplementary relation

$$\frac{\partial\psi_b}{\partial\lambda_b} = \frac{k_BT}{\sqrt{N}} \cdot \frac{\lambda}{\lambda_b^2}\beta_b \tag{2.36}$$

A possible choice of the function ψ_b is [102]

$$\psi_b = \frac{1}{2}E_b \ln^2 \lambda_b \tag{2.37}$$

where E_b has the dimensions of energy and represents the stiffness of the segments. According to this formulation, the resulting force vs. stretch curve overcomes the limitation $\lambda < \sqrt{N}$. In fig. 2.1 such a behavior is compared to the one of a Gaussian and a Langevin Freely Jointed Chain.

2.3.4 Networks of freely jointed chains

Let us consider a network obtained by cross-linking a large number of polymer chains. To incorporate the individual chain statistics into a constitutive framework, it is necessary to have a model that relates the chain stretch of individual chains to the

applied deformation. Among the models available in literature, we are interested in those where the whole network is seen as the repetition of an elementary cell, such as the 3-chains [16], the 4-chains (or Flory-Rehner) [55, 151], the 8-chains [3] and the full network model [156]. In these models, the elastic behavior of the network is governed by the spatial orientation of the chains.

The simplest kind of cell is made of three freely jointed chains in Gaussian region, lying parallel to the local principal axis [143]. Such a network contains n chains per unit volume, each one made of N rigid segments of equal length b. The deformation is assumed to be *affine*, that is to say the deformation of a end-to-end vector is equal to the deformation of the continuum medium in which the chain is embedded in, i.e. $\mathbf{r} = \mathbf{F}\,\mathbf{r}_0$. Under these assumptions, the free energy function is

$$\Psi = \frac{1}{2} n k_B T \left(\lambda_1^2 + \lambda_2^2 + \lambda_3^2 - 3\right) \tag{2.38}$$

where λ_1, λ_2, λ_3 are the three principal stretches of the unit cell. The above expression corresponds to the so-called neo-Hookean model $\Psi = \mu(I_1 - 3)/2$; the comparison of these models provides a microscopic interpretation of the shear modulus $\mu = n k_B T$, which is proportional to the number of chains (and also of cross-links) and to the energy $k_B T$. More general expressions for the elastic constants can be found by considering that the network's cross-links are not in fixed positions, but they can fluctuate around the most probable position [76].

2.3.4.1 Network with non-uniform chain's weight

Since the crosslinking process cannot be controlled precisely, the formation of network whose chains have the same contour length (a so-called *monodisperse network*) is not possible. More often, the network is made of chains with random contour length (*polydisperse network*). Molecular dynamic simulations of the cross-linking process, reported in [63], showed that the number of cross-links per chain follows a Gaussian distribution, while the contour length between two cross-links follows an exponential distribution law. Using the freely jointed chain model, such a distribution can be written [137]

$$P(N) = \frac{1}{N} \exp\left(-\frac{N}{N_{avg}}\right) \tag{2.39}$$

where $P(N)$ is the probability to find a chain formed by N Kuhn segments while N_{avg} is the average number of segments per chain.

Sometimes the presence of multiple networks is a desired feature to improve the mechanical properties of the material [62, 105, 153]. If the polymer is made of a double network with short and long chains, the external loads are bear mainly by the first network and, only after the rupture of the shortest chains, the stress is transferred to the longest ones.

The network's polydispersity leads to the surprising conclusion that, even in a stress-free state, the chains' stretch and force are not homogeneous. The complexity of the internal stress state of the network is highlighted in [150], in which the Authors considered a network where the chains are linked together in series, thus, under a macroscopic stretch, they undergo the same force but different stretch. Under this assumption, they define the number of segments in a chain belonging to an equivalent monodisperse network, which represents the real polydisperse one, as follow

$$N_{eq} = \left(\frac{\sum_{N=1}^{\infty} P(N) N}{\sum_{N=1}^{\infty} P(N) \sqrt{N}} \right)^{1/2} \tag{2.40}$$

where $P(N)$ is the fraction number of chain with N segments, such that $\sum_{N=1}^{\infty} P(N) = 1$. The force in the hybrid representative chain is given by a relation similar to (2.33)

$$f = \frac{k_B T}{b} \mathscr{L}^{-1} \left(\frac{\lambda_{net}}{\sqrt{N_{eq}}} \right) \tag{2.41}$$

where λ_{net} is the macroscopic stretch of the whole hybrid chain. The Authors conclude that the stretch in a chain with N segments is related to the macroscopic stretch through the relation

$$\frac{\lambda_N}{\sqrt{N}} = \frac{\lambda_{net}}{\sqrt{N_{eq}}} \tag{2.42}$$

In the reference, stress-free state, the stretch of a chain with N segments is $\lambda_N^0 = \sqrt{N/N_{eq}}$, thus short chains ($N < N_{eq}$) have $\lambda_N^0 < 1$, while long chains ($N > N_{eq}$) have $\lambda_N^0 > 1$.

2.4 Polymer swelling and gel dynamics

When a polymer with a good fluid affinity is placed in contact with a fluid, the small molecules of the fluid migrate inside the network, which becomes a solution called *gel*, made of a solid solute and a fluid solvent [48]. Fluid absorption increases the volume of the polymer; however the gel is still incompressible because it can change its

volume only by absorbing solvent, but not because of mechanical actions. Rubber can be regarded as a special case of a *dry gel* in which there is no solvent [47]. The amount of fluid absorbed by the polymer depends on the solid-fluid affinity and by the stress state of the network, so the mechanical deformation and the fluid motion are coupled.

The free energy of the gel depends on the deformation state of the network and on the amount of fluid inside the network itself. In polymer physics, a common choice to quantify the presence of solvent is the use of the volume fraction of polymer in the gel (see e.g. [48]), that is, because of its mechanical incompressibility, equal to J^{-1}, where $J = \det\mathbf{F}$ is the volume ratio. In the present work, we adopt the deformation gradient $\mathbf{F}$ and the solvent concentration as state parameter. To a nominal concentration equal to C_s in the reference configuration, corresponds a true concentration $c_s = C_s/J$ in the current configuration.

Following Flory and Rehner [56], the free energy of the gel can be written as the sum of the free energy of the dry polymer $\Psi(\mathbf{F})$ and the free energy of mixing $\Psi_{mix}(C_s)$. A common form of the mixing energy is [104]

$$\Psi_{mix}(C_s) = -\frac{k_B T}{V_s}\left[V_s C_s \ln\left(1+\frac{1}{V_s C_s}\right)+\frac{\chi}{1+V_s C_s}\right] \tag{2.43}$$

where V_s is the volume of the solvent molecules and χ is called *Flory-Huggins mixing parameter*; it measures the chemical dis-affinity between polymer and solvent [117].

The potential energy, i.e. the Lagrangian of the coupled polymer-solvent system can be written as

$$\Pi(\mathbf{F}, C_s) = \Psi(\mathbf{F}) + \Psi_{mix}(C_s) + p(1 + V_s C_s - J) \tag{2.44}$$

where p is the Lagrange multiplier which enforces the condition $J = \det\mathbf{F} = 1 + V_s C_s$ stating that the material can change its volume only by absorbing fluid. Physically, p represents the *osmotic pressure* exerted by the fluid on the network.

The linear momentum balance requires the conditions $\mathrm{Div}\,\mathbf{P} = 0$ in the bulk and $\mathbf{P}\cdot\mathbf{N} = \mathbf{P}_{ext}$ on the boundary, being $\mathbf{P}$ and $\mathbf{P}_{ext}$ the internal and the applied stress, respectively, while $\mathbf{N}$ is the unit vector normal to the boundary of the undeformed body.

Moreover, the solvent's balance requires the conditions $\mathrm{Div}\,\mathbf{Q} = \dot{C}_s$ in the bulk and $\mathbf{Q}\cdot\mathbf{N} = Q_{ext}$ on the boundary, being $\mathbf{Q}$ the vector flow of solvent and Q_{ext} the flow across the boundary, respectively.

The nominal stress can be obtained by deriving the potential Π w.r.t. the gradient tensor, so $\mathbf{P} = \partial\Pi/\partial\mathbf{F} = \partial\Psi/\partial\mathbf{F} + pJ\mathbf{F}^{-T}$, while the chemical potential can be obtained by deriving Π w.r.t. the concentration, $H = \partial\Pi/\partial C_s = \partial\Psi_{mix}/\partial C_s + V_s p$. Such chemical

potential H can be viewed as the agent which moves the solvent, so $H\,dC_s$ is the work related to the mixing of an infinitesimal amount of solvent within the polymer [15].

Following the theory developed by Hong et al. [71], the nominal flux Q_i in the reference configuration can be related to the chemical potential by

$$Q_i = -M_{ik}\frac{\partial H}{\partial X_k} \tag{2.45}$$

where M_{ik} is a symmetric and positive-definite tensor called *mobility tensor* which relates the flux to the gradient of the chemical potential. The above relations have the same structure of the well-known Fick's law of diffusion. Since the mobility tensor depends on the stretch, the solvent diffusion usually is nonlinear and non-isotropic.

Using (2.45), the balance of solvent in the reference configuration becomes

$$\frac{\partial C_s}{\partial t} = -\frac{\partial Q_k}{\partial X_k} = -\frac{\partial}{\partial X_k}\left(M_{kj}\frac{\partial H}{\partial X_j}\right) \tag{2.46}$$

It is worth mentioning that the mobility tensor generally depends on $\mathbf{F}$, as shown in [71], and so the flux exhibits an anisotropy which depends on the applied stretch.

A different theory was proposed earlier by Tanaka et al. [136]. The authors assume that the kinetic energy of the fluid molecules will be dissipated during the swelling process by viscous forces. The dissipated power $\mathscr{R}$, due to such a friction-like effect, can be written in a Rayleigh form as

$$\mathscr{R} = \frac{1}{2}\zeta \dot{C}_s^2 \tag{2.47}$$

where ζ is a dissipation factor. The Lagrange equation for a non-conservative systems provides the evolution of the concentration [47]

$$\frac{\partial \Pi}{\partial C_s} = -\frac{\partial \mathscr{R}}{\partial \dot{C}_s} \qquad \rightarrow \qquad \frac{\partial \Psi_{mix}}{\partial C_s} + pV_s = -\zeta \dot{C}_s \tag{2.48}$$

so the balance between the chemical potential and the osmotic pressure provides the time evolution of the solvent concentration.

2.5 Conclusions

Polymers are among the most diffused materials for industrial and technological application and their micromechanical behavior is quite important because it successfully describes also the response of some tissues and biomaterials. Their structure is made of many long entangled molecules, each obtained by the repetition of an elementary

unit, jointed together at discrete points called cross-links, whose density determine the stiffness of the material.

Synthetic polymers can be roughly subdivided in thermoplastics, thermosets and elastomers. In particular, thermoplastic – differently by thermoset – are characterized by temperature recoverable bonds, while elastomers can undergo very large elastic deformations without losing their mechanical properties.

The description of the mechanical behavior of an elastomeric solid requires the use of non-linear continuum mechanics theory, accounting for the effects of large deformations and displacements.

Within this theoretical framework, the mechanics of polymers is typically described by using a proper hyperelastic constitutive model, which can be derived from phenomenological aspects or, more consistently, through the polymer network's physics. The polymer's elasticity for a not too large deformation regime, is typically ruled by entropy, rather than by the internal energy.

In this thesis the so-called Freely Jointed Chains model, based on the micromechanical features of the involved physical phenomena, is adopted to obtain the hyperelastic constitutive relation for a polydisperse network, i.e. for a network made of chains with different contour length.

Moreover, when a polymer is prone to uptake a fluid (good chemical fluid-polymer affinity), the two substances mix together in a solution called gel; the mechanical behavior in such a case must account also for the swelling phenomenon that becomes fully coupled with the purely mechanical behavior.

CHAPTER 3

TIME-DEPENDENT RESPONSE OF ELASTOMERIC POLYMERS

Natural and synthetic polymers very often show a time-dependent mechanical response, such as creep, stress relaxation, self-healing or energy dissipation due to hysteresis [11, 80]. In the study of biological materials, such as the human myocardium, skin or others tissues, the viscoelasticity is a crucial aspect that should be considered in the constitutive model [64, 111]. Furthermore, the time dependency of the mechanical response of synthetic polymers (such as plastics, rubbers and asphalts) governs their damping and insulating properties against vibration and noise, and plays also an important role in the manufacturing process. Moreover, polymer melts exhibit complex time-dependent behavior, and their response ranges from that of an elastic solid to that of a viscous fluids depending on the rate of stretching [46]. The deformation velocity influences also the ultimate properties of polymers both in terms of strain and stress [26]; in fact, slow deformations usually allow the material to rearrange its internal structure, because the chains tend to align along the loading directions with a subsequent increase of the deformability and of the resistance of the material [30].

Modeling such different behaviors can be addressed through the classical linear models, obtained by combining linear elements such as springs and dashpots. On the other hand, for many materials, the linear theories are not adequate. Dealing with nonlinear viscoelasticy, it is necessary to consider the whole deformation history of the

material from the reference time $t = 0$ to the current one t. A general form of this class of constitutive laws is expressed mathematically as

$$\boldsymbol{\sigma}(t) = \mathscr{F}\left[\mathbf{F}(\theta)|_{\theta=0}^{t}\right] \tag{3.1}$$

where $\mathscr{F}$ is a tensor-valued response functional, θ is a generic time ($0 \le \theta \le t$) and the symbol $\mathbf{F}(\theta)|_{\theta=0}^{t}$ indicates that the whole deformation history is considered. Several forms of the functional $\mathscr{F}$ are available in the literature (e.g. see [155]); most of them can be classified as phenomenological models (see §2.3) because they are based on mathematical considerations instead of the physical nature of the phenomena involved in viscoelasticity.

Another common assumption, alternative to (3.1), is to separate the effects of the deformations from the effects of time with the following relation [80]

$$\boldsymbol{\sigma}(\mathbf{F}, t) = \boldsymbol{\sigma}_0(\mathbf{F})\, g(t) \qquad \text{with} \qquad g(t) = g_\infty + \sum_i g_i e^{-t/\tau_i} \tag{3.2}$$

where τ_i are the relaxation times and $\boldsymbol{\sigma}_0$ is the instantaneous response to the stretch $\mathbf{F}$; the parameters in the dimensionless function $g(t)$ must satisfy the conditions $0 < g_\infty \le 1$, $0 \le g_i < 1$ and $g_\infty + \sum_i g_i = 1$.

The phenomenological models and the models obtained by fitting experimental data are quickly usable for simulations and they are usually accurate if the material's properties and the simulation's conditions are within the range of the calibration tests. Unfortunately, these models have not general validity, and their use is limited by the accuracy of the fitting procedure. Furthermore, such models do not give any information about the material's micro-structure, so they cannot be used to design new materials. In order to overcome these limitations, a strategy can be the development of physics-based models.

In the present work, we develop a physics-based constitutive model able to capture the main aspects of the network's mechanics. The fundamental idea is to focus on the statistical description of the network's state through a proper density function defined in the three-dimensional chains configuration space. The external macroscopic solicitations make the describing function of the network state to evolve, providing a clear and direct correlation between the micro-scale and the macro-scale phenomena.

In the present chapter, we define the configuration space and the «*Chain Configuration Density Function*» (CCDF) that describes the network's state; subsequently we study the network evolution in response to the elastic deformation of the continuum

in which the network is embedded in. After that, we introduce a time-dependency in the mechanical response through the concept of «*dynamic cross-links*» and irreversible deformations through the concept of «*chain unfolding*». Finally, we consider the damage of the network by introducing the chain's failure. The developed theory has general validity, since our attention is on the evolution law of the statistical description of the network state, which is the same for a wide number of polymers. The theory is also flexible and adaptable to the specific chemo-physical properties of the polymer, since different micromechanical models can be adopted: for example, the description of the force-stretch curve of a polymer chain can be achieved by adopting the Gaussian, the Langevin statistic, the worm-like chain model or other models.

3.1 Configuration space

Let us define the *configuration space* as the set of all the possible end-to-end vectors that a polymer chain can assume. Using the Lagrangian approach, the chain is identified by its mean-square end-to-end vector $\mathbf{r}_0$ (see §2.3.3.1), thus the *reference configuration space* Ω_0 can be defined as $\Omega_0 \equiv \{\mathbf{r}_0 \mid \mathbf{r}_0 \in \mathbb{R}^3\}$; by using the affine deformation assumption, the current configuration of a chain can be obtained as $\mathbf{r} = \mathbf{F}\,\mathbf{r}_0$, being $\mathbf{F}$ the deformation gradient tensor. On the other hand, using the Eulerian approach, the chain is identified by its current end-to-end vector $\mathbf{r}$, thus the *current configuration space* Ω can be defined as $\Omega \equiv \{\mathbf{r} \mid \mathbf{r} \in \mathbb{R}^3\}$; the reference configuration of a chain can be obtained as $\mathbf{r}_0 = \mathbf{F}^{-1}\,\mathbf{r}$. In the following, we will use mainly the Eulerian approach for its theoretical convenience; the corresponding Lagrangian relations will be discussed when appropriate.

We assume the reference coordinates system of the configuration space to be parallel to that of the physical space. At each point of the configuration space (identified by the end-to-end vector $\mathbf{r} \in \Omega$), the associated chain force vector $\mathbf{f}$ can be defined, thus the function $\mathbf{f} : \Omega \mapsto \mathbb{R}^3 \mid \mathbf{f} = \mathbf{f}(\mathbf{r})$ can be seen as a vector field. The chain force can be obtained from the chain free energy ψ (see §2.3.2) as

$$\mathbf{f} = \nabla\psi = \frac{\mathrm{d}\psi}{\mathrm{d}\mathbf{r}} = \frac{\mathrm{d}\psi}{\mathrm{d}r}\frac{\mathrm{d}r}{\mathrm{d}\mathbf{r}} = f(r)\,\frac{\mathrm{d}\sqrt{\mathbf{r}\cdot\mathbf{r}}}{\mathrm{d}\mathbf{r}} = f(r)\,\frac{\mathbf{r}}{r} = f(r)\,\hat{\mathbf{r}} \tag{3.3}$$

where $\psi = \psi(r)$ and $f = f(r)$ are the free energy and the force in a chain with end-to-end distance $r = |\mathbf{r}|$, respectively, while $\hat{\mathbf{r}}$ is the unit vector of $\mathbf{r}$, so that $\mathbf{r} = r\,\hat{\mathbf{r}}$. The above expression shows that $\mathbf{f}$ is a central vector field generated by the scalar potential ψ. The

existence of a potential is a necessary and sufficient condition to have a conservative field; thanks to such a property, the curl of the field is identically zero, i.e. $\nabla \times \mathbf{f} = 0$, which implies $f_{i,j} = f_{j,i}$. Furthermore, the work done by the force field when a chain extremity is moved, is path-independent, since it depends only on the initial and final end-to-end vectors; in particular, if the path is closed, the work done is zero.

3.1.1 Chain Configuration Density Function (CCDF)

Let us consider a polymer network and let us define, in the configuration space Ω, a scalar function $\rho : \Omega \to \mathbb{R} \mid \rho = \rho(\mathbf{r})$ which represents the probability density of the chains distribution, so that it provides the number of chains per unit volume with end-to-end vector $\mathbf{r}$. We call such a function *Chain Configuration Density Function* (CCDF). The physical dimensions of the CCDF is $[\mathrm{L}]^{-6}$, since it represents a number of chains per unit volume in the configuration space and per unit volume in the physical space. The CCDF can be written as $\rho : \mathscr{B}_0 \times \Omega \to \mathbb{R} \mid \rho(\mathbf{X}, \mathbf{r}) = n_a(\mathbf{X})\, \varphi(\mathbf{r})$, where $n_a : \mathscr{B}_0 \to \mathbb{R} \mid n_a = n_a(\mathbf{X})$ is the chains density $\left([\mathrm{L}]^{-3}\right)$ in the physical space, while $\varphi : \Omega \to \mathbb{R} \mid \varphi = \varphi(\mathbf{r})$ is the chains density $\left([\mathrm{L}]^{-3}\right)$ in the configuration space.

In order to simplify the notation, let us define the operator $\langle \bullet \rangle$ as the integral over the whole configuration space $\Omega \subseteq \mathbb{R}^3$

$$\langle \bullet \rangle = \int_{\Omega} \bullet \, d\Omega \tag{3.4}$$

The operator $\langle \bullet \rangle$ can be expressed explicitly in rectangular and spherical coordinates as

$$\begin{aligned} \langle \bullet \rangle &= \int_{x=-\infty}^{+\infty} \int_{y=-\infty}^{+\infty} \int_{z=-\infty}^{+\infty} \bullet \, dx\, dy\, dz \\ \langle \bullet \rangle &= \int_{\omega=0}^{2\pi} \int_{\theta=0}^{\pi} \int_{r=0}^{\infty} \bullet \, r^2 \sin\theta \, dr\, d\theta\, d\omega \end{aligned} \tag{3.5}$$

where $(x, y, z) \equiv (r, \theta, \omega)$ are the rectangular and spherical coordinates of a given point of the configuration space, respectively. Furthermore, we define the operator $\langle \bullet \rangle_{\partial}$ as

$$\langle \bullet \rangle_{\partial} = \int_{\partial\Omega} \bullet \, d(\partial\Omega) \tag{3.6}$$

where $\partial\Omega$ represents the boundary of Ω.

Since the normalized function φ represents a probability density, it has the property $\langle \varphi \rangle = 1$ because the integral is performed over the entire domain of definition; as a consequence, the integration of the CCDF over Ω provides the number of chains per unit volume, i.e. $\langle \rho \rangle = n_a \langle \varphi \rangle = n_a$.

3.1.2 Network energy

The energy stored in a network, Ψ, can be obtained by adding the energy stored in each chain composing the network itself, i.e. as $\Psi = \langle \rho\psi \rangle$, being $\psi = \psi(\mathbf{r})$ the free energy of a chain with end-to-end vector $\mathbf{r}$.

Let us consider a material made only of chains not connected each other. The most probable configuration for a free chain is $\mathbf{r} = \mathbf{0}$ (see §2.3.3.1), so the CCDF of such a network can be written as $\rho(\mathbf{r}) = n_a\,\delta(\mathbf{r})$, being $\delta(\mathbf{r})$ the Dirac distribution. The corresponding network's energy results to be zero, since $\Psi = \langle \rho\psi \rangle = \left\langle n_a\,\delta(\mathbf{r})\,\psi(\mathbf{r}) \right\rangle = n_a\,\psi(\mathbf{0}) = 0$. Physically, this zero-energy situation corresponds to a group of molecular chains before the formation of the network.

Let us now consider the same group of chains after the cross-linking process that creates the network. In the stress-free configuration, the network chains are always elongated (see §2.3.3.1) and the most probable end-to-end distance is the mean-square given in (2.26), while the CCDF is the Gaussian distribution with mean $\mathbf{0}$ and standard deviation $b\sqrt{N/3}$ [48]

$$\rho_0(\mathbf{r}) = \overline{\rho}_0(\mathbf{r}) = \frac{n_a}{b^3}\left(\frac{3}{2\pi N}\right)^{3/2} \exp\left(-\frac{3\,|\mathbf{r}|^2}{2Nb^2}\right) \tag{3.7}$$

where we make use of the symbol ρ_0 to indicate the CCDF in the reference state and of the symbol $\overline{\rho}_0$ to indicate the three-dimensional Gaussian function, while N and b are the number and the length of the Kuhn segments, respectively. The free energy in the reference stress-free state can be obtained as $\langle \overline{\rho}_0 \psi \rangle$, thus it is greater than zero, since $\overline{\rho}_0(\mathbf{r}) \geq 0 \quad \forall \mathbf{r} \in \Omega$. Such an energy is stored in the network during the cross-linking process, thus it is pre-existent to any applied external deformation and it is not available to be transformed in mechanical work.

Finally, we stretch the network by applying the (macroscopic) deformation gradient $\mathbf{F}$. According to the affine deformation assumption, the end-to-end vector of a chain evolves from $\mathbf{r}$ to $\mathbf{F}\,\mathbf{r}$ and the CCDF evolves from $\rho_0(\mathbf{r})$ to $\rho(\mathbf{r}) = \rho_0(\mathbf{F}^{-1}\mathbf{r})$. The total amount of energy stored in the network is $\langle \rho\psi \rangle$.

Since the deformation process is assumed to be isothermal and reversible, the free energy corresponds to the deformation work (see eq. 2.21). Moreover, the work done by a conservative force field depends only on the initial and final position of the chain extremities, as recalled in §3.1. The initial and final position of a chain in the configuration space is defined by $\mathbf{r}$ and $\mathbf{F}\,\mathbf{r}$, respectively; under these assumptions, the

deformation free energy Ψ of a network can be obtained as the difference between the energy in the final state (i.e. $\langle \rho\psi \rangle$) and the energy in the reference state (i.e. $\langle \rho_0\psi \rangle$), so that it results

$$\Psi = \left\langle \left(\rho - \rho_0\right)\psi \right\rangle \tag{3.8}$$

for a more detailed explanation we refer to [24]. Using the Lagrangian description, the free energy is written as $\Psi(\mathbf{F}) = \left\langle \left(\rho_0(\mathbf{F}^{-1}\mathbf{r}) - \rho_0(\mathbf{r})\right)\psi \right\rangle$, while using the Eulerain description it is $\Psi(\mathbf{F}) = \left\langle \left(\rho(\mathbf{r}) - \rho(\mathbf{F}\mathbf{r})\right)\psi \right\rangle$. We note that such a formulation respects the condition $\Psi(\mathbf{F} = \mathbf{I}) = 0$ (see §2.2.1).

3.2 Evolution law of the CCDF

We assume that the CCDF, which rules the mechanical response of the polymer network, can evolve in time because of four different mechanisms, described in the following.

The first mechanism is due to the affine deformation assumption, according to which the network undergoes the same deformation of the continuum in which it is immersed in; a detailed description of the effects of such an assumption on the statistical modeling of the network's state can be found in [24].

The second mechanism is due to the presence of *dynamic cross-links*, i.e. we assume that the number of cross-linked chains can vary in time because of a dynamic balance between attachment and detachment of chains, as typically occurs in polymer with physical bonds; more specifically, the model assumes that a stretched chain can detach and subsequently attach in a stress-free state, as proposed in [149] and [30]. Such a mechanism was observed since the 1960s by Tobolsky [140], which reported two types of chain's scission, both leading to stress relaxation: a destructive one, in which the bonds are definitively broken, and a non-destructive one, in which the bonds are regenerated.

The third mechanism we consider is the «*unfolding*» process of the chains, i.e. the fact that the contour length of the network's chains can vary because of the evolution of the entanglement of the network itself. The basic idea is that the entanglement degree of a stretched network is lower than the one of an unstretched network: as a conseguence, the degree of freedom of its chains - represented by the contour lenght - increases with the deformation, since the topological constrain due to the entanglement becomes less strong [7, 97, 106, 123].

The fourth mechanism here considered is the chains failure, represented by the irreversible rupture of the chemical bonds between two consecutive units of a polymer chains, or the rupture of the bonds in a cross-link. The idea to relate the strenght of polymers to the chains scission mechanism was suggested in the 1960s by Lake et al. [90] and successively adopted by many others (see, e.g. [101]); a study about the influence of the chains scission mechanism on the statistical description of the network's state can be found in [148].

In order to take into account the four above mentioned mechanisms, we can formally write the CCDF evolution law as

$$\dot{\rho} = \dot{\rho}_L + \dot{\rho}_{XL} + \dot{\rho}_{un} + \dot{\rho}_f \tag{3.9}$$

where the four contributions to the time derivative $\dot{\rho}$ of the CCDF are: $\dot{\rho}_L$ for the body deformation (through the affine deformation assumption), $\dot{\rho}_{XL}$ for the dynamic cross-links, $\dot{\rho}_{un}$ for the unfolding and $\dot{\rho}_f$ for the chains failure. In the following sections we define in detail each contribution.

3.2.1 CCDF evolution due to the network's deformation

Let us now consider the term $\dot{\rho}_L$ of (3.9), quantifying the evolution of the CCDF due to the deformation of the network, which is assumed to be equal to the deformation of the body.

Let $\Omega^* \subseteq \Omega$ be an arbitrary subset of the configuration space, which contains $\int_{\Omega^*} \rho \, d\Omega$ chains. The time derivative of the amount of chains contained in Ω^* can be evaluated by using the Reynold's transport theorem as

$$\frac{d}{dt}\int_{\Omega^*} \rho \, d\Omega = \int_{\Omega^*} \dot{\rho} \, d\Omega + \int_{\partial\Omega^*} \rho \dot{\mathbf{r}} \cdot \mathbf{m} \, d(\partial\Omega^*) \tag{3.10}$$

where $\mathbf{m}$ is the unit vector normal to the boundary of Ω^*, namely $\partial\Omega^*$. By applying the divergence theorem we obtain

$$\frac{d}{dt}\int_{\Omega^*} \rho \, d\Omega = \int_{\Omega^*} \left(\dot{\rho} + \mathrm{div}(\rho \dot{\mathbf{r}})\right) d\Omega \tag{3.11}$$

Here, the number of cross-linked chains in the network is assumed to be constant, so that no chains are lost or gained, thus the amount of chains contained in Ω^* does not change in time. Since the left-hand side of the above relation is zero and Ω^* is arbitrary, we found

$$\dot{\rho} + \mathrm{div}(\rho \dot{\mathbf{r}}) = 0 \tag{3.12}$$

Interestingly, the above relation has the same structure of the continuity equation commonly used in fluid dynamics. Physically, it means that in a small volume of the configuration space centered in $\mathbf{r}$, the variation of the chains density $\dot{\rho}$ is equal to the flux of chains $\mathrm{div}(\rho\,\dot{\mathbf{r}})$ (assumed positive if outgoing). The divergence can be rewritten as $\mathrm{div}(\rho\,\dot{\mathbf{r}}) = \partial(\rho\dot{r}_i)/\partial r_i = \rho_{,i}\dot{r}_i + \rho\dot{r}_{i,i}$, so that the above relation becomes

$$\dot{\rho} = -\rho_{,i}\dot{r}_i - \rho\dot{r}_{i,i} \tag{3.13}$$

Eq. (3.13) relates the time evolution of the CCDF with the velocity field in the configuration space. By using the affine deformation assumption, such a velocity field can be related to the deformation of the continuum by using the velocity gradient L_{ij} defined in (2.2), so that

$$\dot{r}_i = L_{ij}\,r_j \qquad \dot{r}_{i,i} = \frac{\partial\dot{r}_i}{\partial r_i} = \frac{\partial\left(L_{ij}\,r_j\right)}{\partial r_i} = L_{ij}\,\delta_{ij} = L_{ii} \tag{3.14}$$

where δ_{ij} is the Kronecker's delta tensor. We can obtain the rate $\dot{\rho}_L$ by replacing (3.14) in (3.13) as

$$\dot{\rho}_L = -\left(\rho_{,i}\,r_j + \rho\,\delta_{ij}\right)L_{ij}\,, \qquad \text{or} \qquad \dot{\rho}_L = -\left(\nabla\rho\otimes\mathbf{r} + \rho\,\mathbf{I}\right):\mathbf{L} \tag{3.15}$$

the above evolution law requires the initial condition $\rho(t=0) = \overline{\rho}_0$, being $\overline{\rho}_0$ the initial CCDF defined in (3.7).

Finally, we note that, if the material is incompressible, the divergence of $\dot{\mathbf{r}}$ vanishes (see §2.2.1), thus it results $\dot{r}_{i,i} = \mathrm{tr}(\mathbf{L}) = L_{ii} = 0$ and the above eq. (3.15) reduces to $\dot{\rho}_L = -\rho_{,i}\,r_j\,L_{ij} = -\nabla\rho\otimes\mathbf{r}:\mathbf{L}$. It can be appreciated that, in this particular case, the value of the CCDF in the origin of the configuration space does not change in time, since in that point its time derivative vanishes, i.e. $\dot{\rho}_L(\mathbf{r}=\mathbf{0}) = 0$.

3.2.2 CCDF evolution due to dynamic cross-links

Let us assume that the deformation state in the network is kept constant and both the chains failure and unfolding are absent, so the network's state evolves only because of the dynamic cross-links, such as in polymers with weak physical bonds. The current number of cross-linked chains arises from the dynamic balance between the attachment and the detachment process. In the unit time, the fraction k_a of detached chains becomes attached, while the fraction k_d of attached chains detaches. The two frequencies k_a and k_d are called *attaching* and *detaching rates*, respectively, and are characteristic parameters of the material.

After a sufficiently long time from the polymerization of the material, the dynamic process reaches the steady state in which the number of attached chains does not change anymore. We assume that the shear modulus μ is measured in this steady state condition, thus the corresponding number of attached chains is (see §2.3.4)

$$n_\mu = \frac{\mu}{k_B T} \tag{3.16}$$

The above relation arises from the three-chains model in the so-called Gaussian regime, which is an acceptable assumption for the shear modulus measured for small deformations.

The evolution equation and the initial value of the number of attached chains are, respectively

$$\frac{\partial n_a}{\partial t} = k_a(n_{max} - n_a) - k_d n_a\,, \qquad n_a(t=0) = n_{a0} \tag{3.17}$$

where n_{max} is the total number of chains available to attach, while n_{a0} is the number of attached chains at time $t = 0$. In the above relation, the quantity $k_a(n_{max} - n_a)$ is the number of detached chains that becomes attached in the unit time, while $k_d n_a$ is the number of attached chains that becomes detached in the same time interval. If k_a and k_d are constants, the solution of the above evolution law is

$$n_a(t) = \left(n_{a0} - \frac{k_a}{k_a + k_d} n_{max}\right) e^{-(k_a+k_d)t} + \frac{k_a}{k_a + k_d} n_{max} \tag{3.18}$$

where it can be clearly acknowledged the transient term and the steady state one; the latter is expressed as

$$n_{ss} = \lim_{t\to\infty} n_a(t) = \frac{k_a}{k_a + k_d} n_{max} \tag{3.19}$$

The above value can be obtained directly from (3.17) by using the steady state condition $\dot{n}_a = 0$. Since the shear modulus is measured in the steady state, it results $n_\mu = n_{ss}$, so that the relations (3.16) and (3.19) can be combined to obtain n_{max} as

$$n_{max} = n_\mu \frac{k_a + k_d}{k_a} \tag{3.20}$$

By replacing the above expression in (3.18) we have

$$n_a(t) = \left(n_{a0} - n_\mu\right) e^{-(k_a+k_d)t} + n_\mu \tag{3.21}$$

If we assume that at $t = 0$ the material is already in a steady state condition, it results $n_{a0} = n_\mu$, thus there is no evolution of the number of chains, since from (3.21) we obtain $n_a(t) = n_\mu$.

Now, we can write the term $\dot{\rho}_{XL}$ of (3.9) by modifying (3.17). From the definition of the CCDF, we know that a chain, just before it passes from the attached to the detached state, is associated to the distribution ρ. It is reasonable to assume that the same chain, just after passing from the detached to the attached state, is associated to the stress-free distribution $\overline{\rho}_0$ defined in eq. (3.7). The time derivative of the CCDF at constant deformation, using (3.17) and recalling $\rho = n_a\varphi$, is [30]

$$\dot{\rho}_{XL} = k_a \frac{n_{max} - n_a}{n_a} \overline{\rho}_0 - k_d \rho \tag{3.22}$$

with the initial conditions $n_a(t=0) = n_{a0}$ and $\rho(t=0) = \overline{\rho}_0$.

The rate $\dot{\rho}_{XL}$ can be conveniently rewritten in a easier form by recalling (3.20) and the fact that the number of chains remains constant in time, i.e. $n_a(t) = n_\mu$, so that we have

$$\dot{\rho}_{XL} = -k_d \left(\rho - \overline{\rho}_0\right) \tag{3.23}$$

from which it becomes clear that the effect of the dynamic cross-links is to reduces the current CCDF to the stress-free CCDF (3.7); furthermore, the evolution depends on the detachment rate k_d, but not on the attachment rate.

A chain who detaches, and subsequently attaches, changes its stretch state and consequently changes its deformation energy. Since the amount of chains that in the unit time are subjected to the detachment/attachment process, for a given end-to-end vector, is $\dot{\rho}_{XL}$, the variation of the stored energy due to this process is $\dot{\rho}_{XL}\psi$ and so the internal power dissipated in the whole network can be expressed as

$$D_{XL} = \left\langle \dot{\rho}_{XL}\psi \right\rangle = -k_d \left\langle \left(\rho - \overline{\rho}_0\right)\psi \right\rangle \tag{3.24}$$

where the dissipated power D_{XL} has the physical dimensions of an energy per unit volume (in the physical space) and per unit time. The condition $D_{XL} < 0$, which means energy dissipation, is satisfied when $\dot{\rho}_{XL} < 0$ or, assuming k_d as a material constant, when $\rho > \overline{\rho}_0$.

3.2.3 CCDF evolution due to the chain's unfolding

The so-called reptation theory [45, 115] has been formulated and successfully adopted to interpret the unusual response shown by entangled polymers, enabling the correct explanation of experimental outcomes. The main idea behind this theory is to reduce the complex chains interaction to a simple snakes-like slithering of the polymer chains

through one another. It has been used as a mechanical model to explain viscous flow in amorphous polymers. Entanglement is closely related to reptation and indicates the topological restriction of molecular motion by other chains. It has been shown [91] that polymers disentangle because of correlated constraint release, which leads to a balance of internal deformation modes. Natural elastomeric proteins unfold sequentially when subject to stretching forces; this mechanism allows to a wide variety of natural materials to show high toughness, leading to an efficient shock-absorber system [32]. Upon stretching, such elastomeric proteins show a saw-tooth pattern for the force–extension curves, leading to a significant mechanical stability. Often such elastomeric-like matter refold upon stress removal and recover their initial state [39].

The same idea has been adopted here to simulate the stress relaxation in entangled polymers, in which an irreversible unfolding is assumed to occur at a rate that is related to the applied mechanical stress. The polymer is assumed to be made of entangled molecules whose physical state is characterized by a given number N_p of Kuhn's segments, while only a smaller number of segments N_0 is initially assumed to be available for the deformation process. Under a mechanical stress, the polymer chains tend to unfold at a rate proportional to the applied stress, through a viscous unfolding coefficient. This simple concept is exploited in the following to model the time-dependent mechanical model for polymer network; in some way it represents an alternative to the concept of dynamic cross-links that can be usefully adopted, beyond the effective case of polymers with an internally rearranging microstructure, to simulate the viscous response of polymers.

Let us now consider the term $\dot{\rho}_{un}$ in (3.9) which is here considered to account for two contributions to the evolution of the CCDF: the chain's unfolding and the elastic deformation of the chain's segments. The deformation of the Kuhn segments is a reversible and instantaneous phenomenon (see §2.3.3.3), while the chain's unfolding is assumed to be an irreversible and time-dependent phenomenon, since the number of segments per chains increases permanently in consequence of the applied force. In order to take into account for these effects, we modify the expression of $\dot{\mathbf{r}}$ given in (3.14) and make use of (3.13).

Firstly, we consider a one-dimensional case; we focus on a specific chain whose

end-to-end vector is r (Lagrangian approach) to obtain its time rate $\dot{r}$

$$\begin{aligned}\dot{r} = \frac{\partial}{\partial t}(\lambda r_0) = \dot{\lambda} r_0 + \lambda \dot{r}_0 = \dot{\lambda} b\sqrt{N} + \lambda \frac{\partial}{\partial t}\left(b\sqrt{N}\right) = \dot{\lambda} b\sqrt{N} + \lambda\left(\dot{b}\sqrt{N} + \frac{b}{2\sqrt{N}}\frac{\partial N}{\partial t}\right) = \\ = \lambda b\sqrt{N}\left(\frac{\dot{\lambda}}{\lambda} + \frac{\dot{b}}{b} + \frac{\dot{N}}{2N}\right)\end{aligned} \tag{3.25}$$

where λ is the applied deformation, while b and N are the current segment's length and the current number of segments, respectively, $\dot{\lambda}$ is the stretch rate, $\dot{b}$ is the segments' deformation rate and $\dot{N}$ represents the «*unfolding rate*» of the chain. It is worth mentioning that the unfolding and the segments' deformation affects only the reference mean-square distance r_0; in fact, if these two phenomena were not present ($\dot{b} = 0$ and $\dot{N} = 0$) we would have $\dot{r}_0 = 0$, $r_0 = const$ and so the end-to-end distance rate reduces to $\dot{r} = \dot{\lambda} b\sqrt{N}$. The evaluation of the unfolding rate $\dot{N}$ is discussed in §3.5, while the evaluation of $\dot{b}$ can be performed by using the Extended Freely Jointed Chain model (EFJC, sse §2.3.3.3). From the above relation, the mean-square distance evolves in time as

$$\dot{r}_0 = b\sqrt{N}\left(\frac{\dot{b}}{b} + \frac{\dot{N}}{2N}\right) \tag{3.26}$$

Let us now extend the relation (3.25) to a more general three-dimensional case

$$\begin{aligned}\dot{\mathbf{r}} = \frac{\partial}{\partial t}(\mathbf{F}\,\mathbf{r}_0) = \dot{\mathbf{F}}\,\mathbf{r}_0 + \mathbf{F}\,\dot{\mathbf{r}}_0 = \mathbf{L}\,\mathbf{F}\,\mathbf{r}_0 + \mathbf{F}\,\frac{\partial}{\partial t}\left(b\sqrt{N}\,\hat{\mathbf{r}}_0\right) = \\ = \mathbf{L}\,\mathbf{r} + \mathbf{F}\left(\frac{\partial b}{\partial t}\sqrt{N}\,\hat{\mathbf{r}}_0 + \frac{b}{2\sqrt{N}}\frac{\partial N}{\partial t}\,\hat{\mathbf{r}}_0 + b\sqrt{N}\,\frac{\partial \hat{\mathbf{r}}_0}{\partial t}\right)\end{aligned} \tag{3.27}$$

where $\hat{\mathbf{r}}_0$ is the unit vector of $\mathbf{r}_0$, so that $\mathbf{r}_0 = b\sqrt{N}\,\hat{\mathbf{r}}_0$. Again, if we assume $\dot{b} = 0$ and $\dot{N} = 0$ we recover $\dot{\mathbf{r}} = \mathbf{L}\mathbf{r}$, which is the same relation in (3.14). In the above relation, the term $\partial\hat{\mathbf{r}}_0/\partial t$ represents the time evolution of the unit vector of the chain in the reference state; we assume that the unfolding modifies only the contour length of the chain, but not its orientation in the configuration space; for that reason we assume $\partial\hat{\mathbf{r}}_0/\partial t = 0$. This assumption is supported by the fact that the chain unfolding is driven by the force acting on the chain that, being oriented as its end-to-end vector, does not promote any change of the chain orientation. Relation (3.27) can be rewritten as

$$\dot{\mathbf{r}} = \mathbf{L}\,\mathbf{r} + b\sqrt{N}\left(\frac{\dot{b}}{b} + \frac{\dot{N}}{2N}\right)\mathbf{F}\,\hat{\mathbf{r}}_0 \tag{3.28}$$

From the above relation we conclude that the reference end-to-end vector of a given chain evolves according to

$$\dot{\mathbf{r}}_0 = b\sqrt{N}\left(\frac{\dot{b}}{b} + \frac{\dot{N}}{2N}\right)\hat{\mathbf{r}}_0 \tag{3.29}$$

where N and b are the current values of the number of Kuhn segments and the segments' length, respectively. By noting that $\mathbf{F}\hat{\mathbf{r}}_0 = \mathbf{F}\mathbf{r}_0/r_0 = \mathbf{r}/r_0 = \mathbf{r}/(b\sqrt{N})$, the relation (3.28) can be rewritten as

$$\dot{\mathbf{r}} = \mathbf{L}\,\mathbf{r} + \left(\frac{\dot{b}}{b} + \frac{\dot{N}}{2N}\right)\mathbf{r} \qquad \text{or} \qquad \dot{r}_i = L_{ij}\,r_j + \left(\frac{\dot{b}}{b} + \frac{\dot{N}}{2N}\right)r_i \tag{3.30}$$

The divergence of $\dot{\mathbf{r}}$ can be obtained from the above relation as

$$\dot{r}_{i,i} = L_{ii} + 3\left(\frac{\dot{b}}{b} + \frac{\dot{N}}{2N}\right) \tag{3.31}$$

Replacing $\dot{r}_i$ and $\dot{r}_{i,i}$ in (3.13), after some calculation we obtain

$$\dot{\rho} = \underbrace{-\left(\rho_{,i}\,r_j + \rho\,\delta_{ij}\right)L_{ij}}_{\dot{\rho}_L} \underbrace{-\left(\rho_{,i}\,r_i + 3\rho\right)\left(\frac{\dot{b}}{b} + \frac{\dot{N}}{2N}\right)}_{\dot{\rho}_{un}} \tag{3.32}$$

from which the term $\dot{\rho}_{un}$ can be finally recognized to be

$$\dot{\rho}_{un} = -\left(\rho_{,i}\,r_i + 3\rho\right)\left(\frac{\dot{b}}{b} + \frac{\dot{N}}{2N}\right) \tag{3.33}$$

Interestingly, relation (3.32), accounting for the effect of the deformation and of the chains length variation, can be rewritten as

$$\dot{\rho} = -\left(\rho_{,i}\,r_j + \rho\,\delta_{ij}\right)\left[L_{ij} + \left(\frac{\dot{b}}{b} + \frac{\dot{N}}{2N}\right)\delta_{ij}\right] \tag{3.34}$$

from which we see that the effect of the chain's length variation is superimposed to the network's deformation. It is worth noting that the quantity $\dot{b}/b$ can be neglected if compared to $\dot{N}/N$, since the deformation of the segments depends on atomic bonds, while the unfolding depends on the chains entanglement [102].

3.2.4 CCDF evolution due to failure of chains

The conservation of the chain density is expressed, in the Eulerian approach, through eq. (3.12) as $\dot{\rho} + \mathrm{div}(\rho\dot{\mathbf{r}}) = 0$, in which $\mathrm{div}(\rho\dot{\mathbf{r}})$ physically represents the flow density through a given point in the configuration space. It is possible to take into account for the chains failure by modifying the continuity equation as follows

$$\frac{\partial\rho}{\partial t} = -\mathrm{div}(\rho\dot{\mathbf{r}}) - \omega_f\,\rho \tag{3.35}$$

where $\omega_f : \Omega \to \mathbb{R} \mid \omega_f = \omega_f(\mathbf{r})$ represents the failure rate, i.e. the number of chains per unit volume which fails in the unit time. The expression (3.35) can be recovered, in the Lagrangian approach, by writing the material time derivative of the number of chains contained in an arbitrary subset $\Omega^* \subseteq \Omega$ as

$$\frac{d}{dt}\int_{\Omega^*} \rho \, d\Omega = \int_{\Omega^*} \omega_f \rho \, d\Omega \tag{3.36}$$

and subsequently by using the Reynold's transport theorem (3.10). Finally, the term $\dot{\rho}_f$ in (3.9) can be written, by using (3.35), as

$$\dot{\rho}_f = -\omega_f \rho \tag{3.37}$$

Such a formulation implies a loss of material, leading to a reduction of the bearing capacity of the network. The damage level of the polymer can be measured through the quantity $\mathscr{D}$ defined as

$$\mathscr{D} = 1 - \langle \varphi \rangle \tag{3.38}$$

being $0 \leq \mathscr{D} \leq 1$, with $\mathscr{D} = 0$ for an undamaged polymer and $\mathscr{D} = 1$ for a fully damaged polymer.

3.2.5 CCDF evolution law accounting for all the contributions

Finally we can write explicitly the evolution law (3.9) by using the contributions derived in the previous sections; the final expression reads

$$\dot{\rho} = \underbrace{-\left(\rho_{,i}\, r_j + \rho\, \delta_{ij}\right) L_{ij}}_{\dot{\rho}_L} \underbrace{-k_d \left(\rho - \overline{\rho}_0\right)}_{\dot{\rho}_{XL}} \underbrace{-\left(\rho_{,i}\, r_i + 3\rho\right)\left(\frac{\dot{b}}{b} + \frac{\dot{N}}{2N}\right)}_{\dot{\rho}_{un}} \underbrace{-\omega_f \rho}_{\dot{\rho}_f} \tag{3.39}$$

with the initial condition $\rho(\mathbf{r}, t = 0) = \overline{\rho}_0(\mathbf{r})$, being $\overline{\rho}_0$ the Gaussian function given in (3.7).

It is worth mentioning that the above relation is valid for any polymer, since no hypothesis on the material characteristics have been assumed until now for its derivation. To specify the above relation for a particular polymer, it is necessary to define the proper constitutive models for k_d, which rules the dynamic cross-linking process, for $\dot{b}$, which defines the enthalpic contribution to the deformation energy, for $\dot{N}$, which rules the unfolding mechanism and for ω_f, which rules the damage process.

In the present work, we assume k_d as a constant material parameter, while other Authors have found that it depends on the chain force [149]. Furthermore, we neglect

the term $\dot{b}/b$ with respect to $\dot{N}/N$. A model for the unfolding rate $\dot{N}$ is discussed in §3.5, while the constitutive model for ω_f is discussed in §3.6.

As a final observation, we can prove a particular feature of the CCDF; let us suppose that, at a certain time instant, the CCDF has a central symmetry with respect to the origin of the configuration space, i.e. $\rho(-\mathbf{r},t)=\rho(\mathbf{r},t)$; then, from that moment on, the CCDF remains central-symmetric. In fact, if the CCDF is central-symmetric, its time derivative is also central-symmetric, since

$$\begin{aligned}\dot{\rho}(-\mathbf{r},t) = &-k_d\left(\rho(-\mathbf{r})-\overline{\rho}_0(-\mathbf{r})\right)- \\ &-\left(-\rho_{,i}(-\mathbf{r},t)\,r_j+\rho(-\mathbf{r},t)\,\delta_{ij}\right)\left[L_{ij}+\left(\frac{\dot{b}}{b}+\frac{\dot{N}}{2N}\right)\delta_{ij}\right]-\omega_f\rho(-\mathbf{r},t)=\dot{\rho}(\mathbf{r},t)\end{aligned} \tag{3.40}$$

being $\rho(-\mathbf{r},t)=\rho(\mathbf{r},t)$ by assumption and $\rho_{,i}(-\mathbf{r},t)=-\rho_{,i}(\mathbf{r},t)$ [1], so that $\dot{\rho}(-\mathbf{r},t)=\dot{\rho}(\mathbf{r},t)$. Since $\dot{\rho}$ is central-symmetric, then ρ remains so even after the time increment dt. Since we assume that for $t=0$ the distribution is central-symmetric (i.e. the Gaussian (3.7)), then the CCDF is always central-symmetric.

3.3 Derivation of stress

Let us complete the constitutive model by deriving the stress tensor from the free energy. The second principle of thermodynamics states that, for an isothermal process, the dissipated power D is the difference between the deformation power and the internal power [148], i.e.

$$D=\dot{\Psi}-\boldsymbol{\sigma}:\mathbf{L}\geq 0 \tag{3.41}$$

where the energy dissipation must be positive to ensure the thermodynamic consistency.

In §3.1 we have obtained the internal energy of the network as $\Psi=\left\langle\left(\rho-\rho_0\right)\psi\right\rangle$ with the fundamental assumption of dealing with conservative forces only. On the other hand, in § 3.2 we have introduced non-conservative actions in the network, since the

[1] This statement can be easily proved by evaluating the derivatives of ρ in a generic point of the configuration space with coordinates $(-r_x,-r_y,-r_z)$. By considering, for instance, the derivative w.r.t. r_x, one can obtain

$$\begin{aligned}\frac{\partial\rho}{\partial r_x}(-r_x,-r_y,-r_z,t) &= \lim_{h\to 0}\frac{\rho(-(r_x+h),-r_y,-r_z,t)-\rho(-r_x,-r_y,-r_z,t)}{h}= \\ &= \lim_{h\to 0}\frac{\rho(r_x+h,r_y,r_z,t)-\rho(r_x,r_y,r_z,t)}{h}=\frac{\partial\rho}{\partial r_x}(r_x,r_y,r_z,t)\end{aligned}$$

where the second equality arises from the assumption $\rho(-\mathbf{r},t)=\rho(\mathbf{r})$.

presence of dynamic cross-links, chains unfolding and failure imply a loss of energy. The use of the above mentioned expression, even in presence of non-conservative forces, is desirable for its simplicity, but needs a further justification.

Let us firstly consider the simplest case of no energy dissipation. In the Eulerian approach, the free energy of a single chain, ψ, is a spatial quantity, so it does not depend on time, while the CCDF evolves in time only with the applied deformation, according to (3.15). Then, the internal power can be written as $\dot{\Psi} = \langle (\dot{\rho} - \dot{\rho}_0)\,\psi \rangle = \langle \dot{\rho}\psi \rangle - \langle \dot{\rho}_0 \psi \rangle$, where $\dot{\rho}_0 = \dot{\rho}(t=0)$ is the initial value of the CCDF rate. Using (3.15)

$$\langle \dot{\rho}\,\psi \rangle = -\langle (\rho_{,i}\, r_j + \rho\,\delta_{ij})\,\psi \rangle L_{ij} \tag{3.42}$$

integrating by parts the first term on the right hand side we get

$$\langle \dot{\rho}\,\psi \rangle = -\left[\cancel{\langle \rho\, r_j\, \psi \rangle_\partial} - \left\langle \rho\, \frac{\partial (r_j\,\psi)}{\partial r_i} \right\rangle + \langle \rho\,\delta_{ij}\,\psi \rangle \right] L_{ij} \tag{3.43}$$

being $\langle \rho\, r_j\, \psi \rangle_\partial = 0$ since the CCDF is always zero on the boundary of the configuration space. Furthermore, by developing the derivative w.r.t. r_i we have

$$\langle \dot{\rho}\,\psi \rangle = -\left[-\cancel{\langle \rho\,\delta_{ij}\,\psi \rangle} - \langle \rho\, r_j\, \psi_{,i} \rangle + \cancel{\langle \rho\,\delta_{ij}\,\psi \rangle} \right] L_{ij} = \langle \rho\, f_i\, r_j \rangle L_{ij} \tag{3.44}$$

where we have considered that $\psi_{,i}$ provides the chain's force f_i. The above derivation can be repeated by using ρ_0 instead of ρ. The final expression of the internal power becomes

$$\dot{\Psi} = \langle \dot{\rho}\psi \rangle - \langle \dot{\rho}_0 \psi \rangle = \langle \rho\, \mathbf{f} \otimes \mathbf{r} \rangle : \mathbf{L} - \langle \rho_0\, \mathbf{f} \otimes \mathbf{r} \rangle : \mathbf{L} = \langle (\rho - \rho_0)\, \mathbf{f} \otimes \mathbf{r} \rangle : \mathbf{L} \tag{3.45}$$

In absence of dissipation, the thermodynamic condition (3.41) reduces to $\dot{\Psi} = \boldsymbol{\sigma} : \mathbf{L}$, since $\mathbf{L}$ is the measure of strain rate work-conjugate with the Cauchy stress; by comparing with the above relation, the stress results to be

$$\boldsymbol{\sigma} = \langle (\rho - \rho_0)\, \mathbf{f} \otimes \mathbf{r} \rangle \tag{3.46}$$

Interestingly, the same conclusion can be recovered by applying the time derivative to the chain's energy, instead of to the CCDF

$$\dot{\Psi} = \langle (\rho - \rho_0)\, \dot{\psi} \rangle = \left\langle (\rho - \rho_0)\, \frac{\partial \psi}{\partial r_i} \frac{\partial r_i}{\partial t} \right\rangle = \langle (\rho - \rho_0)\, f_i\, L_{ij}\, r_j \rangle = \langle (\rho - \rho_0)\, f_i\, r_j \rangle L_{ij} \tag{3.47}$$

even if the quantity $\langle (\rho - \rho_0)\,\dot{\psi} \rangle$ does not have a clear physical meaning.

Let us now consider the presence of both conservative and non-conservative forces. When the body is stretch-free ($\mathbf{F} = \mathbf{I}$), the energy stored in the material is equal to $\overline{\mathscr{E}}_0$; after the application of the stretch λ, the stored energy becomes $\mathscr{E} = \overline{\mathscr{E}}_0 + \mathscr{E}_{el}$, where $\mathscr{E}_{el}$ is the elastic (reversible) energy, corresponding to the difference between the final and initial energy $\mathscr{E} - \overline{\mathscr{E}}_0 = \mathscr{E}_{el}$. If the material loses the energy $\mathscr{E}_d$ because of dissipative effects, the final stored energy is $\mathscr{E} = \overline{\mathscr{E}}_0 + \mathscr{E}_{el} - \mathscr{E}_d$, so that the difference between final and the initial energy is $\mathscr{E} - \left(\overline{\mathscr{E}}_0 - \mathscr{E}_d\right) = \mathscr{E}_{el}$. By comparing these two expressions we can note that the effect of the energy dissipation can be included in the initial energy, which can be rewritten as the difference between the initial and the dissipated energy as $\mathscr{E}_0(t) = \overline{\mathscr{E}}_0 - \mathscr{E}_d(t)$.

In the case of a polymer network, the stored energy is $\mathscr{E} = \langle \rho\, \psi \rangle$, the initially stored energy is $\overline{\mathscr{E}}_0 = \langle \overline{\rho}_0\, \psi \rangle$, the elastic energy is $\mathscr{E}_{el} = \int_0^t \boldsymbol{\sigma} : \mathbf{L}\, dt$ and the dissipated energy is $\mathscr{E}_d = \int_0^t D\, dt$, so that

$$\langle \rho\, \psi \rangle = \langle \overline{\rho}_0\, \psi \rangle + \int_0^t \boldsymbol{\sigma} : \mathbf{L}\, dt - \int_0^t D\, dt \tag{3.48}$$

If we write the dissipation in the form $D = \langle \dot{\rho}_d\, \psi \rangle$, in which ρ_d can be interpreted as a «chain density loss», we can rewrite (3.48) as

$$\left\langle \left[\rho - \left(\overline{\rho}_0 - \int_0^t \dot{\rho}_d\, dt \right) \right] \psi \right\rangle = \int_0^t \boldsymbol{\sigma} : \mathbf{L}\, dt \tag{3.49}$$

from which it appears clearly that the effect of the non-conservative forces is to modify the reference CCDF from the initial Gaussian distribution $\overline{\rho}_0$ to the one corresponding to the current state ρ_0

$$\rho_0 = \overline{\rho}_0 - \int_0^t \dot{\rho}_d\, dt \tag{3.50}$$

We can easily evaluate the *current reference* CCDF ρ_0 at time t by locking all the non-conservative contributions, and subtracting the elastic energy from $\langle \rho\, \psi \rangle$ by mapping $\mathbf{r}$ into $\mathbf{F}\,\mathbf{r}$ (as recalled in §3.1.2), so that

$$\rho_0(\mathbf{r}) = \rho(\mathbf{F}\,\mathbf{r}) \tag{3.51}$$

We use the expression «current reference configuration» to highlight the fact that the initial (reference) configuration must be updated with the non-conservative effects.

3.4 Full-network model

Relation (3.8) can be regarded as a generalization of the so-called *full-network model*. Such a model was suggested by Thomas [138], that determined the free energy of a

monodisperse polymer by assuming the chains to be randomly oriented in the space. Treloar and Riding [146] developed a bi-dimensional full network using Langevin statistic. Wu and van der Giessen [156] proposed a three-dimensional full network model for a monodisperse polymer with Langevin statistic; they defined the distribution of the chains orientation as a function $C(\theta,\omega,\lambda_i)$, depending on the two orientation angles θ and ω and on the principal macroscopic stretches λ_i. The plot of the chain orientation function C in two orthogonal planes, for three different deformations, is illustrated in fig. 3.1. In the stretch free state ($\lambda_1 = \lambda_2 = \lambda_3 = 1$) the function C is greater than zero and it has spherical symmetry. The function C increases with the stretch along the deformation directions, since the chains are preferentially oriented in the loading direction. They obtained the free energy of the network by using the affine deformation assumption and by integrating the energy of the chains over all the possible orientations:

$$\Psi = n\int_0^{\pi}\int_0^{2\pi} \psi C(\theta,\omega,\lambda_i)\sin\theta d\theta d\omega \tag{3.52}$$

Exploiting the spherical chains arrangement, the authors found that the distribution of the orientations depends on the macroscopic stretches λ_i

$$C(\theta,\omega;\lambda_i) = \frac{1}{4\pi}\lambda^3(\theta,\omega;\lambda_i) \qquad \lambda = \left(\sum_i \frac{m_i^2}{\lambda_i^2}\right)^{-1/2} \tag{3.53}$$

where $\lambda(\theta,\omega;\lambda_i)$ is the chain stretch, for a given set of external stretches λ_i, of a chain whose current orientation is defined by θ and ω, while m_i are the components of the unit vector $\mathbf{r}/\|\mathbf{r}\|$.

The Authors provided an expression of the principal Cauchy stresses through the equation [156]

$$\sigma_i = \frac{1}{4\pi} n k_B T\sqrt{N}\int_0^{\pi}\int_0^{2\pi} \mathscr{L}^{-1}\left(\frac{\lambda}{\sqrt{N}}\right)\lambda^4 m_i^2 \sin\theta d\theta d\omega - p \tag{3.54}$$

where p is the unknown pressure that enforce the incompressibility constraint. Once the principal stresses are known, the stress tensor is expressed as $\boldsymbol{\sigma} = \sum_i \sigma_i(\mathbf{e}_i \otimes \mathbf{e}_i)$, where $\mathbf{e}_i$ are the principal axis of the Eulerian triad.

By comparing (3.52) with (3.8), is appears that the model proposed by Wu and van der Giessen does not take into account for the distribution of the chain density along r; furthermore, they considered such a distribution as a mere consequence of

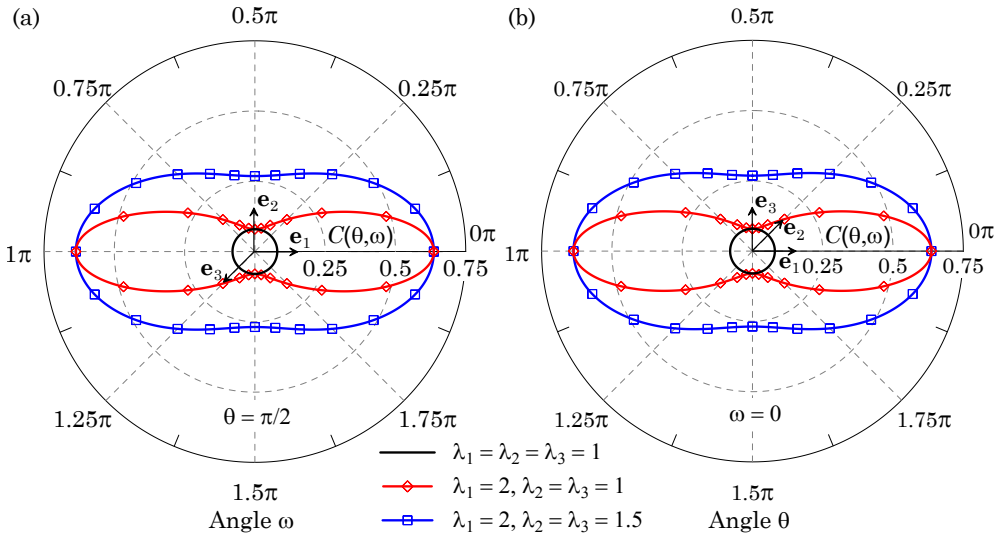

Figure 3.1: *Chain orientation distribution function C (see [156]) vs. orientation angles ω and θ. Plot of C vs. ω in the plane* $\mathbf{e}_1 - \mathbf{e}_2$ *(a) and C vs. θ in the plane* $\mathbf{e}_2 - \mathbf{e}_3$ *(b).*

the spherical geometry. Finally, the network is assumed to be perfectly elastic and the distribution function changes only in response to external deformations.

As the author pointed out, the full network can be seen as a generalization of the 3-chains and 8-chains models. These two latter models can be recovered by using an orientation function allowing to account for preferential directions. Their work were reviewed and compared by other models (3,4,8-chains) by Beatty [9] and used by Puso [121]. A full network scheme were adopted by Miehe et al. [107] with a non-affine deformation assumption. Subsequently, the full network model was extended by Verron and Gros [150] and by Itskov and Knyazeva [74] to the case of polydispersed polymers. Tehrani and Sarvestani [137] used it for polydispersed polymers by accounting for the Eyring-like bond rupture.

3.5 Unfolding rate

In this section we propose a model for the unfolding rate $\dot{N}$ (see §3.2.3). Let us consider a particular chain of the network, having in the reference state N_0 Kuhn segments

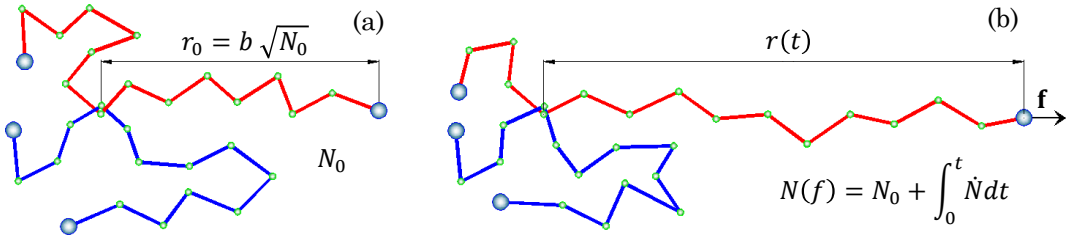

Figure 3.2: *Scheme of the chain's unfolding under an applied stretch starting from the initial state (a) to a generic one (b). The unfolding mechanism ends when the number of Kuhn segments reaches the maximum physical chain length* N_p.

available to deform, while its physical length (maximum number of Kuhn segments that can take part of the deformation) is $N_p \geq N_0$. The remaining $N_p - N_0$ Kuhn segments are entangled with others chains, so they are not initially available to take part to the deformation process (fig. 3.2).

Upon stretching, the chain portion available to deform starts to elongate (fig. 3.2(b)); because of the chain force increases, it is reasonable to assume that such a force triggers the chain unfolding, i.e. a fraction of the previously unavailable segments enters into the deformation process. In general, at a generic time instant, the full chain length has still to be attained, since the chain has not completely deployed until the maximum number of segments N_p has been made available to deform.

We assume that, for a given chain, its number of segments increases in time since the chain undergoes a force greater than that existing in the reference state. In particular, because of the unfolding of the polymer segments during the deformation process, the actual effective length $N(t)$ of the chain whose end-to-end vector is $\mathbf{r}$ (i.e. the number of segments available to deform) can be assumed to fall within the range $N_0 \leq N(t) \leq N_p$ (fig. 3.2(b)), i.e. the current chain length is greater than the initial one and less than the physical length N_p of the polymer chain in turn; the ratio

$$0 \leq e_p(t) = 1 - \frac{N(t) - N_0}{N_p - N_0} \leq 1 \tag{3.55}$$

can be assumed as a measure of the entanglement degree of the chain: $e_p = 1$ indicates a fully entangled chain, while $e_p = 0$ corresponds to the chain with the minimum entanglement degree, corresponding to a completely unfolded state.

Let us consider all the chains with end-to-end vector $\mathbf{r}$; during the deformation

process the contribution of that chain to the whole stress can be expressed as

$$\mathbf{s} = (\rho - \rho_0)\,\mathbf{f} \otimes \mathbf{r} \tag{3.56}$$

being $\boldsymbol{\sigma} = \langle \mathbf{s} \rangle$ from (3.46). Since the chains are oriented in every direction of the configuration space, the hydrostatic part of $\mathbf{s}$, i.e. $\mathrm{tr}(\mathbf{s})/3$, can be assumed to be the cause of the segments unfolding. The governing law for such an unfolding mechanism can be assumed to obey to a Maxwell-like relationship law in the form

$$\dot{N}(t) = \frac{N_p - N(t)}{\eta} \cdot \frac{\mathrm{tr}(\mathbf{s})}{3} \tag{3.57}$$

where η is a viscous-like parameter governing the unfolding rate. Since the chain force is coaxial with $\mathbf{r}$, we can write $\mathbf{f} = f\,\hat{\mathbf{r}}$ (see eq. (3.3)), thus the trace of $\mathbf{s}$ can be rewritten $\mathrm{tr}(\mathbf{s}) = (\rho - \rho_0) f r\, \mathrm{tr}(\hat{\mathbf{r}} \otimes \hat{\mathbf{r}})$. Moreover, being $\mathrm{tr}(\hat{\mathbf{r}} \otimes \hat{\mathbf{r}}) = 1$, we obtain $\mathrm{tr}(\mathbf{s}) = (\rho - \rho_0) f r$, then we can rewrite the evolution law (3.57) as

$$\dot{N}(t) = \frac{N_p - N(t)}{\eta} \cdot \frac{(\rho - \rho_0) f r}{3} \tag{3.58}$$

The proposed model is illustrated in fig. 3.3 where some polymer-related quantities vs. the applied stretch are displayed for a simple case by varying η. An increasing monotonic stretch starting from $\lambda = 1$ up to $\lambda = 4$ is assumed to be applied to the material in the time interval $t \in [0, t_{max}]$. It can be appreciated that the viscosity parameter η plays a key role in the mechanics of polymer unfolding: in fact, low values of the viscosity promote the unfolding mechanism, while high values induces the chain to maintain its initial number of Kuhn segments (N_0). The entanglement degree, defined according to (3.55), starts from unity and tends to zero as the unfolding proceeds (fig. 3.3(a)), meanwhile the chain force shows a transition behavior, changing from an initial increasing trend for moderate unfolding, to a decreasing phase when the disentanglement is more pronounced; finally it starts to increase again when the unfolding is almost complete, i.e. when N approaches the physical length of the polymer N_p (fig. 3.3(b)). In fig. 3.3(c) the current number of segments available to deform divided by the maximum number of segments of the chain, N/N_p, is displayed, while in fig. 3.3(d) the unfolding rate vs the applied stretch is illustrated; as far as $\dot{N}$ is concerned, it can be observed that it starts from zero at the beginning of the deformation process, reaches a maximum and then tends to zero as $N \to N_p$.

The effect of the strain rate on the mechanical response can be appreciated in fig. 3.4, where the chain force vs. stretch is shown by changing the time required to reach

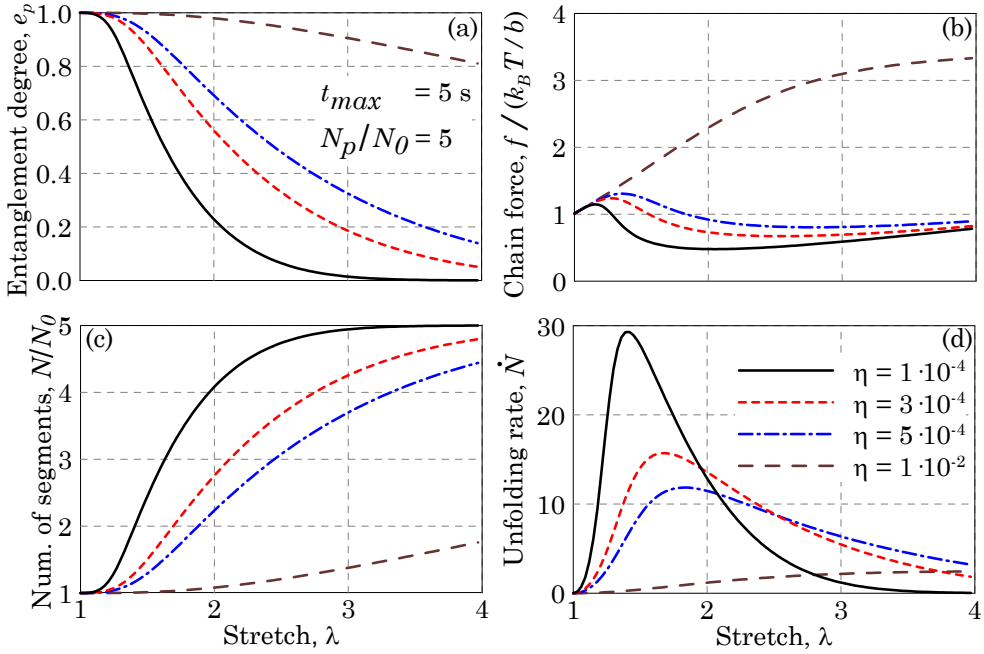

Figure 3.3: *Stretching of a folded chain. Entanglement degree vs. applied stretch λ for four polymers with different values of the unfolding viscosity parameter η (a). Chain force vs. λ (b), ratio between current and initial number of segments vs. λ (c) and unfolding rate vs. λ (d). In the present case the initial and maximum number of Kuhn segments have been assumed equal to $N_0 = 10$ and $N_p = 50$, respectively.*

the maximum deformation, t_{max}. Lower strain rates (fig. 3.4(a)) allow the chains to unfold more easily, leading to lower value of the chain force; on the other hand, by adopting a higher strain rate, the response is much more rigid, since the chains have not enough time to unfold (fig. 3.4(b)).

3.6 Failure rate of the polymer chains

In this section we formulate a model for the failure rate ω_f. The kinetic of bonds rupture can be modeled with the reaction rate theory of Eyring [36, 61, 128]. The number of chains with N segments and separation $\mathbf{r}$ that fails in the unit time, can be

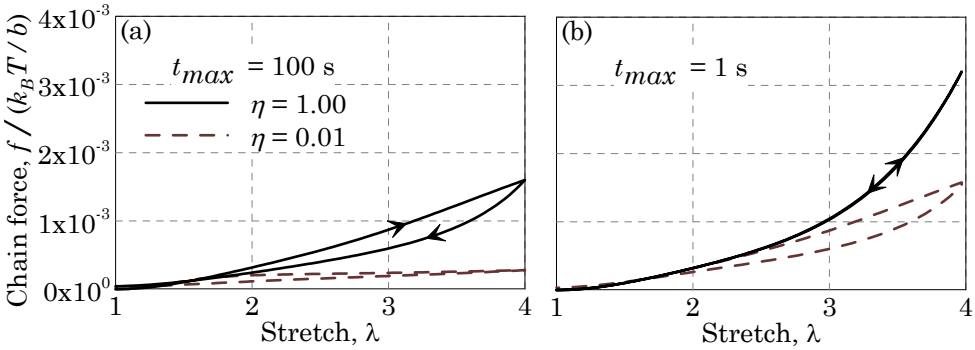

Figure 3.4: *Chain force vs. λ for two different values of the viscosity-like parameter η and a strain rate equal to $\dot{\lambda} = 0.03\ s^{-1}$ (a) and $\dot{\lambda} = 3\ s^{-1}$ (b).*

evaluated through the statistical thermal fluctuations of the energy as [93]

$$\omega_f = \frac{N}{\tau} \exp\left(\frac{w}{k_B T}\right) \tag{3.59}$$

where w is the work done the by the chain force and τ a characteristic time. Following [102], w can be identified with the enthalpic part of the chain's free energy (see §2.3.3.3), so that $w = \psi_b$, with ψ_b defined in (2.37). The characteristic time τ can be expressed as [72]

$$\tau = \frac{h}{k_B T} \exp\left(\frac{\overline{w}}{k_B T}\right) \tag{3.60}$$

where h is the Planck's constant ($h = 6.626 \cdot 10^{-34}$ Js) and $\overline{w}$ is the bond's strength expressed in term of energy. With such a definition of τ, the failure rate becomes

$$\omega_f = \frac{k_B T}{h} N \exp\left(\frac{\psi_b - \overline{w}}{k_B T}\right) \tag{3.61}$$

The failure rate can be interpreted as the probability of chains to break, evaluated on the basis of the chain's stored energy. It is worth noting that it is proportional to N since the rupture of a single segment entails the failure of the whole chain.

3.7 Parametric tests

In the present section we use the above described model by simulating some simple cases. In order to show separately the effects of each considered phenomenon, we activate one contribution at a time. We consider a representative elementary volume of an

incompressible polymer subjected to a uniaxial stretch. The tests are performed on such a sample by controlling the three principal stretches, whose values - according to the incompressibility condition - are $\lambda_1 = \lambda$, $\lambda_2 = \lambda_3 = \lambda^{-1/2}$. Once the body's deformations are known, the evolution of the CCDF is evaluated by using eq. (3.39) and the corresponding reference CCDF ρ_0 is evaluated by using eq. (3.51). Then, eq. (3.46) provides the stress tensor $\boldsymbol{\sigma}$, which must be corrected by applying the hydrostatic pressure p in order to ensure the incompressibility of the material; the unknown pressure is evaluated from the boundary condition $\sigma_2 = \sigma_3 = 0$, which leads to $p = -\sigma_2 = -\sigma_3$. For the details of the numerical integration in the configuration space we refer to chapter 5.

The effects of the applied deformation, without other phenomena involved, are shown in §3.7.1, while the effects of the dynamic cross-links are tested in §3.7.2, the effects of the unfolding mechanism in §3.7.3 and the effects of the chains failure in §3.7.4.

The values of the parameters adopted for the simulations are the same for all the cases, except when differently indicated. The assumed polymer is made of a single network with $N = 50$, with shear modulus equal to $\mu = 1$ MPa, while the length of each chain segments is $b = 1$ nm and the temperature is $T = 300$ K.

3.7.1 Purely elastic polymer

In the first case we evaluate the stress arising in the polymer because of the elastic deformation of the network, which is governed by the affine deformation assumption.

The stress vs. stretch curves of two different polymers, characterized by $N = 20$ and $N = 50$, respectively, are illustrated in fig. 3.5. The stress is evaluated by using two different models for the chain energy ψ, i.e. the formulation based on the Gaussian (2.27) and the Langevin (2.32) statistic. The polymer with the shortest chains ($N = 20$) appears to be more stiff than the one with the longest chains ($N = 50$). Moreover, the curves obtained with the Gaussian statistic are closer to the corresponding curves based on the Langevin formulation for the polymer with $N = 50$ than for the polymer with $N = 20$; this result can be justified by the fact that the polymer with $N = 20$ is influenced by the nonlinear terms of the force vs. extension curve of the Langevin model for lower deformation level than the polymer with $N = 50$.

The CCDF φ of the two considered polymers is depicted in fig. 3.6 for the same deformation level $\lambda = 3.5$. The CCDF in the plane $r_z = 0$ of the configuration space, i.e. the function $\varphi = \varphi(r_x, r_y, 0)$, is illustrated through the contour plot of fig. 3.5(a)

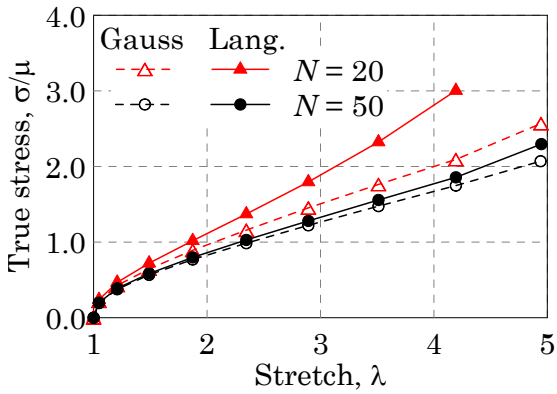

Figure 3.5: *Stress vs. stretch curves evaluated with the Gaussian and the Langevin statistic for two polymers, characterized by* $N = 20$ *and* $N = 50$*, respectively.*

for the polymer with $N = 50$ and in fig. 3.5(b) for the polymer with $N = 20$. In both cases, the density function is not isotropic but it is deformed along the direction of the applied external deformation, in accordance with the affine deformation assumption, since we assume that the reference system of the configuration space is parallel to that of the physical space. The CCDF along the deformation direction, i.e. the function $\varphi = \varphi(r_x, 0, 0)$, is plotted, with the corresponding reference CCDF φ_0, in fig. 3.6(c) and 3.6(d) for the polymer with $N = 50$ and $N = 20$, respectively. The distribution for the polymer with $N = 50$ (fig. 3.6(c) and (e)) appears to be more disperse than the one for the polymer with $N = 20$ (fig. 3.6(d) and (f)). Along the x-direction (fig. 3.6(c) and (d)), the distribution φ is always greater than the distribution φ_0, while along the y-direction (fig. 3.6(e) and (f)) the distribution φ is lower than φ_0. As previously noted (see §3.2.1) the value of φ in the origin of the configuration space does not change during the deformation process, i.e. $\varphi(\mathbf{r} = \mathbf{0}) = \varphi_0(\mathbf{r} = \mathbf{0})$.

3.7.2 Polymer with dynamic cross-links

Let us now consider a representative volume of a polymer whose chains can attach and detach dynamically in time. We assume that the total number of chains remains constant, that is to say the polymer has reached a steady state condition before the application of the load (see §3.2.2). The stress vs. time curves of a polymer characterized

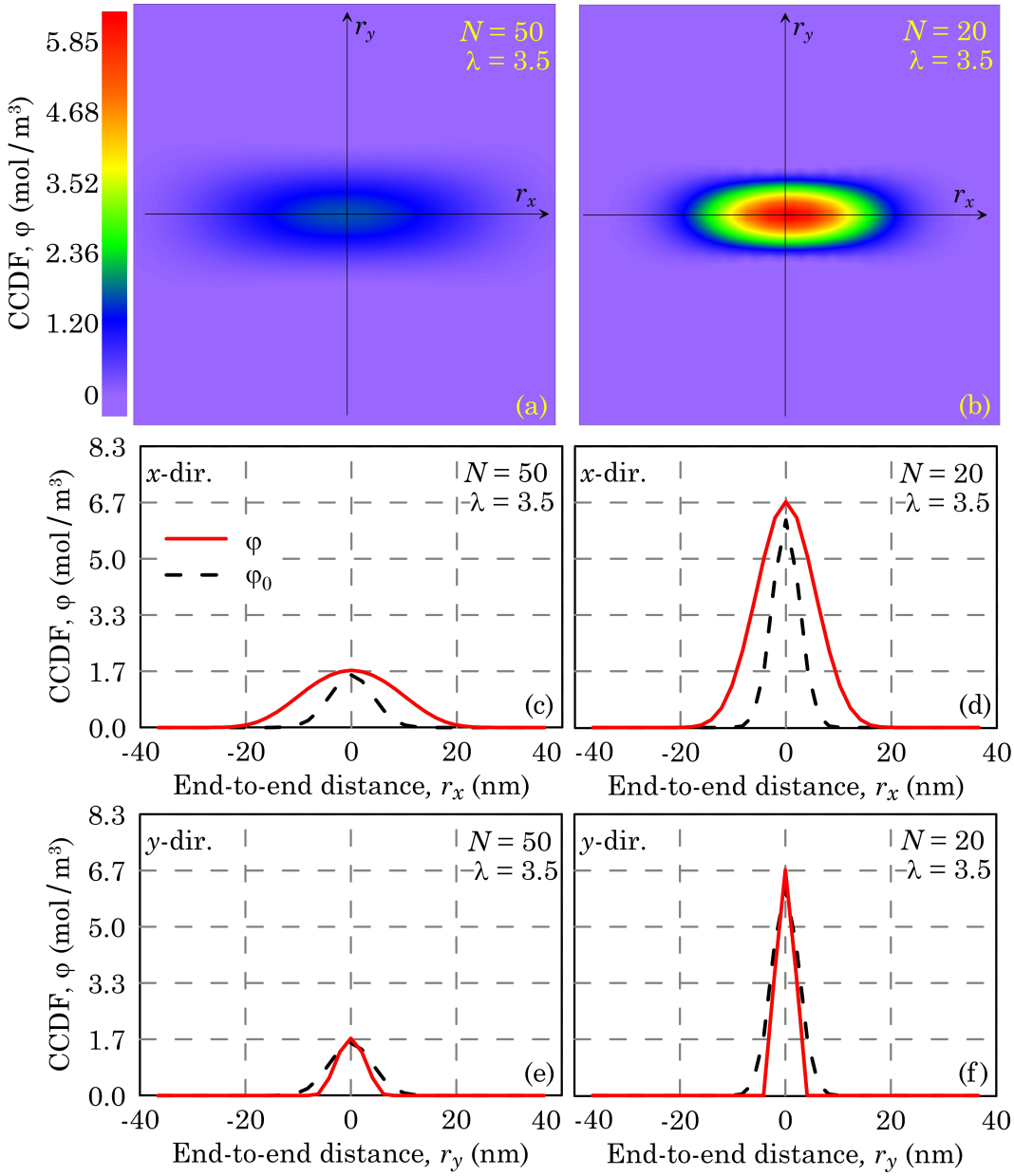

Figure 3.6: *CCDF of the two considered polymers ($N = 50$ and $N = 20$) for the stretch $\lambda = 3.5$. Contour plot of the CCDF in the plane $r_z = 0$ for the polymer with $N = 50$ (a) and for the polymer with $N = 20$ (b); plot of the CCDF along the stretching direction for the polymer with $N = 50$ (c) and $N = 20$ (d); plot of the CCDF along the direction normal to the applied stretch for the polymer with $N = 50$ (e) and $N = 20$ (f).*

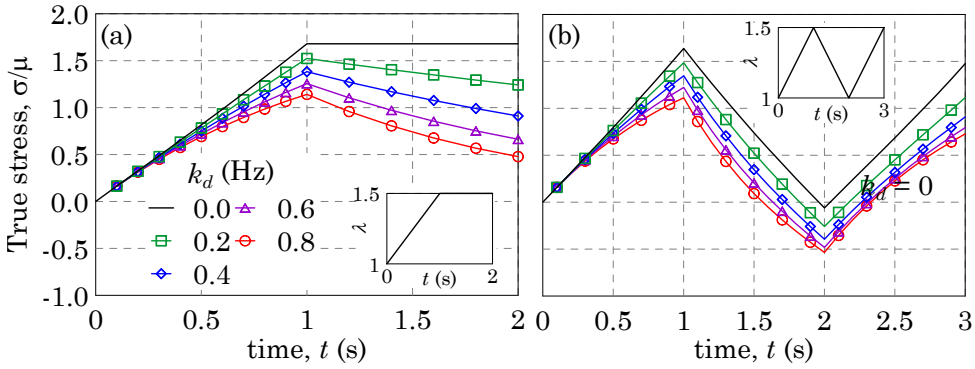

Figure 3.7: *Stress vs. time curves of polymers characterized by different values of the detachment rate k_d compared with the elastic response ($k_d = 0$). Monotonic stretch history with a final constant part (a) and cyclic stretch history (b).*

by $N = 50$, for two different load histories and different values of the detachment rate k_d, are illustrated in fig. 3.7.

In the case reported in fig. 3.7(a), for $0 < t < 1$ s, the stretch increases linearly from $\lambda = 1$ up to $\lambda = 1.5$, then it is kept constant at $\lambda = 1.5$ when $1 < t < 2$ s. The stress vs. time curve relative to the case of no dynamic cross-links (i.e. $k_d = 0$) corresponds to the purely elastic response of the material. As expected, by increasing the detachment rate ($k_d = 0.2, 0.4, 0.6, 0.8$ Hz, respectively), the dynamic cross-links mechanism increases its effectiveness in inducing the stress relaxation of the material, which quicker tends to return to the stress-free state.

In the case reported in fig. 3.7(b), the deformation history is composed of three parts: in the first one ($0 < t < 1$ s) the stretch increases linearly from $\lambda = 1$ to $\lambda = 1.5$, then ($1 < t < 2$ s) the stretch goes back to $\lambda = 1$ and in the third one ($2 < t < 3$ s) the stretch increases again up to $\lambda = 1.5$. Again, the elastic response ($k_d = 0$) is compared to the relaxing behavior induced by the dynamic cross-links, for different values of the deactivation rate k_d. At the end of the second part of the stretch history, when the applied stretch is near to 1, the corresponding stretch results to be negative for all the considered cases, except for the elastic one; furthermore, the compression stress increases as the deactivation rate increases. This behavior is justified by the fact that the network, under the effect of the dynamic cross-links, rearrange its structure and

tends to the stress-free CCDF; as a result, after the application of a stretch, it is necessary to compress the polymer to recover the initial shape of the sample. This aspect underlines the difficulties in defining a proper reference configuration for the polymer, since such a configuration evolves in time. It is worth mentioning that the assumed values of the detachment rate k_d have been chosen according to the adopted time scale, i.e. the characteristic time of the detachment rate should be comparable to the physical stretching time interval.

3.7.3 Effects of chains unfolding

Let us now consider the effect of the unfolding mechanism on the constitutive response of a representative volume of polymer. According to (3.57), the unfolding process is governed by three parameters: the number of segments per chain in the folded (N_0) and fully unfolded (N_p) state and the viscosity-like parameter η, which rules the unfolding rate.

We consider, again, a representative elementary volume of an incompressible polymer subjected to uniaxial stretch. The stress vs. stretch curves of a polymer with $N_0 = 50$ and $N_p = 70$ are reported in fig. 3.8(a). Two different values of the unfolding viscosity η are considered ($\eta = 1$ kPa·s and $\eta = 5$ kPa·s). The responses of such materials are compared with the behaviors of two purely elastic polymers (i.e. without unfolding), with $N = 50$ and $N = 70$, respectively. For a given value of the stretch, the corresponding stress decreases by reducing the unfolding viscosity, since a faster unfolding implies a reduction of the chains stretch.

The curves related to the polymers subjected to the unfolding process are, for small stretch, close to response of the purely elastic polymer with $N = 50$; by increasing the stretch, the response of the polymer with the lowest viscosity ($\eta = 1$ kPa·s) starts to deviate from the elastic behavior, followed, for larger stretch, by the curve of the polymer with the highest viscosity ($\eta = 5$ kPa·s), which, nevertheless, remains close to the elastic curve with $N = 50$. By increasing again the stretch, the two curves tend to the response of the purely elastic polymer with $N = 70$. The two elastic behaviors can be considered as limit curves, since the polymer subjected to unfolding can reproduce the elastic curve with $N = 50$ when $\eta \to \infty$, while it can reproduce the curve with $N = 70$ when $\eta \to 0$. Moreover, the unfolding mechanism moves the limit stretch of a given chain from $\sqrt{N_0}$ to $\sqrt{N_p} > \sqrt{N_0}$.

The stress vs. stretch curves of a polymer, characterized by different values of the

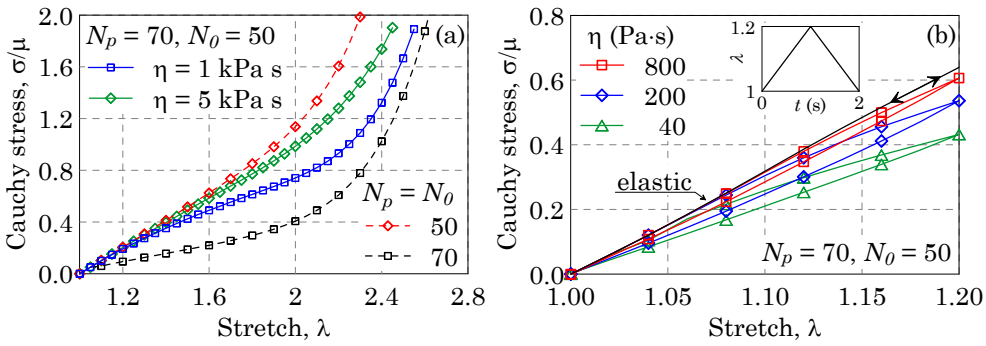

Figure 3.8: *Stress vs. stretch curves of networks with different values of the unfolding viscosity parameter η compared to the response of an elastic network: monotonic stretch history (a) and cyclic stretch history (b).*

unfolding viscosity and subjected to a stretch cycle, are reported in fig. 3.8(b). The load cycle is composed of two part, as shown in the insert of fig. 3.8(b); in the first one, the applied stretch increases linearly from 1 to 1.2 in 1 s, while in the second one it goes back linearly from 1.2 to 1 in 1 s. The polymer is characterized by $N_0 = 50$ and $N_p = 70$, while three different values of the unfolding viscosity are tested, i.e. $\eta = 40$, 200, 800 Pa·s, respectively; the obtained stress vs. stretch curves are compared with the response of a purely elastic polymer. Again, by decreasing the viscosity, the unfolding process becomes faster, and tends to reduce the stress; in fact, for a given stretch, the corresponding stress measured during the first part of the stretch cycle is lower for low viscosity values. Furthermore, the area under the curve increases by decreasing the viscosity, since the energy dissipation becomes more pronounced when the unfolding is faster.

3.7.4 Effect of bond strength on chains failure

In the last case we consider the mechanical response of a polymer whose chains can fail according to the criterion (3.61), written in terms of the bond energy evaluated through the Extended Freely Jointed Chain (EFJC) model (see §2.3.3.3).

The stress vs. stretch curve of two polymers with different values of the normalized bond strength $\overline{w}/k_BT$, subjected to a load cycle, are shown in fig. 3.9(a); the curves are compared with the curve relative to an elastic, undamaged, network. The applied

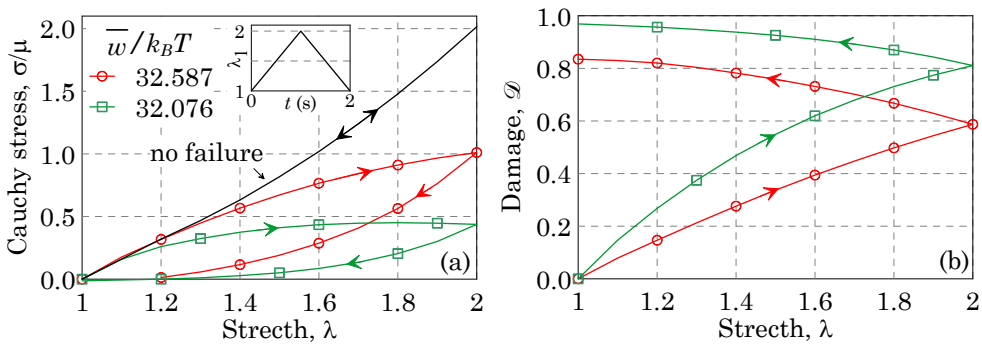

Figure 3.9: *Polymer networks with breakable bonds under a displacement history. Cauchy stress vs. stretch curve of two polymers with different bond strength compared to that of an elastic network (a); Damage vs. stretch curve for the same polymers (b).*

stretch cycle is reported in the insert of the same figure 3.9(a): from the stress-free state, the stretch increases up to $\lambda = 2$ in 1 s, and subsequently returns to $\lambda = 1$ in 1 s. The curve related to the elastic behavior is the same for both the loading and the unloading phase of the cycle, while when the chains failure is taken into account, the curve takes a different path during the unloading part of the cycle. As expected, by decreasing the failure energy the damage becomes more pronounced. The evolution of the damage $\mathscr{D}$ of the polymer, as defined in (3.38), with the applied stretch is illustrated in fig. 3.9(b). The damage increases during the whole deformation history because of the stretch of the network's chains, but in the loading phase of the history ($0 \le t \le 1$) the damage increases faster than in the unloading phase. We have still a damage increase during unloading, because the chains are still more stretched than in their reference configuration ($\lambda = 1$).

Finally, a double network polymer, in which each network has different bond strength, is considered. In the first case, the networks are assumed to have the same normalized bond strength $\overline{w}_1 = \overline{w}_2 = 33.69\,k_BT$, while in the second case the bond strength of the second network falls at $\overline{w}_2 = 32.59\,k_BT$ and in the third case it further reduces to $\overline{w}_2 = 32.08\,k_BT$. The two networks are both characterized by $N = 50$ and by the same volume fraction, equal to 50%. In fig. 3.10(a), the Cauchy stress vs. stretch curves of the three considered polymers are reported. For a given stretch, the overall stress in the polymer decreases with the bond strength of the weakest network. Simi-

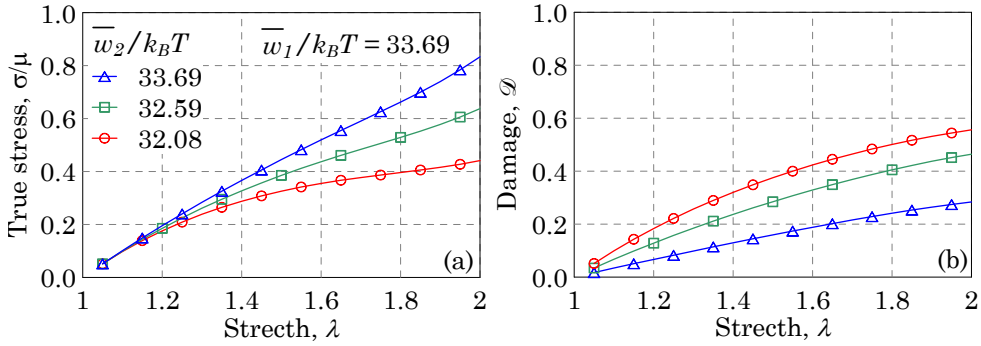

Figure 3.10: *Double network polymers made of networks with different bond strength. Cauchy stress vs. applied stretch curves (a) and damage vs. stretch curves (b) for three double network polymers. The strongest network has bond strength* $\overline{w}_1$*, while the weakest one has bond strength* $\overline{w}_2 \leq \overline{w}_1$.

larly, the damage of the material increases when the second network becomes weaker, as it can be seen in fig. 3.10(b), in which the damage of the polymers vs. the stretch is reported.

3.8 Conclusions

Polymeric materials exhibit a complex time-dependent mechanical response, that generally depends on the load history.

In the present chapter, a theoretical constitutive model based on the statistical description of the polymeric network, has been presented and discussed. The state of a representative volume of a polymer network is described by the *Chain Configuration Density Function* (CCDF) defined in the three-dimensional configuration space. Such a function provides the connection between the micro-scale and the continuum scale level. The evolution law of the CCDF has been derived by taking into account for: (i) the deformation applied to the material, (ii) the dynamic process of chains attachment and detachment, (iii) the chains unfolding mechanism and (iv) the chains failure. Once the CCDF and its evolution with the applied deformation are known, the stress state in the material can be evaluated. The developed micromechanical model allows for a simple determination of the involved parameters thanks to its physic-based nature.

Finally, some numerical tests carried out through the proposed model, have been presented and discussed in terms of stress vs. stretch curves.

CHAPTER 4

POLYMERS WITH STIMULI-RESPONSIVE MOLECULES

The introduction of properly designed molecules can lead to the development of a new class of polymers, capable to respond to external stimuli by changing their own physical or chemical properties [154]. Stimuli-responsive polymers have been synthesized to be responsive to temperature [120], pH [43], mechanical stress [96], electric and magnetic fields [99], light [78], etc.

Among this wide class of materials, we focus on *mechanochemically responsive polymers*, i.e. materials with embedded molecules that undergo chemical transformations triggered by chemical and/or mechanical actions. Mechanoresponsive materials are obtained by adding proper functional groups, called *mechanophores*, to the polymer. According to Brantley et al. [17], a mechanophore is «*any chemical entity that possesses mechanically labile bonds; that is, a functional group that changes under the influence of exogenous mechanical forces*».

Most of the mechanophores reported so far are characterized by the presence of strategically weakened bonds [57], electrocyclic ring-opening reactions [68], isomerizations [94], release of small molecules [92] or activation of latent transition metal catalysts [118].

4.1 Switchable molecule-based mechanophores

A possible strategy to obtain a molecular actuator is to exploit the so-called *molecular switch*. A mechanophore with such a property possesses, at least, two molecular stable states called *isomers* [100]; the transition from an isomer to another is triggered and tuned through proper external stimuli such as chemical, temperature, light, electric and/or magnetic fields, mechanical stress, etc [83, 112, 119]. The stable states are characterized by different geometrical, physical and sometimes chemical properties. When the switching mechanism implies a change in the geometry of the molecule, such a mechanism can be exploited to get a molecular-level actuator [23].

The phenomenon is often called stereoisomerism or conformational switching if the positions of the atoms change in space without modification of the atomic bonds. In other cases, the switching implies the rearrangement of the molecule, with breaking of some bonds and the formation of others. Another switching mechanism is related to redox reactions or pH variations, when the molecules are charged by electrons or protons, respectively. The change in the electronic configuration of the molecule often induces a change of the geometrical configuration [142].

Since the conformation change takes place at the molecular level, the actuating response of the material can be obtained at any dimensional scale, enabling their use in a very wide scale range, useful for advanced applications, such as in nanodevices.

4.1.1 Switching mechanism

From the energetic point of view, the isomers are distinct stable molecular configurations that correspond to local minima of the Gibbs energy. In fig. 4.1 it is represented a possible trend of the Gibbs energy vs. the mechanophore's conformation. The two stable states of the mechanophore are separated by an energy barrier, and the conformation switch implies to pass through an unstable state. The Gibbs energy required to overcome the barrier derives from the thermal agitation of the molecules itself, or from an external source, such as a mechanical work or a chemical potential. A possible measure of the mechanophore's conformation is the molecule's size. For that reason, the switching mechanism can be considered as an instability phenomenon (analogous to the well-known snap through phenomenon in structual mechanics), triggered by external stimuli capable to provide the energy required to overcome the energy barrier [22]. In the present study we consider switchable molecules with two distinct stable

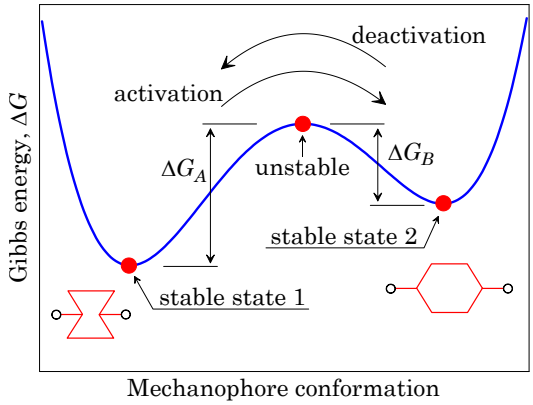

Figure 4.1: *Gibbs energy vs. mechanophore's conformation. The «active» and «inactive» conformations are stable states, while the intermediate conformation is unstable. The switching between the two stable conformations requires to overcome an energy barrier.*

states, identified as «*inactive*» and «*active*», where the word «activation» is synonymous of switching.

Let us consider a large number of mechanophores and let us indicate the fraction of active molecules - among all the mechanophores - with h. The evolution law of the active fraction can be obtained from a standard kinetic equation [66, 152], which has the same form of Eq. (3.17) describing the attached fraction of polymer chains [23]

$$\frac{dh}{dt} = k_A(1-h) - k_D h \tag{4.1}$$

where k_A and k_D are the activation and deactivation rates, respectively. These rates can be obtained with a thermodynamic approach to the transition state theory, that leads to the well-known Arrhenius equation [2, 20]

$$k_{A0} = C_A \exp\left(-\frac{\Delta G_{A0}}{k_B T}\right) \qquad k_{D0} = C_D \exp\left(-\frac{\Delta G_{D0}}{k_B T}\right) \tag{4.2}$$

where C_A and C_D are the so-called frequency factors or pre-exponential factors, while ΔG_{A0} and ΔG_{D0} are the Gibbs energy barriers associated to the activation ad deactivation reactions in absence of external stimuli, respectively. Such energy barriers can be experimentally measured, for instance, by the Nuclear Magnetic Resonance (NMR) spectroscopy [109] or numerically determined through Molecular Dynamics simulations [82].

In the present study, we focus on mechanophores responsive to mechanical and chemical stimuli. The mechanical stimuli comes from the force transmitted by the polymer chains to the mechanophore, while the chemical stimuli is induced by the presence of a proper solvent carring the molecules that react with the mechanophores [22].

The effect of the mechanical stress or of the triggering solvent is to promote the activation reaction and hinder the deactivation one, since these actions modifies the energy barriers from ΔG_{A0} to ΔG_A and from ΔG_{D0} to ΔG_D [31], i.e.

$$\Delta G_A = \Delta G_{A0} - f\,\delta s_{sw} - \Delta G_{A0}\frac{C_s}{\hat{C}_s}\,, \qquad \Delta G_D = \Delta G_{D0} + f\,\delta s_{sw} + \Delta G_{D0}\frac{C_s}{\hat{C}_s} \tag{4.3}$$

where f is the polymer chain's force, δs_{sw} is the displacement traveled by the force f, C_s is the solvent concentration inside the polymer and $\hat{C}_s$ is the solvent concentration required to activate all the mechanophores present in the unit volume. We emphasize that $f\,\delta s_{sw}$ represents the mechanical work done by the chain force times the displacement corresponding to the mechanophore's switching, thus δs_{sw} is a physical property of the mechanophore, depending on its size change. Using (4.3) the activation and deactivation rates can be finally expressed as

$$k_A = k_{A0}\exp\left(\frac{f\,\delta s_{sw}}{k_B T}\right)\exp\left(\frac{\Delta G_{A0}}{k_B T}\cdot\frac{C_s}{\hat{C}_s}\right) \qquad k_D = k_{D0}\exp\left(-\frac{f\,\delta s_{sw}}{k_B T}\right)\exp\left(-\frac{\Delta G_{D0}}{k_B T}\cdot\frac{C_s}{\hat{C}_s}\right) \tag{4.4}$$

Let us consider the particular case characterized by a constant applied stretch and solvent concentration in time, so that also k_A and k_D are constant. The solution of (4.1), by adopting the initial condition $h(t=0)=0$, is

$$h(t) = \frac{k_A}{k_A + k_D}\left[1 - e^{-(k_A+k_D)t}\right] \tag{4.5}$$

that correspond, at the steady state, to an active fraction of molecules equal to $h = k_A/(k_A+k_D) \le 1$.

4.2 Polymer chain with a bi-stable molecule

Let us consider a single polymer chain connected to a mechanophore which has two stable conformational states. If we ideally perform a tensile test on such a chain by controlling the displacement of its free ends (as shown in fig. 4.2), we obtain the force vs. extension curve reported in fig. 4.2(a) [23].

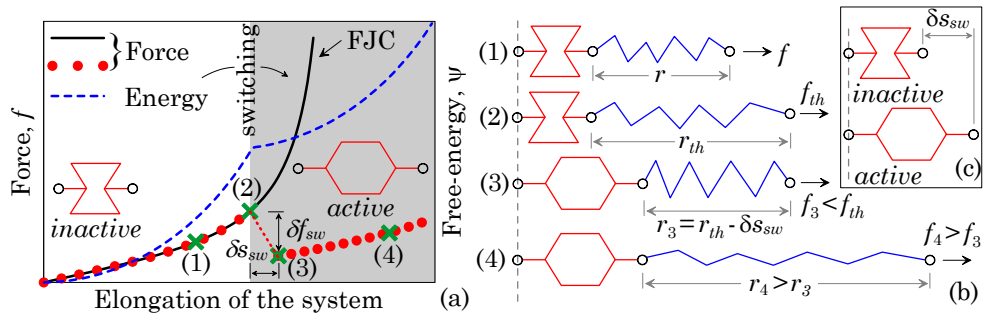

Figure 4.2: *Mechanical response of a polymer chain linked to a bi-stable mechanophore: plot of the force and the chain energy vs. the elongation for a Freely Jointed Chain with a mechanophore (a); scheme of the bi-stable chain in four different states (b); active and inactive states of the element representing the mechanophore.*

In the scheme of fig. 4.2(b), the mechanophore is represented by an element whose left end is kept fixed and its right end is linked to a chain; the mechanophore is characterized by a size change between the two states equal to δs_{sw}.

In the state labeled with (1) in fig. 4.2(b), the force f_1 corresponding to the separation r_1 arises from the FJC model, meanwhile the mechanophore is inactive. In the state (2) the force reaches the threshold value f_{th} at which the mechanophore becomes instantaneously active. During the activation, i.e. in the transition between (2) and (3), the mechanophore increases its size of the quantity δs_{sw}; at the same time, the chain reduces its extension of the same quantity, since the activation is instantaneous and its right end does not change position. The activation leads to an instantaneous drop of the force and, after this point, in the range (4), the behavior goes back to that of the FJC model as in the range (1) (fig. 4.2(a)).

Such a force drop can be observed in the force vs. extension curve of long folded molecules, such as DNA [41], RNA [31, 97] or synthetic polymers [10]; in these studies, the force vs. extension curve of single polymer chain were experimentally measured by using Atomic Force Microscopy [13].

The presence of a range in which the function $f(r)$ has a decreasing trend (see fig. 4.2(a)) implies that, in such an interval, the stiffness of the chain is negative; therefore, the free energy results to be non-convex, being the stiffness the second derivative of the energy itself.

A similar force drop can be considered as a local mechanical instability phenomenon, since a small variation of the force causes a large variation of the displacement, until a new stable configuration is reached. The force acting on the mechanophore is equal to the force in the chain, so it can be written [21]

$$f_m = \frac{k_B T}{b} \mathscr{L}^{-1}\left(\frac{r - \mathscr{H}\,\delta s_{sw}}{Nb}\right) \tag{4.6}$$

where the step function $\mathscr{H}$,accounting for the inactive ($\mathscr{H} = 0$) or active ($\mathscr{H} = 1$) state of the mechanophore, is defined as

$$\mathscr{H} = \mathscr{H}_f(f) + \mathscr{H}_s(n_s) - \mathscr{H}_f(f)\,\mathscr{H}_s(n_s) \tag{4.7}$$

$$\mathscr{H}_f(f) = \begin{cases} 0 & \text{if} \quad f < f_{th} \\ 1 & \text{if} \quad f \geq f_{th} \end{cases} \qquad \mathscr{H}_s(n_s) = \begin{cases} 0 & \text{if} \quad n_s < S_r \\ 1 & \text{if} \quad n_s \geq S_r \end{cases} \tag{4.8}$$

being f_{th} the threshold force required to activate the mechanophore (i.e. the force in the state (2) of fig. 4.2), n_s the number of solvent molecules available for the reaction and S_r is the number of solvent molecules required to activate the mechanophore, i.e. it represents the stoichiometric ratio that activates the reaction.

In the following, we indicate with f the chain's force evaluated for an end-to-end length r, while f' is the force evaluated for $r' = r - \delta s_{sw}$, namely

$$f = \frac{k_B T}{b} \mathscr{L}^{-1}\left(\frac{r}{Nb}\right) \qquad f' = \frac{k_B T}{b} \mathscr{L}^{-1}\left(\frac{r - \delta s_{sw}}{Nb}\right) \tag{4.9}$$

Finally, we can define the free energy associated to the switching, ψ_{sw}, as the work done by the chain force times the switching displacement

$$\psi_{sw} = \int_{sw} f_m(r)\, dr \approx \delta f_{sw}\, \delta s_{sw} \tag{4.10}$$

where the integral is evaluated during the switching mechanism, and δf_{sw} is the force drop.

4.2.1 Mechanophore switching as an unstable mechanical phenomenon

Let us consider the dynamic linear momentum balance in presence of inertia actions and viscous effects; using the Eulerian approach it reads

$$m\ddot{\mathbf{u}} = \operatorname{div} \boldsymbol{\sigma} - \eta\, \dot{\mathbf{u}} \tag{4.11}$$

where m is the mass density, $\mathbf{u}$ is the displacement from the reference to the current configuration, η is the coefficient of viscous damping and $\boldsymbol{\sigma}$ is the Cauchy stress tensor. The stability of the system can be studied by perturbing the above dynamic equilibrium equation, i.e. by introducing a variation of the displacement $\delta\mathbf{u}$ and assuming that the CCDF does not change in consequence of such a variation. Under these assumption, the corresponding variation of the Cauchy stress is

$$\delta\boldsymbol{\sigma} = \left\langle \left(\rho - \rho_0\right) \delta\mathbf{f} \otimes \mathbf{r} \right\rangle \tag{4.12}$$

where the variation of the chain force is $\delta\mathbf{f} = \frac{k_B T}{b} \mathscr{L}^{-1}\left(\frac{\delta r}{bN}\right)\hat{\mathbf{r}}$. In this case, the variation of the chains forces is induced by the mechanophore switching, whose effect is to reduce the chain's end-to-end distance of the quantity $\delta r = \delta s_{sw}$. At the chain-scale level, the mechanophore switching induces a snap-through instability in the mechanophore-chain system (see fig. 4.2), while the free energy ψ appears to be non convex [130].

4.3 Network with switchable molecules

Let us consider a representative volume of a network whose chains are linked to bistable molecules; a deformation history is applied to the material, which is further assumed to be immersed in a fluid (solvent). Our goal is to obtain the internal stress state and the fraction of active mechanophores when the external actions on the material are known.

In §4.1.1 the quantity h is defined as the fraction of active mechanophores; here we specify that $h : \Omega \times \mathscr{T} \to [0,1] \,|\, h = h(\mathbf{r},t)$ is a function defined in the configuration space Ω and in the time interval $\mathscr{T}$, which returns the fraction of active mechanophores, for a given end-to-end vector $\mathbf{r}$ and for a given time instant t. Moreover, we define $\overline{h}$ as the total fraction of active mechanophores in the representative volume, i.e. the number of active molecules divided by the number of mechanophores in the network. With the above definitions, the total active fraction can be computed as

$$\overline{h}(t) = \left\langle h(\mathbf{r},t)\, \varphi(\mathbf{r},t) \right\rangle \tag{4.13}$$

where φ is the normalized CCDF.

We quantify the amount of mechanophores in the network through the parameter α_{sw}, which represents the volume fraction of the material occupied by the mechanophores at $t = 0$; correspondingly, the volume fraction of the polymer is $1 - \alpha_{sw}$.

The switching mechanism usually implies a conformation change of the mechanophore, i.e. a change in shape and size; we quantify the deformation induced in the material through the corresponding deformation gradient tensor $\mathbf{F}_{sw}$ whose principal components are λ_{sw1}, λ_{sw2} and λ_{sw3}. Let us consider a fictitious material made only of mechanophores uniformly oriented in every direction of the 3D space. The deformation gradient in such a material, induced by the switch of all the mechanophores, can be obtained by an integration over all the possible orientations, i.e.

$$\overline{\mathbf{F}}_{sw} = \frac{1}{4\pi}\int_S \mathbf{A}\mathbf{F}_{sw}\mathbf{A}^T dS = \frac{\lambda_{sw1}+\lambda_{sw2}+\lambda_{sw3}}{3}\mathbf{I} \tag{4.14}$$

where S represents the unit sphere and $\mathbf{A}$ the three-dimensional rotation tensor. The volume ratio of this fictitious material made of switched mechanophores is

$$J_{sw} = \det\overline{\mathbf{F}}_{sw} = \left(\frac{\lambda_{sw1}+\lambda_{sw2}+\lambda_{sw3}}{3}\right)^3 \tag{4.15}$$

Since we are also in presence of a fluid phase, the absorption of the fluid by the polymer and the consequent swelling of the material must be taken into account. The chemical affinity of the mechanophores with the solvent is assumed to be negligible, so that only the polymer fraction of the material is responsible for the solvent absorption and volume swelling (the theory of polymer swelling is recalled in §2.4). Here we need to modify the potential energy of the polymer-solvent mixing given in (2.44), because of the presence of the mechanophores.

For sake of simplicity, here we neglect the chains attachment/detachment mechanism (i.e. we assume $k_a = k_d = 0$), unfolding ($\dot{N} = 0$), enthalpic deformation ($\dot{b} = 0$) and failure ($\omega_f = 0$). With the above hypothesis the CCDF's evolution law (3.39) reduces to $\dot{\rho} = -\left(\rho_{,i}\, r_j + \rho\,\delta_{ij}\right)L_{ij}$. The potential energy of the coupled system made of polymer, solvent and mechanophores becomes [22]

$$\Pi = \left\langle \left(\rho-\rho_0\right)\left[(1-\alpha_{sw})\,\psi - \alpha_{sw}\,h\,\psi_{sw}\right]\right\rangle + (1-\alpha_{sw})\Psi_{mix} + p\,(J-1-V_sC_s-J_{sw}) \tag{4.16}$$

where ψ is the free energy of a polymer chain (defined in §2.3.3), ψ_{sw} is the work associated to the mechanophore's activation (defined in (4.10)), Ψ_{mix} is the mixing energy given in (2.43), C_s is the solvent concentration measured in the reference configuration, V_s is the molar volume of the fluid, while p is the hydrostatic pressure enforcing the constraint

$$J = 1 + V_sC_s + J_{sw} \tag{4.17}$$

where J is the volume ratio of the material, $V_s C_s$ is the (dimensionless) volume of the absorbed solvent and J_{sw} is the volume ratio due to the mechanophores expansion. Since the polymer is assumed to be incompressible, the above expression reduces to $J = 1$ in absence of solvent and mechanophores activation.

The potential energy Π depends on two unknowns: the deformation gradient F_{ij} and the solvent concentration C_s. As recalled in §2.4, the stress state can be obtained from $P_{ij} = \partial\Pi/\partial F_{ij}$, while the chemical potential from $H = \partial\Pi/\partial C_s$. Following the procedure discussed in §3.3, the first Piola-Kirchhoff and the Cauchy stress tensors are, respectively

$$P_{ij} = \left\langle \left(\rho - \rho_0\right) \left[\alpha_{sw}\, h\, f_i' + (1 - \alpha_{sw}\, h) f_i\right] r_k \right\rangle F_{kj}^{-T} + p J F_{ij}^{-T}\, \delta_{ij} \tag{4.18}$$

$$\sigma_{ij} = \left\langle \left(\rho - \rho_0\right) \left[\alpha_{sw}\, h\, f_i' + (1 - \alpha_{sw}\, h) f_i\right] r_k \right\rangle + p\, \delta_{ij} \tag{4.19}$$

where the symbol F_{ij}^{-T} refers to the ij-component of tensor $\mathbf{F}^{-T}$, and similarly for $\dot{F}_{kj}^{-T}$ and L_{kj}^{-T}. The solvent concentration evolution law is given by eq. (2.48). It is worth noting that the stress and swelling coupling takes place through the pressure p.

4.4 Solution procedure

In this section we summarize the mathematical procedure adopted to solve the above described mechanical problem.

Unknowns. We start from the known data of the problem: the deformation history applied to the material $\mathbf{F} = \mathbf{F}(t)$, the initial conditions of the evolution laws for C_s and h, and the material parameters. The unknowns of the problem are the stress state $\boldsymbol{\sigma}$, the solvent concentration C_s and the active fraction h of the mechanophores.

Initial conditions. At time $t = 0$ the material is assumed to be in a stress-free state, with all the mechanophores inactive, i.e. $h(\mathbf{r}, t = 0) = 0 \;\; \forall \mathbf{r} \in \Omega$. The initial dimensionless CCDF is $\varphi(\mathbf{r}, t = 0) = \varphi_0(\mathbf{r})$, where $\varphi_0(\mathbf{r})$ is the Gaussian distribution given in (3.7). The initial solvent concentration inside the material is $C_s(t = 0) = C_{s0}$, while the initial value of the hydrostatic pressure is $p(t = 0) = 0$. Furthermore, in the following examples, the number of cross-links is assumed to be constant ($n_a(t) = n_\mu$), the segments are assumed rigid ($\dot{b} = 0$) and the chains unfolding is neglected ($\dot{N} = 0$).

Procedure flowchart. To solve the problem we use the following procedure:

1. the evolution law $\dot{\rho} = -\left(\rho_{,i}\, r_j + \rho\, \delta_{ij}\right) L_{ij}$ is used to update the CCDF, starting from the initial reference function $\rho_0(\mathbf{r}) = n_\mu\, \varphi_0(\mathbf{r})$, by using the velocity of deformation L_{ij};

2. the solvent concentration $C_s(t)$ is updated by using the evolution law (2.48), starting from the initial concentration C_{s0} and the initial value of the hydrostatic pressure p;

3. for each end-to-end vector $|\mathbf{r}|$ and for each value of N (if the polymer is polydisperse, i.e. it contains more than one network), the chain forces f and f' are determined using (4.9); then the activation and deactivation rates are evaluated using (4.4). Finally, the active fraction function $h = h(\mathbf{r}, t)$ is updated for the current $\mathbf{r}$ by using (4.1);

4. since the current CCDF, the solvent concentration C_s and $h = h(\mathbf{r}, t)$ are now known for the current time, the stress state can be evaluated using (4.19), in which the hydrostatic pressure p is determined from the boundary conditions of the problem.

The above described procedure is repeated through the time steps adopted, until the whole deformation history is completed.

4.5 Simulations

The above discussed procedure is used to simulate the mechanical response of a representative volume of an incompressible polymer containing switchable mechanophores; the effects of the solvent and of the applied deformation history are considered. The goal of the simulations is to determine the stress state and the total active fraction of mechanophores. Three parametric cases are reported and discussed in order to underline the role played by the different mechano-chemical stimuli.

Except when differently specified, the polymer under study is formed by a double network with the following characteristics: the first network is made of chains with N_1 Kuhn's segments and contributes to the 50% of the total volume, while the second one is made of chains with N_2 Kuhn's segments and occupies the remaining 50% of the volume. In order to study the effect of polydispersity on the switching mechanism, we

assume $N_1 = 100$ for the first network, while for the second one we tests three different values, i.e. $N_2 = 100$, $N_2 = 60$ and $N_2 = 40$. The volume fraction of switchable molecules is $\alpha_{sw} = 2\%$ in all cases.

The values of the other parameters, common to all the simulations, are the following: polymer's shear modulus $\mu = 5$ MPa, absolute temperature $T = 300$ K, Flory-Huggins dimensionless parameter $\chi = 0.4$ (typical value for a good polymer-solvent affinity), mechanophore's size variation $\delta s_{sw} = 10b$ (being $b = 1$ nm the length of a Kuhn segment), solvent molar volume $V_s = 5$ dm^3/mol, stoichiometric ratio $S_r = 10$ (number of solvent molecules required to activate one mechanophore), swelling's friction coefficient $\zeta = 60.2$ kJm^{3}s, Gibbs energy for the activation $\Delta G_A = 0.30$ J/mol, Gibbs energy for the deactivation $\Delta G_D = 6022$ J/mol, activation frequency $C_A = 10^{-10}$ Hz and deactivation frequency $C_D = 10^{-5}$ Hz.

4.5.1 Polymer under the effect of a monotonic deformation

Let us consider an incompressible polymer enriched with switchable molecules, under the action of an uniaxial stretch, without any chemical agent triggering the mechanophores activation.

We apply a deformation along the principal direction 1, while in the other directions the material is unconstrained. The applied deformation history is as follows: for $0 \le t \le 6$ ks the material is unstretched ($\lambda_1(t) = 1$), for $6 \le t \le 12$ ks the stretch λ_1 increases linearly from 1 to 1.5, for $12 \le t \le 18$ ks the deformation is kept constant at the value $\lambda_1 = 1.5$ and for $18 \le t \le 24$ ks the stretch increases linearly from 1.5 to 2. The initial unstretched time period is adopted to reach the steady state for the switching mechanism, according to the kinetic law (4.1). The dimensionless true stress in the stretching direction σ_1/μ vs. the applied stretch λ_1 is illustrated in fig. 4.3(a).

For the same deformation value, the stress in the polymer increases when the number N_2 of segments in the second network decreases. During the time intervals 0 $\div$ 6 ks and 12 $\div$ 18 ks the mechanophores activation is due to the kinetic switching equilibrium, thus no significant deformation takes place in the networks and the arising stress is negligible. In fig. 4.3(b) the evolution of the total active fraction $\overline{h}$ is illustrated. When the deformation is kept constant ($0 \le t \le 6$ ks and $12 \le t \le 18$ ks), the fraction of switched molecules increases because of the evolution of the kinetic equilibrium; instead, when the stretch increases ($6 \le t \le 12$ ks and $18 \le t \le 24$ ks) the active fraction $\overline{h}$ increases significantly because of the tensile forces induced in the network's chains.

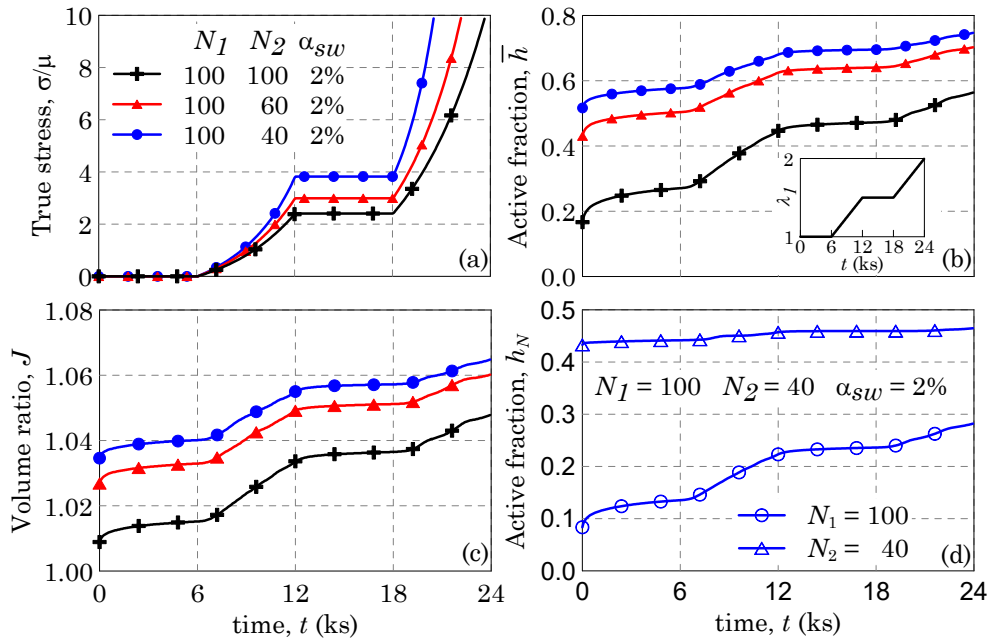

Figure 4.3: *Uniaxial stretch of three different polymers with embedded switchable molecules. The polymers consists of two networks, both with volume fraction of 50%, characterized by N_1 and N_2 segments per chain and a content equal to 2% of swithcable molecules. Plot of the stress vs. time curves (a), of the active fraction vs. time curves (b) and of the volume ratio of the material (c) for the monotonic deformation history depicted in (a). In (d) the evolution of the active fraction for the polymer with $N_1 = 100$ and $N_2 = 40$ is reported where the contributions of two networks are singularly indicated.*

It's worth noting that $\overline{h}$ increases when N_2 decreases since the network becomes more stiff and the force in the chains are greater for the same applied deformation value; the mechanical stimulus is thus more effective in inducing the mechanophore switching for low values of N_2. The volume ratio of the material is proportional to the active fraction of mechanophores, since the polymer itself is incompressible and in this example there is no swelling due to solvent uptake. The time evolution of the volume ratio, $J = J(t)$, is depicted in fig. 4.3(c).

In fig. 4.3(d) the time evolution of the active fraction of mechanophores for the polymer with $N_1 = 100$ and $N_2 = 40$ is illustrated by showing separately the contribution of the two networks: again, the shortest network ($N_2 = 40$) displays higher values of

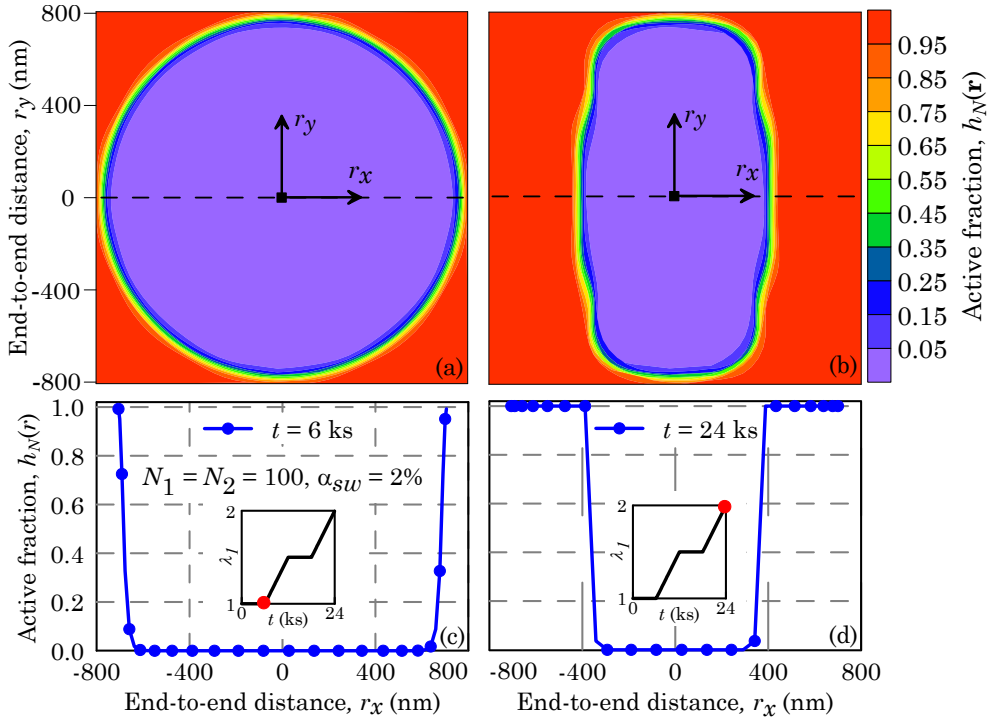

Figure 4.4: *Uniaxial stretch of a monodisperse polymer with embedded switchable molecules. Plot of the function* $h = h(r_x, r_y, r_z = 0)$ *for* $t = 6$ *ks (a) and for* $t = 24$ *ks (b) in the plane* $r_x - r_y$ *of the configuration space. The three-dimensional surface* $h = h(r_x, r_y, r_z = 0)$ *is sectioned in* $r_y = 0$ *and the plot of the obtained function* $h = h(r_x, r_y = 0, r_z = 0)$ *is reported in (c) and (d) for the corresponding time instants.*

the function h_N, because of the higher values of the forces arising in its chains with respect to those of the longer network.

Finally, in fig. 4.4 the contour plot of the function $h(r_x, r_y) = h_{N=N_1}(r_x, r_y, r_z = 0)$, for the case $N_1 = N_2 = 100$, is illustrated for two representative time instants, $t = 6$ ks and $t = 24$ ks. In the same figure is reported, moreover, the plot of the function $h_{N=N_1}(r_x, r_y = 0, r_z = 0)$ vs. the component r_x of the end-to-end vector $\mathbf{r}$. For $t = 6$ ks, the function $h(r_x, r_y)$ is close to zero for $|\mathbf{r}| < 600$ nm, irrespectively of the direction, while it is close to 1 for end-to-end distance greater than such a value, with a sharp increase. At the beginning the distribution is isotropic since the activation is driven by the kinetic equilibrium in absence of external stimuli. For $t = 24$ ks the distribution is

not isotropic, since in the x-direction the function $h(r_x, r_y)$ shows a sharp transition in $r_x \approx 400$ nm, while it changes slightly in the y-direction.

4.5.2 Polymer under the effect of a permeating solvent

In this example the polymer is exposed to a chemical agent; the material absorbs the fluid from the surrounding environment, thus it increases its volume because of the swelling; furthermore, the chemical agent enter in contact with the mechanophores, causing the switching to occur.

In fig. 4.5(a) the time evolution of the solvent concentration C_s for the three polymers considered in §4.5.1 is reported. The initial value of the concentration is $C_s(t = 0) \approx 0$ and after a transient time interval it reaches a steady state value. It appears that the most compliant polymer (i.e. that with $N_1 = N_2 = 100$) allows a more easily solvent diffusion, so the concentration is higher.

The time evolution of the active fraction of mechanophores, $\overline{h}$, is shown in fig. 4.5(b); as expected, $\overline{h}$ tends to an asymptotic value representing the steady state condition of the kinetic equilibrium. For a given time, the polymer with higher stiffness presents a higher value of the active fraction $\overline{h}$, since a greater chain's force promotes the activation process.

The volume ratio due only to the switching mechanism, $\overline{J}_{sw}$, is illustrated in fig. 4.5(c); the trend of such curves is proportional to that shown in fig. 4.3(b) for $\overline{h}$. Again, the volume change induced by the switching mechanism increases its effectiveness with the stretching of the network, i.e. for lower values of N_2.

In fig. 4.5(d) the polymer with $N_1 = 100$ and $N_2 = 40$ is considered to study the contribution of the two networks; again, the shortest network ($N_2 = 40$) is more effective in inducing the activation of the switchable molecule.

Finally, fig. 4.6 shows the contour plot of the function $h(r_x, r_y) = h_{N=N_1}(r_x, r_y, r_z = 0)$ for the polymer with $N_1 = N_2 = 100$ for $t \approx 0$ (fig. 4.6(a)) and for $t = 2$ ks (fig. 4.6(b)). It can be appreciated that the function is isotropic during the whole process, so in the three-dimensional configuration space (r_x, r_y, r_z) it has spherical symmetry, since the chemical-induced activation does not have preferential directions and the stretch induced by the swelling is isotropic. We assume the reference system (r_x, r_y, r_z) in the configuration space to be *coaxial* with the principal reference system (r_1, r_2, r_3) in the physical space. The section of the function $h(r_x, r_y)$ for $r_y = 0$ vs. the x-component of the end-to-end vector $\mathbf{r}$ is reported in fig. 4.6(c) and 4.6(d) for the two time instants.

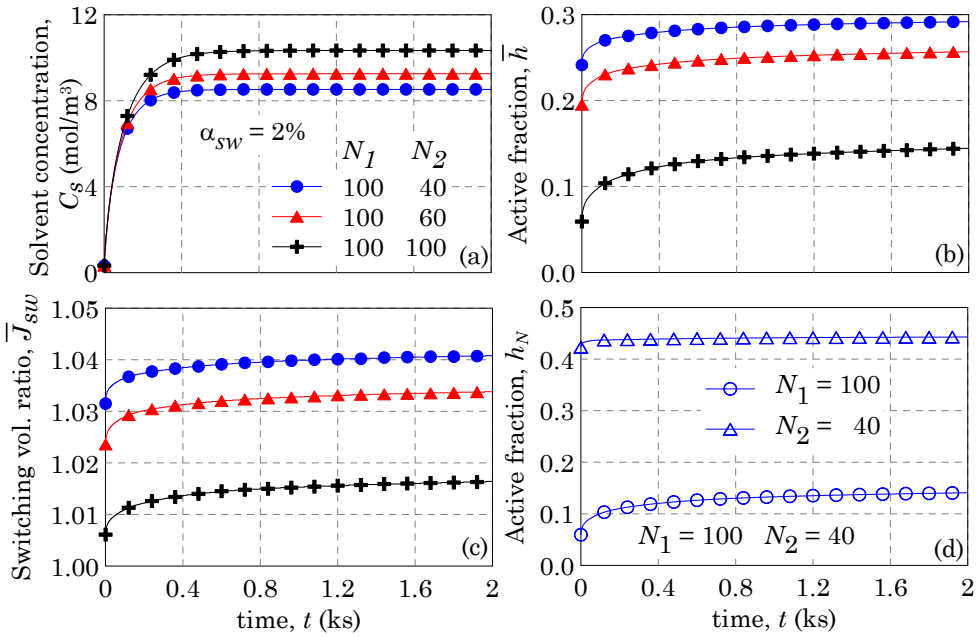

Figure 4.5: *Effect of a fuild solvent on three different polymers with embedded switchable molecules. The polymers consists of two networks, both with volume fraction of 50%, characterized by N_1 and N_2 segments per chain and a content equal to 2% of swithcable molecules. Plot of the solvent concentration (a), of the active fraction (b) and of the volume ratio of the material due only to the switching (c) versus time. Active fraction for the polymer with $N_1 = 100$ and $N_2 = 40$ represented separately for the two networks (d).*

At the very beginning of the simulation, only the molecules connected to chains with $|\mathbf{r}| > 800$ nm are active, while at the steady state the active molecules can be found for $|\mathbf{r}|$ greater than about 700 nm. The fraction of switched mechanophores is initially greater for large values of r_x, being the chains along this direction the most elongated ones and so the more stressed. Furthermore, the function $\overline{h}$ increases also because of the swelling expansion induced by the solvent absorption.

4.5.3 Polymer under cyclic loading in presence of a solvent phase

In the last parametric analysis we investigate the effects, on a monodisperse polymer with switchable molecules, of an imposed deformation history in combination with the presence of a solvent phase. The deformation history applied to the material is shown

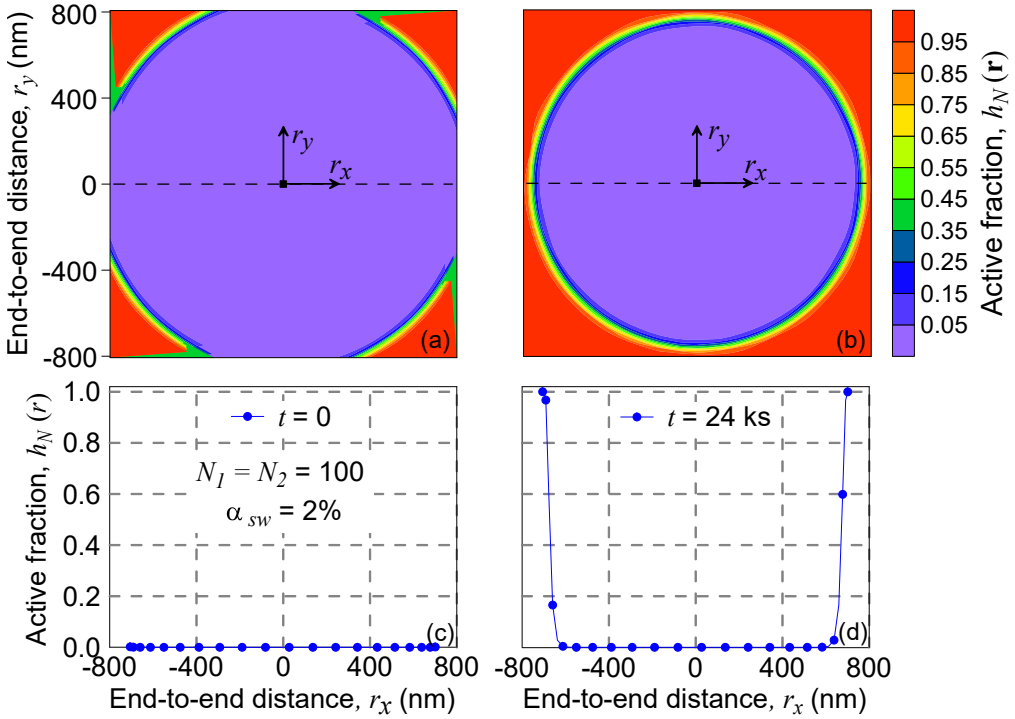

Figure 4.6: *Effect of a fluid solvent on a monodisperse polymer (N=100) with embedded switchable molecules ($\alpha_{sw} = 2\%$). Contour plot of the function $h = h(r_x, r_y, r_z = 0)$ for $t \approx 0$ (a) and for $t = 2$ ks (b) on the $r_x - r_y$ plane of the configuration space. Plot of the function $h = h(r_x, r_y = 0, r_z = 0)$ vs. the x-component of the end-to-end vector* **r** *for the same time instants, (c) and (d).*

in the insert of fig. 4.7(a): in the time interval $0 \le t \le 1$ ks no external deformation is applied to the material in order to let the material reaching the steady state for the swelling and the switching mechanism; then, a tensile cycle is applied by stretching the material linearly for 1 ks ($1 \le t \le 2$ ks) up to $\lambda_1 = 1.6$, by keeping the deformation constant for 1 ks ($2 \le t \le 3$ ks) and by reducing the stretch to $\lambda_1 = 1$ in 1 ks ($3 \le t \le 4$ ks); after that, a smaller compressive cycle is applied, by reaching the stretch $\lambda_1 = 0.6$ in 1 ks ($4 \le t \le 5$ ks), by maintaining this value for 1 ks ($5 \le t \le 6$ ks) and then going back to $\lambda_1 = 1$ in 1 ks ($6 \le t \le 7$ ks), while in the last interval $7 \le t \le 8$ ks $\lambda_1 = 1$ is kept constant.

In this example, the polymer is characterized by $N = 100$, the Flory-Huggins

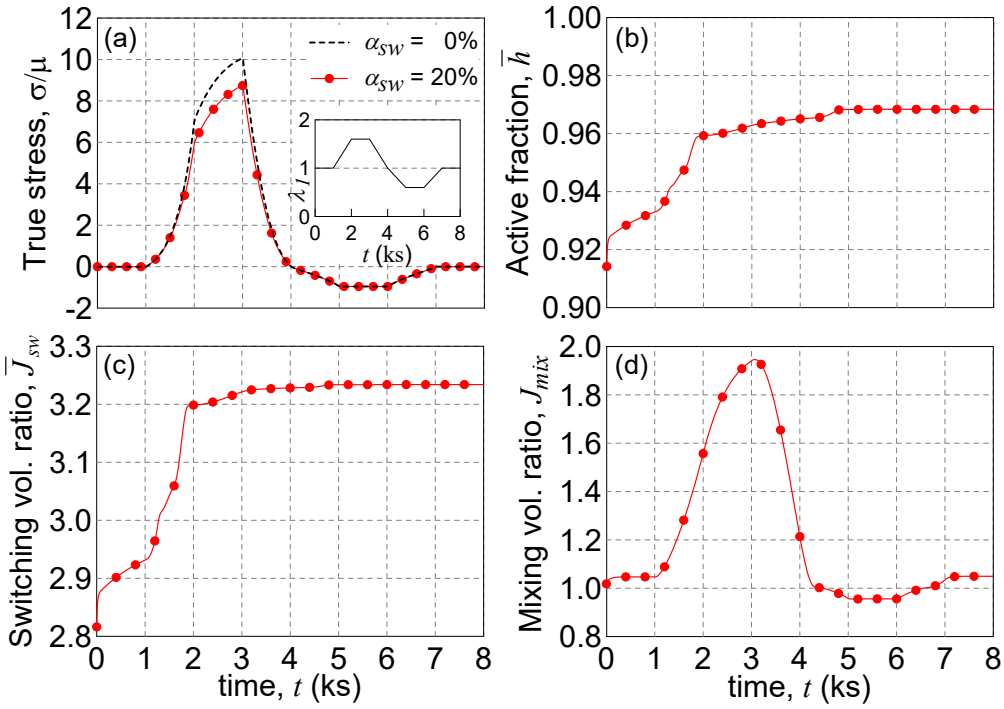

Figure 4.7: *Effect of a fluid solvent and of a mechanical action on a polymer with embedded switchable molecules. Plot of the true stress vs. time (a) for the polymer with* $\alpha_{sw} = 20\%$ *of mechanophores and for a blank polymer* ($\alpha_{sw} = 0\%$). *Active fraction (b), switching volume ratio (c) and swelling volume ratio (d) vs. time*

parameter is $\chi = 1.8$ (corresponding to a low polymer-solvent affinity), the size variation associated to the mechanophores activation is $\delta_{sw} = 50b$, while the mechanophores contents is assumed to be $\alpha_{sw} = 0\%$ or 20%.

In fig. 4.7(a) the true stress vs. time is reported for the two considered mechanophores contents. During the tensile cycle, the stress in the polymer with mechanophores ($\alpha_{sw} = 20\%$) reaches a lower value than in the case without mechanophores ($\alpha_{sw} = 0$), because no stress relaxation induced by the mechanophores activation in the chains takes place in the second case.

The time evolution of the active fraction $\bar{h}$ is reported in fig. 4.7(b); in the time interval $0 \div 1$ ks the fraction evolves because of the chemical stimulus, while in $1 \div 2$ ks it increases faster because of the mechanical action. During the unloading phase

(2÷3 ks), the fraction of active mechanophores does not change significantly, because the switching mechanism is sensible only to tensile forces, being the compression not allowed to occur in the polymer chains. A further small increase of the active fraction occurs during the compressive cycle (4÷7 ks), due to the stretch increase of the chains normal to the load.

Again, the volume ratio of the material due only to the switching mechanism, $\overline{J}_{sw}$, is proportional to the active fraction $\overline{h}$, fig. 4.7(c). The swelling of the material, quantified by the volume ratio $J_{mix} = C_s V_s$, is illustrated in 4.7(d) for the polymer with mechanophores. It appears that an increase of the applied stretch promotes the fluid absorption (1÷3 ks and 6÷7 ks), while a stretch reduction (3÷5 ks) induces the expulsion of the solvent.

Finally, in fig. 4.8 the contour plot of the function $h = h(r_x, r_y, r_z = 0)$ is illustrated for $t = 1$ ks (fig. 4.8(a)) and for $t = 3$ ks (fig. 4.8(b)). As expected, when the activation is promoted only by the chemical stimulus, the function has spherical symmetry, while the stretch increases the active fraction preferentially along the x-axis. In fig. 4.8 (c) and (d) the function $h = h(r_x, r_y = 0, r_z = 0)$ is represented for the same time instants; it is appreciable the reduction, in the configuration space, of the number of chains jointed to inactive mechanophores.

4.6 Comparision with experimental tests

In this section we compare the results obtained through the above described model with those from some experimental tests. Firstly, we simulate the test reported in [136] related to the swelling of a polyacrylamide gel; then we consider the test reported in [132] considering the activation of a spiropyran mechanophore in a glassy polymer matrix; finally, we attempt to reproduce the results of an experiment [142] on the activation of a quinoxaline cavitand mechanophore embedded in a PDMS elastomer under the exposure to an acid vapor.

4.6.1 Swelling of a polyacrylamide gel

In [136] the results of an experimental campaign on the free swelling of spherical polyacrylamide gel samples immersed in water are reported. For the details about the sample preparation and the test execution, we refer to the cited paper. The spherical samples has an initial radius of 0.315 mm; after 700 minutes in water, the radius

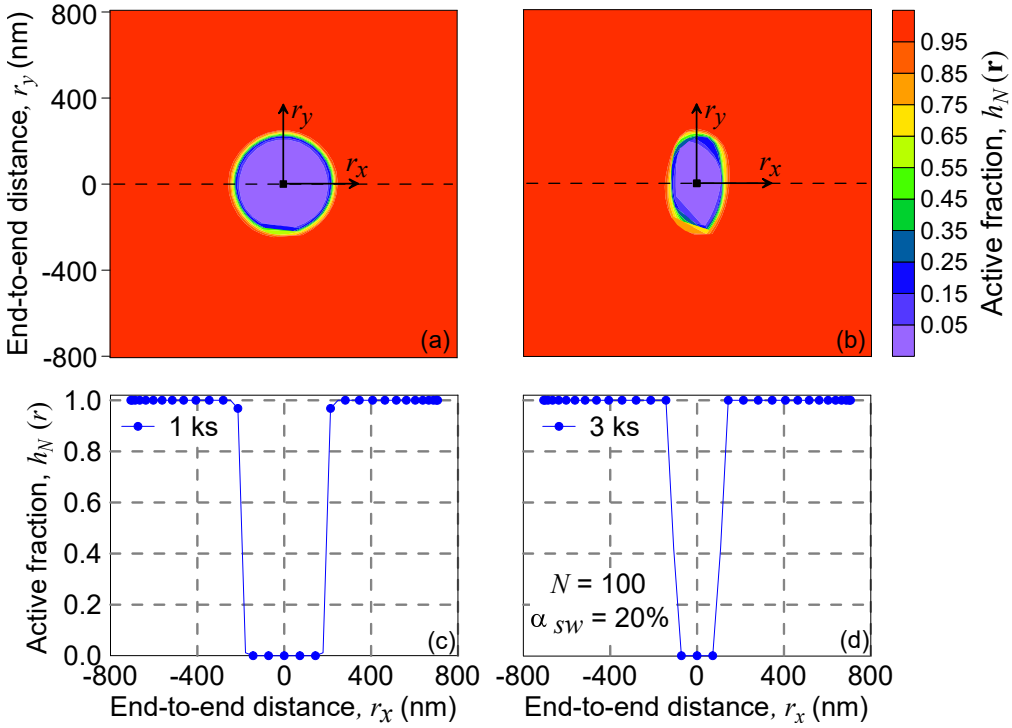

Figure 4.8: *Effect of a fluid solvent combined to a mechanical action on a polymer with embedded switchable molecules. Contour plot of the function* $h = h(r_x, r_y, r_z = 0)$ *for* $t = 1$ *ks (a) and for* $t = 3$ *ks (b) on the* $r_x - r_y$ *plane of the configuration space. Plot of the function* $h = h(r_x, r_y = 0, r_z = 0)$ *vs. the x-component of the end-to-end vector* $\mathbf{r}$ *for the same time instants, (c) and (d).*

became 0.338 mm. The Authors measured the sphere's radius during the swelling process, thus it is possible to compute the volume ratio of the sphere, assuming an homogeneous expansion, as $J(t) = \big(r(t)/r(t=0)\big)^3$, where $r(t)$ is the radius of the sphere at time t and $r(t=0) = 0.315$ mm is the radius at $t = 0$.

In fig. 4.9 the experimental curve $J = J(t)$, obtained from the data reported in [136], is compared with three curves obtained with the model for three different values of the ζ parameter, i.e. $\zeta = 24, 36, 54$ kJm^{3}s, since the exact value for the present material is not provided in literature. The shear modulus of the polyacrylamide gel is assumed to be $\mu = 40$ kPa [110], while the Flory-Huggins parameter is $\chi = 0.4986$ for the polyacrylamide-water interaction [95].

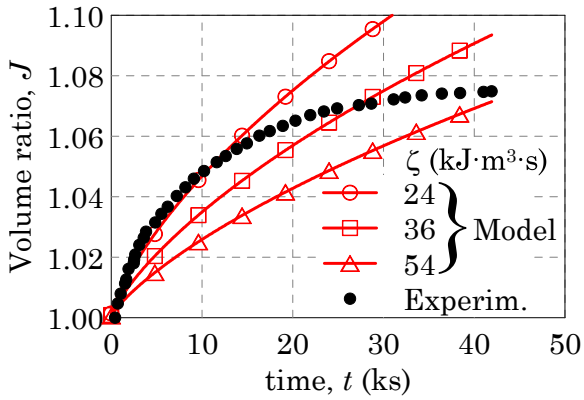

Figure 4.9: *Swelling of a polyacrylamide gel in water. Evolution of the volume ratio with time. Experimental results derived from [136] and results of simulations for three different values of the ζ-parameter.*

4.6.2 Responsive PMMA under mechanical load

In [132] some tests on a polymethyl methacrylate (PMMA) polymer enriched with a spiropyran mechanophores have been reported. Such a mechanophore has two stable isomers, called *spiropyran* and *merocyanine*; the merocyanine is fluorescent and thus can be easily detected under UV light. The PMMA sample is mechanically tested by applying a torsion load meanwhile the activation level of the mechanophores is quantified by measuring the fluorescence intensity. We identify the «inactive» state with the spiropyran and the «active» state with the merocyanine, thus we associate the measured fluorescence intensity to the fraction $\overline{h}$ of active molecule.

As reported in [132], the shear modulus of the PMMA sample is $\mu = 0.74$ GPa, while the mechanophore is characterized by a Gibbs energy $\Delta G_{A0} = 48.2$ kJ/mol for the activation and $\Delta G_{D0} = 150.6$ kJ/mol for the deactivation, respectively. The torsion load increases monotonically with constant rate, while the test is performed at room temperature and no solvent is present. From the experimental results, the activation phenomenon appears to be slightly influenced by the strain rate.

In order to fit the measured fluorescent of the sample, the polymer is assumed to be monodisperse with $N = 2000$, the characteristic size variation between spiropyran and merocyanine is assumed to be $\delta s_{sw} = 5b$ and the activation and deactivation rates are

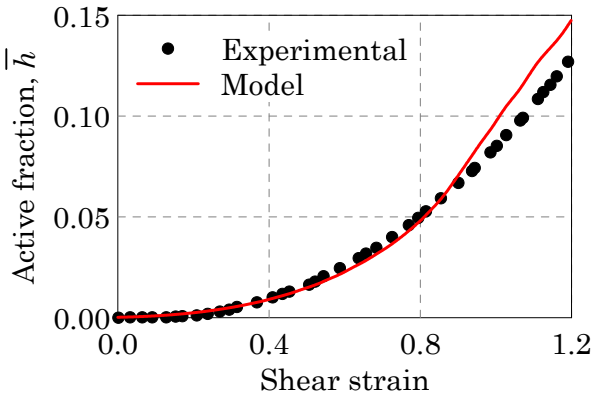

Figure 4.10: *Torsion test on a PMMA polymer enriched with spiropyran mechanophores. Evolution of the active fraction with the applied shear deformation. Experimental data from [132] compared with the results of a simulation.*

assumed to be $k_{A0} = 10^{-22}$ Hz and $k_{D0} = 10^{-5}$ Hz, respectively. We highlight that the assumed rate values are related to the time scale adopted in the experimental tests.

In fig. 4.10 the results of the simulation, i.e. the active fraction vs. shear deformation curve, is illustrated and compared with the experimental data reported in [132]. The numerical and the experimental data appear to be in a satisfactory agreement, in particular for strain values lower than about 0.9.

4.6.3 Responsive PDMS elastomer exposed to an acid

The last example is related to a polydimethylsiloxane (PDMS) elastomer containing, as responsive mechanophores, quinoxaline cavitands. We consider the experimental tests reported in [142] on unconstrained samples exposed to trifluoroacetic acid vapor, which permeates the elastomer and promotes the mechanophores activation. During the test, performed at room temperature, the polymer samples increase their volume because of the swelling and the own expansion of the mechanophores during their conformational change. The volumetric deformation of the samples were measured by using a Digital Image Correlation technique.

The two conformational stable isomers, called *vase* and *kite* [89], of the quinoxaline cavitand are depicted in fig. 4.11, with some representative dimensions. The chains of

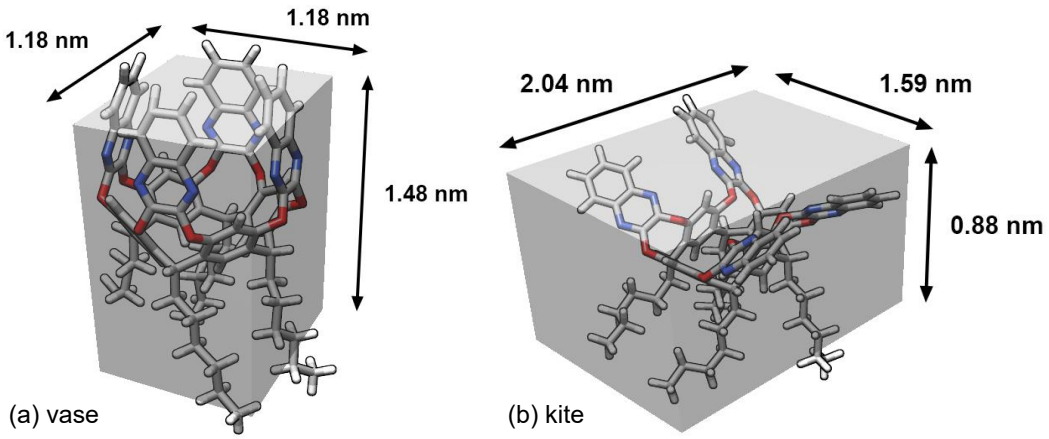

Figure 4.11: *Conformational stable states of the Quinoxaline cavitand: vase (a) and kite (b).*

the hosting polymer are connected to the cavitands wings in the top plane of fig. 4.11, while the other arms are not connected [141]. For that reason, the deformation due to the conformational change is more effective in that plane. The volume ratio associated to the vase-kite transition for a material made of quinoxaline cavitands only can be computed by using (4.15); by adopting the dimensions showed in fig. 4.11 it results $J_{sw} = 5.67$.

The experimental results of the tests are reported in fig. 4.12 in term of surface strain vs. time for a sample containing mechanophores and for a control sample without mechanophores; the control sample is necessary to quantify the swelling contribution to the whole expansion. In the same figure the results of the numerical simulation carried out with the proposed model are also reported. The parameter used to perform the simulation are the following: volume fraction of mechanophores $\alpha_{sw} = 0.41\%$ ($\alpha_{sw} = 0\%$ for the reference sample), shear modulus of the PDMS elastomer $\mu = 0.5$ MPa, Flory-Huggins parameter $\chi = 0.6$, Gibbs energy $\Delta G_{A0} = 13.7$ kJ/mol for the mechanophores activation and $\Delta G_{D0} = 28.1$ kJ/mol the deactivation, respectively, stoichiometric ratio for the quinoxaline cavitand-trifluoroacetic acid reaction $S_r = 4$ (i.e. 4 moles of acid are required to activate 1 mole of cavintands), ζ-parameter $\zeta = 180.7$ kJm^{3}s, size variation of the mechanophore $\delta s_{sw} = 0.86$ nm, number of segments per chain $N = 100$. Being the specimens thin flat plates, we use the surface expansion as a representative measure of the volume expansion of the material.

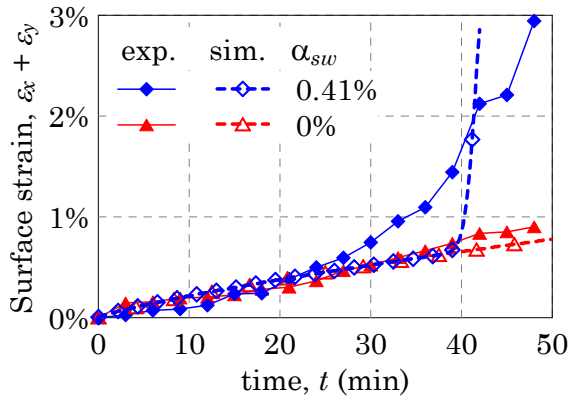

Figure 4.12: *PDMS elastomer with quinoxaline cavitands exposed to an acid. Surface strain of the samples vs. time: experimental and numerical results for the mechanophores-added polymer and for a reference one with* $\alpha_{sw} = 0\%$.

The numerical simulation appears to be in good agreement with the experimental outcomes for the reference sample, while for the sample enriched with mechanophores the simulation predict a more abrupt volume increase than in the test.

4.7 Conclusions

Stimuli responsive materials are capable to respond to external stimuli by changing their physical or chemical properties. Mechanochemically responsive polymers can be obtained by introducing inside the network special molecules, called mechanophores, capable to change their conformation in response to external stimuli.

In the present chapter, a micromechanical model has been developed to study the mechanical response of polymers enriched with switchable mechanophores characterized by two stable states, characterized by different sizes.

The conformation change has been considered to be induced by both mechanical or chemical stimuli; the equilibrium condition is determined on the basis of a kinetic equilibrium law. Since the assumed chemical stimulus is driven by the presence of an «active» solvent, the absorption mechanism of such a fluid has been considered (swelling).

The effect of the abrupt size change of the mechanophores on the polymers chains can be considered as an unstable phenomenon and so the corresponding mechanical description can be done also by taking advantag of the theory of material or pointwise instability. The mechanical response of the whole network have been obtained by upscaling the micromechanical model to the macroscale through the network's model developed in chap. 3.

Some parametric examples of polymer enriched with mechanophores subjected to mechanical and/or chemical stimuli have been discussed. Finally, the results of three experimental tests on different polymers, have been reported and simulated through the proposed model.

CHAPTER 5

NUMERICAL MODELING

The mechanical problem we are interested in requires to calculate the displacement, the strain, the stress, the solvent concentration and the active fraction of mechanophores in each point of a continuum body, by knowing the geometry of the body itself, the external actions (mechanical or chemical) and the kinematic boundary conditions.

In this chapter we present the numerical solution of such a problem through a Finite Element approach, implementing the model discussed in the previous chapters. Firstly, we recall the set of relations to be solved (strong form formulation); secondly, we discuss the formulation of the mechanical problem in term of variational principles (weak form formulation); then the linearization of the weak form problem and the discretization of the continuum body are presented; finally, we illustrate the implementation of the numerical procedure in a in-house Finite Element code. At the end of the chapter, some parametric tests performed with the FE algorithm are presented and discussed.

5.1 Strong form formulation

The strong form of the mechanical problem we need to solve is composed of two sets of equations: the linear momentum balance (2.14), corrected because of the presence of a linear energy dissipation due to the solvent uptake, and the solvent concentration

evolution law (2.48).

5.1.1 Linear momentum balance equation

By adopting a Lagrangian description, the linear momentum balance equation, accounting for a viscous-like dissipation, is [136]

$$\mathrm{Div}\,\mathbf{P} + \mathbf{G} = \zeta\,\dot{\mathbf{u}} \quad \text{in} \quad \mathscr{B}_0 \tag{5.1}$$

where $\mathbf{P}$ is the first Piola-Kirchhoff stress tensor, $\mathbf{G}$ is the body force vector, ζ is the polymer-solvent friction coefficient and $\dot{\mathbf{u}}$ is the velocity field. The Cauchy problem is completed by the boundary conditions

$$\mathbf{u} = \overline{\mathbf{u}} \quad \text{on} \quad \partial\mathscr{B}_{0u}\,, \qquad \mathbf{P}\,\mathbf{N} = \overline{\mathbf{T}} \quad \text{on} \quad \partial\mathscr{B}_{0\sigma} \qquad \text{with} \qquad \partial\mathscr{B}_0 = \partial\mathscr{B}_{0u} \cup \partial\mathscr{B}_{0\sigma} \tag{5.2}$$

where $\overline{\mathbf{u}}$ are the displacements applied to the boundary region $\partial\mathscr{B}_{0u}$, $\mathbf{N}$ is the unit vector normal to the body's boundary $\partial\mathscr{B}_0$ and $\overline{\mathbf{T}}$ is the stress vector applied to the boundary region $\partial\mathscr{B}_{0\sigma}$.

5.1.2 Evolution law of the solvent concentration

Following the theory developed by Tanaka et al., the evolution law for the solvent concentration evolution is [136]

$$\frac{\partial \Psi_{mix}}{\partial C_s} + pV_s = -\zeta \dot{C}_s \tag{5.3}$$

where Ψ_{mix} is the mixing free energy defined in (2.43), p is the osmotic pressure and V_s is the volume of the incoming solvent molecules. The initial condition of the above evolution law is

$$C_s(t=0) = C_{s0} \quad \text{in} \quad \mathscr{B}_0 \tag{5.4}$$

being C_{s0} the initial concentration.

5.2 Weak form formulation

The above strong form problem can be conveniently rewritten in a weak form. We choose as independent field variables the displacements $\mathbf{u} : \mathscr{B}_0 \times \mathscr{T} \to \mathbb{R}^3 \mid \mathbf{u} = \mathbf{u}(\mathbf{X}, t)$ and the solvent concentration $C_s : \mathscr{B}_0 \times \mathscr{T} \to \mathbb{R} \mid C_s = C_s(\mathbf{X}, t)$, being $\mathscr{T}$ the time domain.

Formally, the weak form formulation of eq. (5.1) has the form $\mathscr{G}(\mathbf{u},\dot{\mathbf{u}},\delta\mathbf{u}) = 0$, where $\delta\mathbf{u}$ is a test function representing an arbitrary infinitesimal variation [1] of the displacement field $\mathbf{u}$ and $\mathscr{G}$ is the following functional

$$\mathscr{G}(\mathbf{u},\dot{\mathbf{u}},\delta\mathbf{u}) = \int_{\mathscr{B}_0} \left[\mathbf{P} : \mathrm{Grad}(\delta\mathbf{u}) - (\mathbf{G} - \zeta\,\dot{\mathbf{u}})\cdot\delta\mathbf{u}\right] d\mathscr{B}_0 - \int_{\partial\mathscr{B}_{0\sigma}} \overline{\mathbf{T}}\cdot\delta\mathbf{u}\, d(\partial\mathscr{B}_{0\sigma}) \doteq 0 \tag{5.5}$$

The linear momentum balance (5.5) is valid for any material mechanical behavior, since it does not require the knowledge of the constitutive properties of the material.

Let us now introduce the hypothesis that the material is characterized by an hyperelastic behavior (see §2.2.1), so that we can define the energy density $\Pi = \Pi(\mathbf{F}(\mathbf{u}), C_s)$, whose derivatives w.r.t. $\mathbf{F}$ are the nominal stress, while the derivative w.r.t. C_s is the chemical potential (see § 2.4). Under the hyperelasticity assumption, the weak form formulation of the coupled equations (5.1) and (5.3) takes the form $\mathscr{G}(\mathbf{u}, C_s) = 0$, where the functional $\mathscr{G}(\mathbf{u}, C_s)$ is now defined as

$$\mathscr{G}(\mathbf{u}, C_s) = W_{\mathrm{int}}(\mathbf{u}, C_s) + W_{\mathrm{ext}}(\mathbf{u}) \tag{5.6}$$

$$W_{\mathrm{int}}(\mathbf{u}, C_s) = \int_{\mathscr{B}_0} \Pi(\mathbf{F}(\mathbf{u}),\, C_s)\, d\mathscr{B}_0 \tag{5.7}$$

$$W_{\mathrm{ext}}(\mathbf{u}) = -\int_{\mathscr{B}_0} \mathbf{G}\cdot\mathbf{u}\, d\mathscr{B}_0 - \int_{\partial\mathscr{B}_{0\sigma}} \overline{\mathbf{T}}\cdot\mathbf{u}\, d(\partial\mathscr{B}_{0\sigma}) \tag{5.8}$$

where $W_{\mathrm{int}}(\mathbf{u}, C_s)$ and $W_{\mathrm{ext}}(\mathbf{u})$ are the potential energies of the internal and external actions, respectively, while $\Pi(\mathbf{F}(\mathbf{u}), C_s)$ is the energy per unit volume previously defined in (4.16) as

$$\Pi(\mathbf{F}(\mathbf{u}),\, C_s) = \Psi(\mathbf{F}(\mathbf{u})) + (1-\alpha_{sw})\Psi_{mix}(C_s) + p\,(J - 1 - V_s C_s - \overline{J}_{sw}) \tag{5.9}$$

The energy density Π takes into account for the physical phenomena described in the previous chapters: the network's deformation, the stress relaxation due to the dynamic cross-links, the chains unfolding, the mechanophores activation, the mixing with the fluid and for the constraint represented by the incompressibility of the polymer.

The solution of the problem written in the weak form requires the functional $\mathscr{G}(\mathbf{u}, C_s)$ to be stationary with respect to the unknown fields $\mathbf{u}$ and C_s. Since the energy dissipation due to the polymer-solvent interaction is linear (see eq. (5.1)), we can define the Rayleigh's dissipation function $\mathscr{R} = \mathscr{R}(\dot{C}_s)$ as in eq. (2.47). The variational principle $\delta\mathscr{G}(\mathbf{u}, C_s) = 0$ can be explicitly written as [47]

$$\frac{\delta\mathscr{G}(\mathbf{u}, C_s)}{\delta\mathbf{u}} = -\frac{\partial\mathscr{R}}{\partial\dot{\mathbf{u}}} = \mathbf{0}\,, \qquad \frac{\delta\mathscr{G}(\mathbf{u}, C_s)}{\delta C_s} = -\frac{\partial\mathscr{R}}{\partial\dot{C}_s} \tag{5.10}$$

[1] The operator $\delta(\bullet)$ has the following properties: $\delta(\mathrm{Grad}\,\bullet) = \mathrm{Grad}(\delta\,\bullet)$ and $\delta\int_X \bullet\, dX = \int_X \delta\bullet\, dX$.

where the first identity is justified since $\mathscr{R}$ does not depend on the velocity. The above system of nonlinear equation is hereafter solved through a staggered technique: each field is determined independently, by using the latest calculated value of the other field, assumed to be constant during the current time step increment. The iterative calculation is repeated until a proper convergence criterion is fulfilled.

5.3 Linearization and discretization

We adopt the Finite Element technique to find the numerical solution of the above discussed problem. The Finite Element method requires to linearize the nonlinear equations (5.5) involved in the weak form formulation and the discretization of the continuum domain in a finite number of elements characterized by nodal degrees of freedom.

5.3.1 Linearization

Let $\mathbf{u}$ be a given displacement field and $\Delta\mathbf{u}$ an unknown displacement increment such that $\mathbf{u}+\Delta\mathbf{u}$ satisfies (5.5), i.e. $\mathscr{G}(\mathbf{u}+\Delta\mathbf{u})=0$. The functional $\mathscr{G}$ can be linearized through a first-order series expansion as $\mathscr{G}(\mathbf{u}+\Delta\mathbf{u})=\mathscr{G}(\mathbf{u})+\Delta\mathscr{G}(\mathbf{u},\Delta\mathbf{u})$, where $\Delta\mathscr{G}(\mathbf{u},\Delta\mathbf{u})$ represents the increment of $\mathscr{G}$ due to the increment $\Delta\mathbf{u}$ for a fixed $\mathbf{u}$. The linearization of eq. (5.5) leads to

$$\mathscr{G}(\mathbf{u})+\Delta\mathscr{G}(\mathbf{u},\Delta\mathbf{u})=0 \tag{5.11}$$

The term $\Delta\mathscr{G}(\mathbf{u},\Delta\mathbf{u})$ in the above expression is the slope of δW_{int} in the direction of $\mathbf{u}$ times the displacement increment $\Delta\mathbf{u}$; formally it can be expressed as

$$\Delta\mathscr{G}(\mathbf{u},\Delta\mathbf{u})=\frac{\partial(\delta W_{\text{int}})}{\partial\mathbf{u}}\Delta\mathbf{u}=\Delta\mathscr{G}_g(\mathbf{u},\Delta\mathbf{u})+\Delta\mathscr{G}_m(\mathbf{u},\Delta\mathbf{u}) \tag{5.12}$$

where $\Delta\mathscr{G}_g(\mathbf{u},\Delta\mathbf{u})$ is the so-called geometric part of $\Delta\mathscr{G}(\mathbf{u},\Delta\mathbf{u})$, while $\Delta\mathscr{G}_m(\mathbf{u},\Delta\mathbf{u})$ is the so-called material part. Using the Total Lagrangian approach, the geometric contribution is

$$\Delta\mathscr{G}_g(\mathbf{u},\Delta\mathbf{u})=\int_{\mathscr{B}_0}\text{Grad}(\delta\mathbf{u})\otimes\text{Grad}(\Delta\mathbf{u}):\mathbf{S}\,d\mathscr{B}_0 \tag{5.13}$$

while the material contribution is

$$\Delta\mathscr{G}_m(\mathbf{u},\Delta\mathbf{u})=\int_{\mathscr{B}_0}\mathbf{F}^T\text{Grad}(\delta\mathbf{u}):\mathbb{C}:\mathbf{F}^T\text{Grad}(\Delta\mathbf{u})\,d\mathscr{B}_0 \tag{5.14}$$

where $\mathbf{S}$ is the second Piola stress tensor, and $\mathbb{C}$ is the fourth-order elasticity tensor, that can be obtained from (5.9) as

$$\mathbb{C} = \frac{\partial^2 \Pi}{\partial \mathbf{F}\, \partial \mathbf{F}}\,, \qquad \mathbb{C} = \mathbb{C}_0 = \frac{\partial^2 \Pi_0}{\partial \mathbf{F}\, \partial \mathbf{F}} \tag{5.15}$$

where the first expression refers to the so-called *tangent stiffness method*, while the second to the *initial stiffness method*, being Π_0 the energy density (5.9) evaluated in the reference configuration. In the present study we adopt the initial stiffness method.

5.3.2 Discretization

The Finite Element method requires to discretize the domain $\mathscr{B}_0$ in a finite number of elements

$$\mathscr{B}_0 \approx \bigcup_{e=1}^{nele} \mathscr{B}_0^e \tag{5.16}$$

The mapping between the natural and the reference coordinates of a given element is provided by the shape functions N_I, $I = 1, \ldots, nnod$. By adopting the isoparametric formulation, the geometry and the displacement are interpolated with the same shape functions, so that

$$\mathbf{X}(\boldsymbol{\xi}) \approx \sum_{I=1}^{nnod} N_I(\boldsymbol{\xi})\, \mathbf{X}_I\,, \qquad \mathbf{u}(\boldsymbol{\xi}) \approx \sum_{I=1}^{nnod} N_I(\boldsymbol{\xi})\, \mathbf{u}_I \tag{5.17}$$

where $\mathbf{X}_I$ and $\mathbf{u}_I$ are the coordinates and the displacement vector of the I-th node of the considered element, while $\boldsymbol{\xi}$ are the coordinates (in the natural reference system of the element) of a generic finite element's point, corresponding to the material point $\mathbf{X}$ in the reference configuration. The material gradient of the displacement vector $\mathbf{u}$ can be evaluated as

$$\mathrm{Grad}(\mathbf{u}) \approx \sum_{I=1}^{nnod} \mathbf{u}_I \otimes \mathrm{Grad}(N_I) \tag{5.18}$$

while the material gradient of the increments $\delta\mathbf{u}$ and $\Delta\mathbf{u}$ are

$$\mathrm{Grad}(\delta\mathbf{u}) \approx \sum_{I=1}^{nnod} \delta\mathbf{u}_I \otimes \mathrm{Grad}(N_I)\,, \qquad \mathrm{Grad}(\Delta\mathbf{u}) \approx \sum_{I=1}^{nnod} \Delta\mathbf{u}_I \otimes \mathrm{Grad}(N_I) \tag{5.19}$$

Finally, the material gradient of the shape functions is

$$\mathrm{Grad}(N_I) = \mathbf{J}_e^{-T} \frac{\mathrm{d}N_I}{\mathrm{d}\boldsymbol{\xi}} \qquad \text{with} \qquad \mathbf{J}_e = \frac{\mathrm{d}\mathbf{X}}{\mathrm{d}\boldsymbol{\xi}} = \sum_{I=1}^{nnod} \mathbf{X}_I \otimes \frac{\mathrm{d}N_I}{\mathrm{d}\boldsymbol{\xi}} \tag{5.20}$$

The weak-form of the problem requires the stationarity (5.10) of the potential energy W, i.e. $\delta W = 0$; the discretized form of such relations, for each finite element e, is

$$\delta W^e = \delta W^e_{int} - \delta W^e_{ext} = 0 \tag{5.21}$$

The discretized internal and external potential energies are

$$\delta W^e_{int} = \sum_{I=1}^{nnod} \delta \mathbf{u}_I \cdot \mathbf{f}^{int}_I \,, \qquad \delta W^e_{ext} = \sum_{I=1}^{nnod} \delta \mathbf{u}_I \cdot \mathbf{f}^{ext}_I \tag{5.22}$$

where $\mathbf{f}^{int}_I$ and $\mathbf{f}^{ext}_I$ are the internal and external nodal forces, respectively, referred to the I-th node

$$\mathbf{f}^{int}_I = \int_{\mathscr{B}^e_0} \mathrm{Grad}(N_I)\, \mathbf{S}\, d\mathscr{B}^e_0 \,, \qquad \mathbf{f}^{ext}_I = \int_{\mathscr{B}^e_0} N_I\, \mathbf{b}\, d\mathscr{B}^e_0 + \int_{\partial\mathscr{B}^e_0} N_I\, \mathbf{T}\, d(\partial\mathscr{B}^e_0) \tag{5.23}$$

being $\mathbf{S}$ the second Piola stress tensor (2.6).

Let us define the umbalanced force vector for the I-th node $\mathbf{R}_I$ as the difference between the internal and external nodal forces, i.e. $\mathbf{R}_I = \mathbf{f}^{int}_I - \mathbf{f}^{ext}_I$. The nodal equilibrium equation requires $\mathbf{R}_I = \mathbf{0}$ for each node $I = 1, \ldots, nnod$. The solution of such an equation can be found, for instance, through a Newton-Raphson iterative solution technique, which can be written, for the k-th iteration, as $\mathbf{R}^{k+1}_I = \mathbf{R}^k_I + \Delta\mathbf{R}^k_I = 0$, where the increment $\Delta\mathbf{R}^k_I$ is

$$\Delta\mathbf{R}^k_I = \sum_{J=1}^{nnod} \frac{\mathrm{d}\,\mathbf{R}_I}{\mathrm{d}\,\mathbf{u}_J}\, \Delta\mathbf{u}_J \tag{5.24}$$

In the above expression, the derivative $\mathrm{d}\mathbf{R}_I/\mathrm{d}\mathbf{u}_J$ represents the tangent stiffness matrix , i.e.

$$\mathbf{K}_{IJ} = \frac{\mathrm{d}\,\mathbf{R}_I}{\mathrm{d}\,\mathbf{u}_J} = \int_{\mathscr{B}^e_0} \left[\mathrm{Grad}(N_I)\cdot\mathbb{C}\cdot\mathrm{Grad}(N_J) + \big(\mathrm{Grad}(N_I)\cdot\mathbf{S}\cdot\mathrm{Grad}(N_J)\big)\mathbf{I}\right] d\mathscr{B}^e_0 \tag{5.25}$$

where $\mathbb{C}$ is he fourth-order elasticity tensor defined in (5.15) and $\mathbf{S}$ is the second Piola-Kirchhoff stress tensor. The global stiffness matrix $\mathbf{K}$, the global umbalanced forces vector $\mathbf{R}$ and the global displacement vector $\mathbf{D}$ can be obtained through the following standard assembling operation

$$\mathbf{K} = \bigcup_{e=1}^{nele} \mathbf{K}^e, \qquad \mathbf{R} = \bigcup_{e=1}^{nele} \mathbf{R}^e, \qquad \mathbf{D} = \bigcup_{e=1}^{nele} \mathbf{D}^e \tag{5.26}$$

where $\mathbf{K}^e$ is the stiffness matrix (with dimension $nnod \times nnod$) of the element e, while $\mathbf{R}^e$ and $\mathbf{D}^e$ are the unbalanced force vector and the displacement vector (both with

dimension $nnod$) relative to the element e, respectively. Finally, the nodal equilibrium equations become

$$\mathbf{R}^k + \mathbf{K}^k \Delta \mathbf{D}^k = \mathbf{0} \qquad \text{with} \qquad \Delta \mathbf{D}^k = \mathbf{D}^{k+i} - \mathbf{D}^k \tag{5.27}$$

the iterative procedure - involving the above equations - provides the solution for the discretized displacement field $\mathbf{D}$ at each time instants.

5.4 Implementation in a Finite Element Code

The above discussed formulation has been implemented in a in-house Finite Element code whose flowchart is illustrated in fig. 5.1. The algorithm can solve 2D problems in plane stress, plane strain or axisymmetric condition.

The algorithm discretizes the time in a finite number of steps and, for each step, solves the mechanical problem with a non-linear iterative procedure. At the beginning of each step, the global stiffness matrix $\mathbf{K}$ is evaluated with the current nodal displacements by using (5.25) and assembled through (5.26); the external nodal force vector $\mathbf{f}^{ext}$ is evaluated by using (5.23) and finally the constraints are applied by using the so-called penalty method.

After these initial operations, the iterative solution procedure starts. The internal nodal force vector $\mathbf{f}^{int}$ is evaluated for the current stress state by using (5.23) and the reaction forces in the constrained nodes are updated accordingly. Then, the unbalanced (or residual) force vector $\mathbf{R}^k$ is evaluated for the current k-th iteration as the difference between the internal and external nodal forces. Since the umbalanced forces are known, it is possible to compute the increment of nodal displacement for the current iteration $\Delta \mathbf{D}^k$ by using (5.27) as $\Delta \mathbf{D}^k = -\mathbf{K}^{-1}\mathbf{R}^k$, being $\mathbf{K}^{-1}$ the inverse of the stiffness matrix for the current step. After that, the global displacement vector is updated as $\mathbf{D}^k = \mathbf{D}^{k-1} + \Delta \mathbf{D}^k$, and also the coordinates of the nodes and of the elements' Gauss point are updated accordingly. Thus, the stress arising at each Gauss point is evaluated by following the procedure described in §5.4.1. Finally, if the convergence criteria are fulfilled, the execution proceeds to the next step, otherwise a further iteration is performed. The convergence of the iterative procedure to an acceptable solution is assumed to be fulfilled when both the following inequalities are fulfilled

$$\frac{|\Delta \mathbf{D}^k|}{|\mathbf{D}^k|} \leq toll_D \,, \qquad \frac{|\Delta \mathbf{R}^k|}{|\mathbf{R}^k|} \leq toll_R \tag{5.28}$$

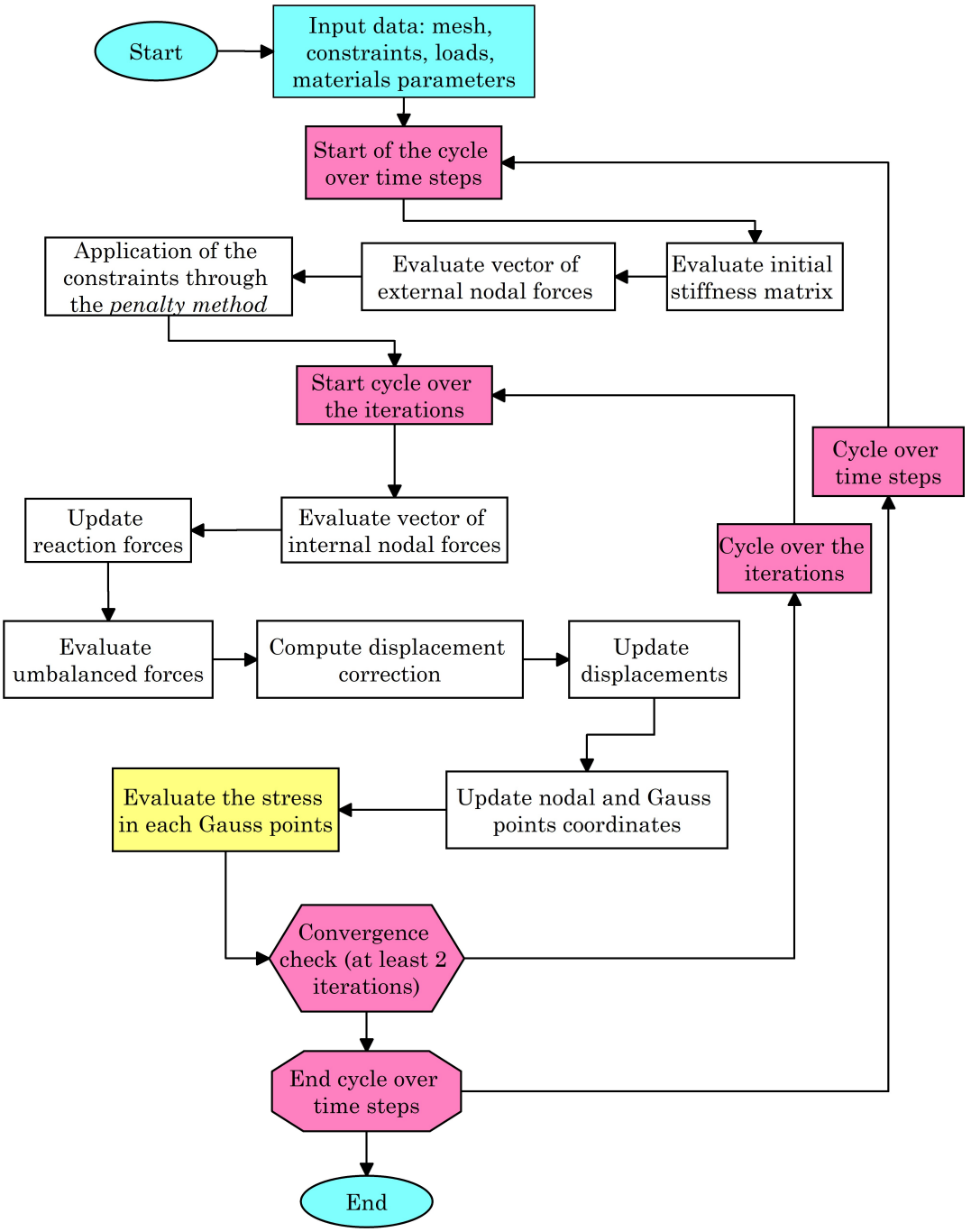

Figure 5.1: *Flowchart of the algorithm of the developed Finite Element code.*

where the operator $|\bullet|$ indicated the usual Euclidean norm, while the tolerances $toll_D$ and $toll_R$ are assumed sufficiently small.

5.4.1 Numerical evaluation of the stress state

The evaluation of the stress state at the Gauss points is performed by following the flowchart of fig. 5.2. The algorithm evaluates the deformation gradient tensor $\mathbf{F}$ and the velocity gradient $\mathbf{L}$ at each Gauss point of the mesh, by interpolating the nodal displacement with the shape functions of the element to which the Gauss point belongs. The z-term of the deformation gradient, i.e. the deformation gradient term related to the direction normal to the plane of the 2D problem, cannot be evaluated by interpolating the displacement field, but it arises from the assumption of plane state. Since we are dealing with a 2D problem, the nonzero terms of the deformation gradient tensor are

$$\mathbf{F} = \begin{pmatrix} F_x & F_{xy} & 0 \\ F_{yx} & F_y & 0 \\ 0 & 0 & F_z \end{pmatrix} \tag{5.29}$$

In particular, the term F_z in plane stress condition is evaluated from the incompressibility condition $\det\mathbf{F} = 1$, leading to $F_z = (F_x F_y - F_{xy}F_{yx})^{-1}$; in plane strain condition it is, by definition of plane strain, $F_z = 1$; in axisymmetry it is $F_z = r/R$, being r and R the current and reference distance of the point from the axis of symmetry, respectively. Once the deformation and the velocity gradient tensors, $\mathbf{F}$ and $\mathbf{L} = \dot{\mathbf{F}}\mathbf{F}^{-1}$, are known in the Gauss point, the stress state can be evaluated with the model discussed in the previous chapters (see below). Finally, the Green-Lagrange deformation tensor and the first Piola stress tensor are derived.

The evaluation of the stress state in a given Gauss point is performed by following the flowchart depicted in fig. 5.3. The integration domain in which the operator $\langle\bullet\rangle$ is defined is a finite subset of the configuration space Ω, and it is defined by $\{\mathbf{r} \in \mathbb{R}^3 \mid |r_i| \leq r_{max}, \quad i = x,y,z\} \subset \Omega$, where r_{max} is the (finite) dimension of the integration domain. The numerical integration is performed, in the configuration space, by using a $n \times n \times n$ grid ($n = 30$) of integration points, whose positions are determined according to the Gauss' quadrature rule, so that the operator $\langle\bullet\rangle$ becomes

$$\langle\bullet\rangle = \sum_{inet=1}^{nnet} q_{inet} \sum_{i=1}^{n}\sum_{j=1}^{n}\sum_{k=1}^{n} \bullet \, \Delta\Omega \tag{5.30}$$

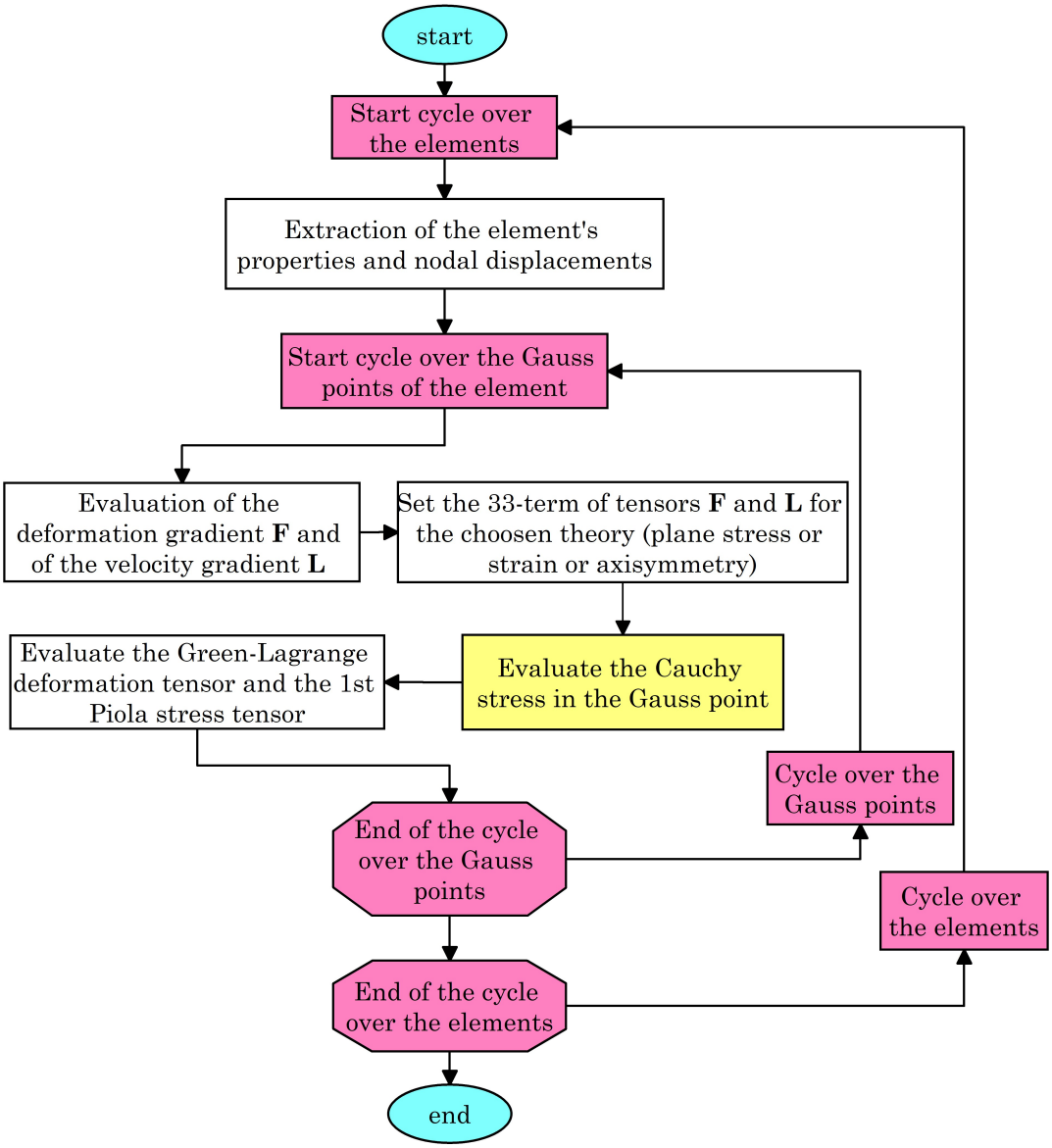

Figure 5.2: *Flowchart of the algorithm for the evaluation of the stress state in the discretized body.*

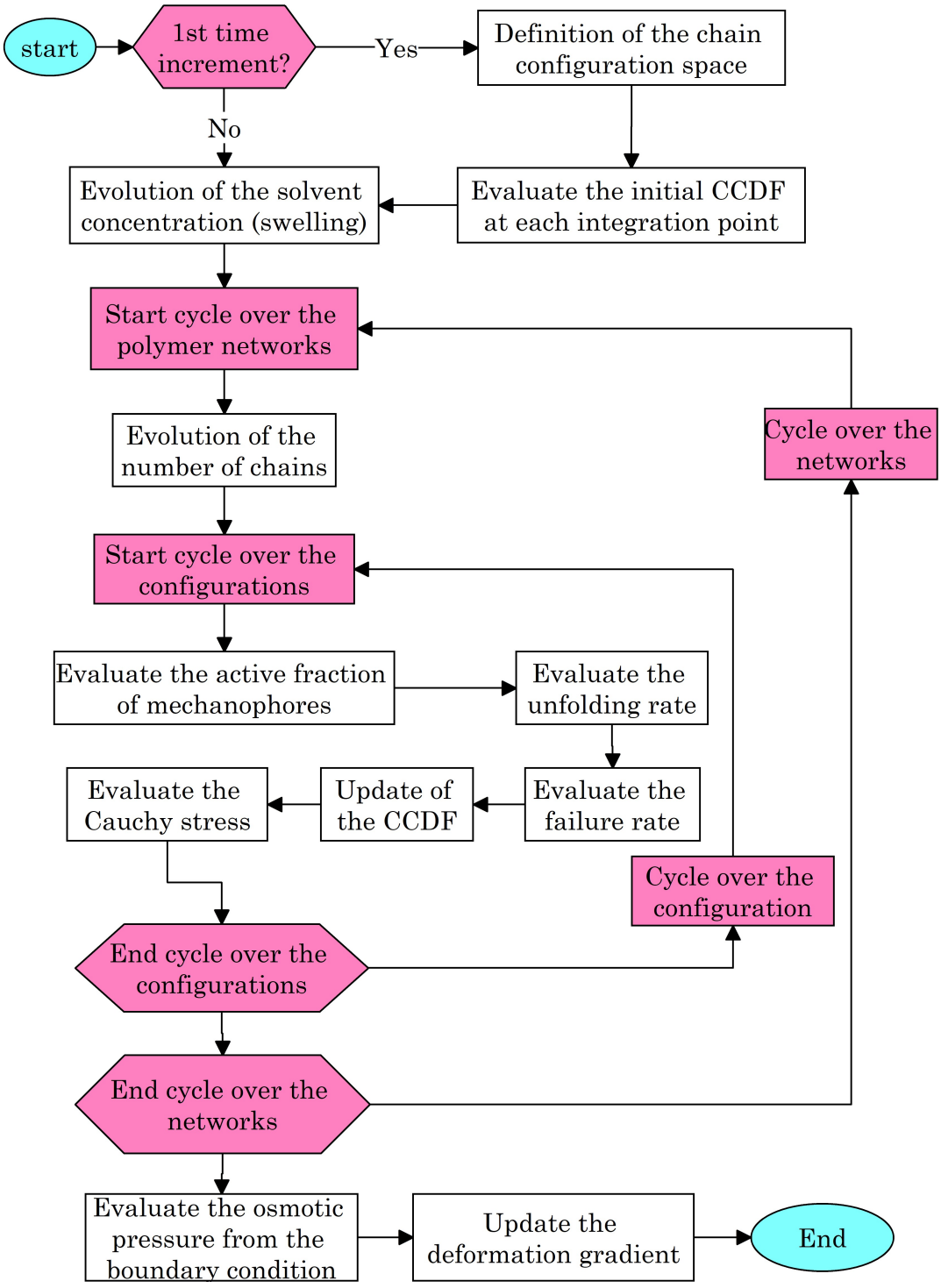

Figure 5.3: *Flowchart of the algorithm for the evaluation of the stress state in a given Gauss point.*

where $nnet$ is the number of networks present in the polymer, q_{inet} is the volume fraction of each network, so that $\sum_{inet=1}^{nnet} q_{inet} = 1$, and $\Delta\Omega$ is the weight of each Gauss point. At $t = 0$ the CCDF of each network is set to a standard Gaussian distribution with mean value equal to 0 and standard deviation equal to $b\sqrt{N/3}$. The gradient of the CCDF $\nabla\rho$ is numerically evaluated through a quadratic interpolation of the discretized CCDF in the chain configuration space.

For every iteration, the solvent concentration C_s is updated by using the evolution law (2.48), while the evolution of the chains concentration is evaluated for each network by using the evolution law (3.17).

Then, for each chain configuration, provided by the end-to-end vector $\mathbf{r} = (r_x, r_y, r_z)$, the active fraction of mechanophores h is evaluated by using the kinetic equilibrium (4.1), while the unfolding rate $\dot{N}$ is evaluated by using (3.58) and the failure rate ω_f by using (3.61). Once all these contributions are known, it is possible to compute the CCDF time derivative defined in (3.39) and to update the CCDF. Thus, the CCDF $\rho_0(\mathbf{r})$ is evaluated as indicated in eq. (3.51) as $\rho_0(\mathbf{r}) = \rho(\mathbf{F}\,\mathbf{r})$ by interpolating, with linear shape functions, the values of ρ in the three-dimensional grid of the integration point. Finally, the Cauchy stress are evaluated by using (3.46).

Once the Cauchy stress tensor in the Gauss point is known, it is possible to compute the osmotic pressure which enforces the incompressibility constraint; in plane stress such a pressure can be obtained from the boundary conditions along the z-direction, $\sigma_3 = 0$, while in plane strain or axisymmetric situations it is obtained from the constraint condition required by the deformation. Once the osmotic pressure is known, the stress tensor is correct accordingly. Finally, the deformation gradient is updated by taking into account the expansion due to the fluid absorption and the volumetric deformation effect due to the mechanophores activation.

5.5 Parametric FE analysis

In this section we present the results of some parametric tests performed with the Finite Element algorithm. The body considered for the tests is the $5 \times 1 \times 0.1$ m cantilever beam subjected to a vertical displacement $\overline{\delta} = 0.3$ m applied to the top-right corner of the element. The geometry of the body is illustrated in fig. 5.4(a), while the adopted mesh and boundary condition is illustrated in fig. 5.4(b).

The material is assumed to be an incompressible polymer with shear modulus $\mu = 1$

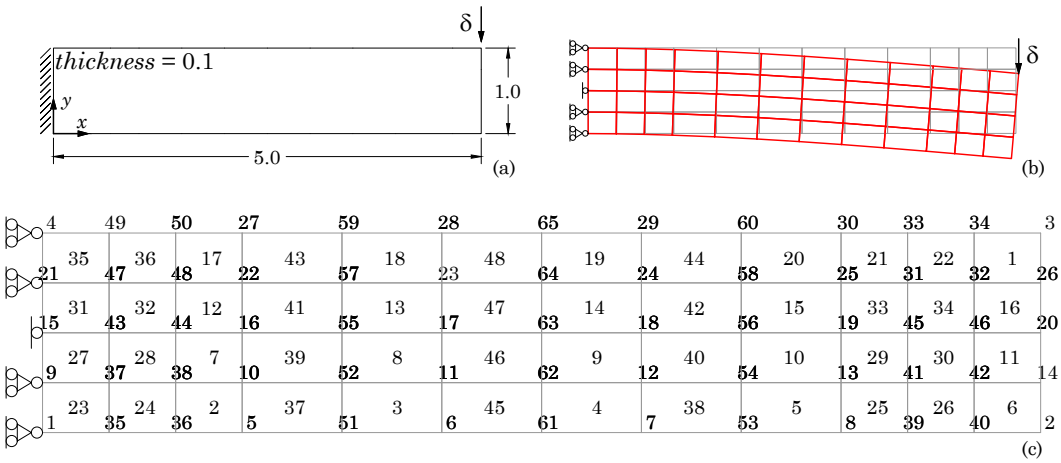

Figure 5.4: *Cantilever beam subjected to an imposed vertical displacement. Geometry of the problem (dimensions in meters) (a), deformed mesh for* $\delta = 0.3\,\mathrm{m}$ *(b) and adopted FE mesh whit the constraints (c).*

MPa for all the considered cases. The applied displacement history is assumed to be made of two phases: in the first one ($0 \le t \le 1$ s) the displacement factor $\alpha(t)$ (such that $\delta(t) = \overline{\delta} \cdot \alpha(t)$) increases linearly from 0 to 1, while in the second phase ($1 \le t \le 2$) it goes back to 0 (see insert of fig. 5.5).

In §5.5.1 the results related to the beam made of a polymer with dynamic cross-links is presented, while in §5.5.2 the material is assumed to be characterized by the unfolding phenomenon and, finally, in §5.5.3 the polymer damage is considered.

5.5.1 FE analysis of a beam made of polymers with dynamic cross-links

In the present case, the material composing the beam is assumed to be a polymer with dynamic cross-links. Three polymers, characterized by different values of the deactivation rate k_d (k_d = 0.6, 1.8 and 3.0 Hz, respectively) are considered. The polymer is made of a single network with $N = 50$.

The vertical reaction force at the restraint vs. time for the three considered polymers and for a purely elastic polymer is illustrated in fig. 5.5(a). The effect of the dynamic cross-links is to induce a stress relaxation, which becomes more pronounced as the deactivation rate increases. In fig. 5.5(b) the stress σ_x vs. time evaluated in the upper part of the constrained section of the beam is illustrated. Again, the stress relaxation

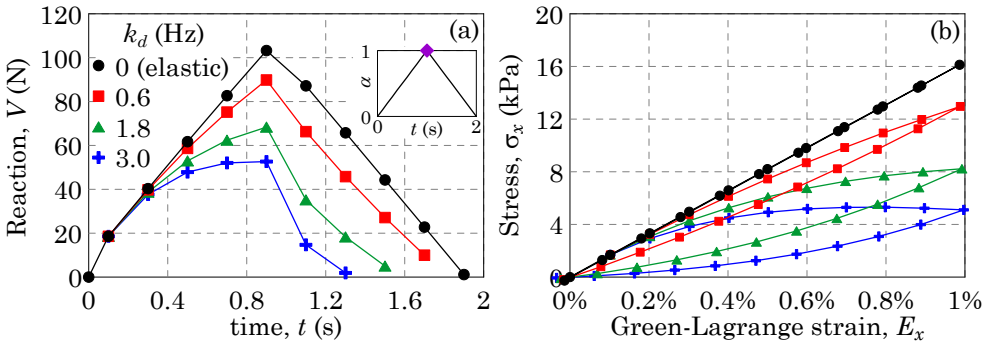

Figure 5.5: *FE parametric test on a cantilever beam made of polymers with dynamic cross-links. Vertical reaction force in the clamped section vs. time (a). Cauchy stress σ_x vs. Green-Lagrange strain E_x for the different values of the deactivation rate k_d; the stress and the strain are evaluated in the point highlighted in fig. 5.6* (b).

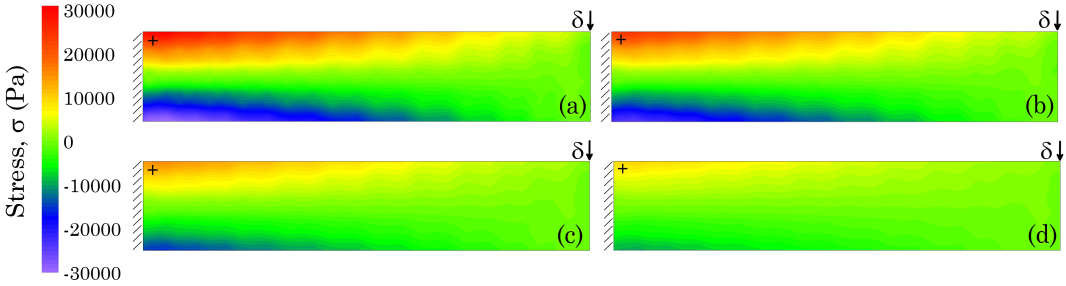

Figure 5.6: *FE parametric test on a cantilever beam made of polymers with dynamic cross-links. Contour plot of the Cauchy stress σ_x for $\delta = \overline{\delta} = 0.3\,\mathrm{m}$ (see insert of fig. 5.5). $k_d = 0$ (elastic case) (a), $k_d = 0.6\,\mathrm{Hz}$ (b), $k_d = 1.8\,\mathrm{Hz}$ (c), $k_d = 3\,\mathrm{Hz}$ (d).*

is clearly evident. The contour plot of the axial stress σ_x in the beams, for the four assumed values of the deactivation rates k_d, are illustrated in fig. 5.6 at the time instant $t = 1$ s (i.e. when the load factor is equal to $\alpha = 1$ and the applied displacement is equal to δ). By increasing the deactivation rate, the stress decreases in all the points of the beam.

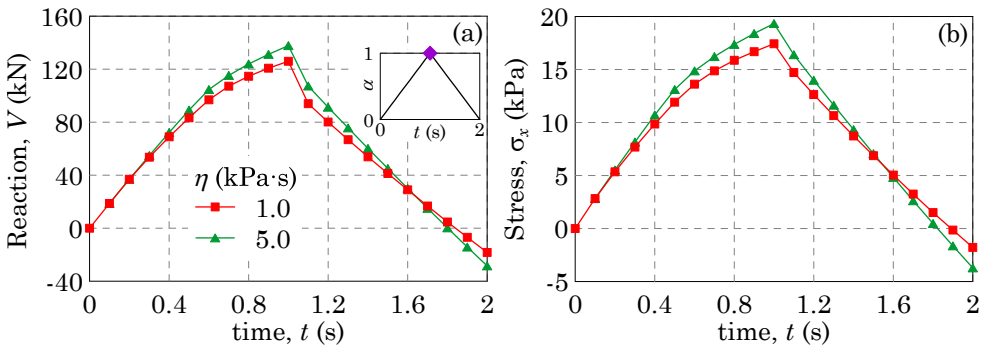

Figure 5.7: *FE parametric test on a cantilever beam made of polymers with unfolding chains. Vertical reaction force in the clamped section vs. time (a). Cauchy stress σ_x vs. time for the two values of the unfolding parameter η (b); the stress is evaluated in the point highlighted in fig. 5.8.*

5.5.2 FE analysis of a beam made of polymers with unfolding chains

In the present case, the material composing the beam is assumed to be a polymer whose chains are subjected to the unfolding phenomenon. Two polymers, characterized by different values of the viscosity-like unfolding parameter η ($\eta = 1.0$ kPa·s and $\eta = 5.0$ kPa·s, respectively) are considered. The polymer is made of a single network with folded length $N_0 = 50$ and physical length $N_p = 70$ (see §3.5).

The vertical reaction force at the restraint vs. time for the considered polymers is illustrated in fig. 5.5(a). The effect of the unfolding phenomenon is that to induce a stress relaxation, which becomes more pronounced for low values of the viscosity-like parameter η, since the unfolding process takes place more becomes more rapidly. During the unloading phase of the displacement cycle, the resulting reaction force becomes negative, which means that it is necessary to push the beam with a force directed along $+y$ to recover the original position of the control point, i.e. $\delta = 0$. In fig. 5.5(b) the stress σ_x vs. time evaluated in the upper part of the constrained section of the beam is illustrated. The stress changes sign during the last part of the load cycle, according to the sign of the reaction.

The contour plot of the axial stress σ_x in the beams, for the two assumed values of the unfolding parameter η, are illustrated in fig. 5.8 at the time instant $t = 1$ s (i.e. when the load factor is equal to $\alpha = 1$). By reducing the viscosity parameter, the unfolding

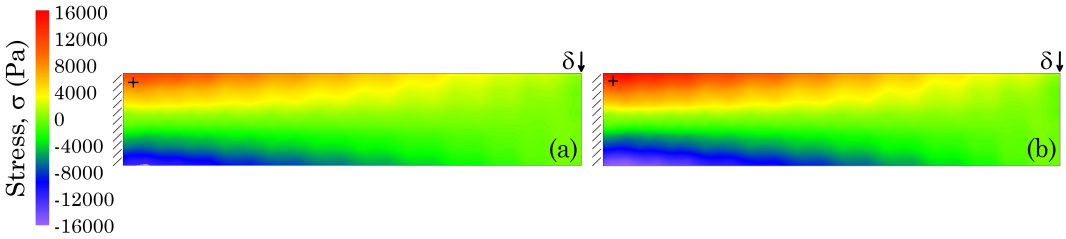

Figure 5.8: *FE parametric test on a cantilever beam made of polymers with unfolding chains. Contour plot of the Cauchy stress* σ_x *for* $\delta = \overline{\delta} = 0.3\,\mathrm{m}$ *(see insert of fig. 5.7).* $\eta = 1.0\,\mathrm{kPa}\cdot\mathrm{s}$ *(a),* $\eta = 5.0\,\mathrm{kPa}\cdot\mathrm{s}$ *(b).*

mechanism becomes faster and the stress decreases.

5.5.3 FE analysis of a beam made of polymers with breakable chains

In the present case, the effect of the failure of the polymer chains is considered in the FE analysis of the beam. Two different polymers, with different values of normalized bond strength $\overline{w}/k_BT$, i.e. 32.59 and 32.08, are considered. The polymer is made of a single network with $N = 50$.

The evolution of the vertical reaction force in time for the two considered beams and for a beam made of an elastic polymer is illustrated in fig. 5.9. The effect of the chains failure produces a reduction of the bearing capacity of the material; the reduction is more pronounced for low values of the bond strength. The time evolution of the horizontal stress in a representative point of the beam (i.e. in the upper part of the constrained section, as indicated in fig. 5.10) is showed in fig. 5.9(b). For the same applied displacement, the material with the lower bond strength ($\overline{w} = 32.08\,k_BT$) shows lower stress than the material with the higher bond strength ($\overline{w} = 32.59\,k_BT$). In fig. 5.10 the contour plot of the axial stress σ_x in the two beams with breakable chains for the same applied displacement δ (i.e. for $\alpha = 1$ at $t = 1$ s) is represented. The beam with lower bond strength shows lower values of the stress with respect to the beam with the higher bond strength. It is worth noting that the stress reduction is the same for the tensile part and for the compressed part of the beam. In fig. 5.11 the contour plot of the damage parameter $\mathscr{D}$ (see eq. (3.38)) for the stress levels depicted in fig. 5.10 is represented; the beam with higher bond strength (fig. 5.11(a)) shows lower damage values than the beam with low strength (fig. 5.11(b)), furthermore the damage becomes more pronounced in the region close to the beam's constraint.

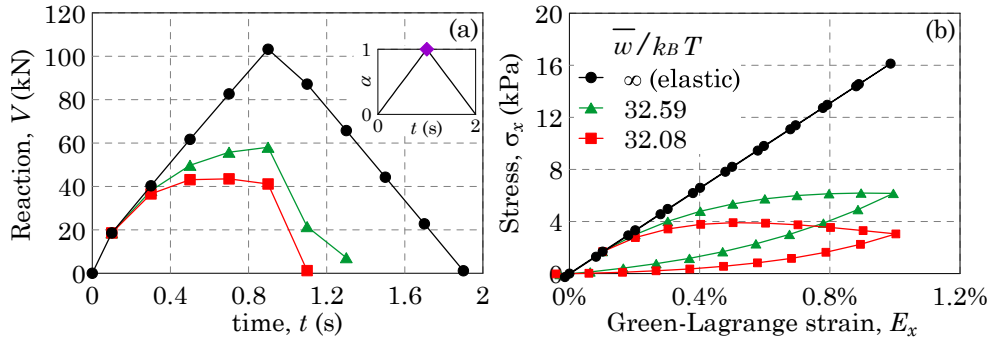

Figure 5.9: *FE parametric test on three beams made of polymers with breakable chains. Reaction force vs. time (a) and axial stress vs. Green-Lagrange strain (b) for the different values of the normalized bond strength $\overline{w}/k_BT$; the stress and the strain are evaluated in the point highlighted in fig. 5.10.*

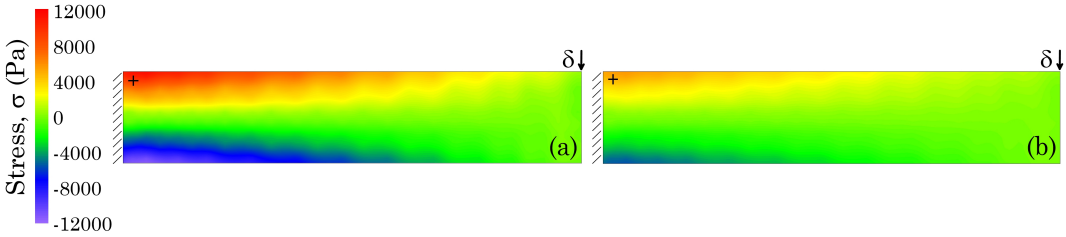

Figure 5.10: *FE parametric test on two beams made of polymers with breakable chains. Contour plot of the Cauchy stress σ_x for $\delta = 0.3\,\mathrm{m}$ ($\alpha = 1$ at $t = 1\,\mathrm{s}$, see fig. 5.5): polymer with normalized bond strength $\overline{w}/k_BT = 32.59$ (a) and 32.08 (b).*

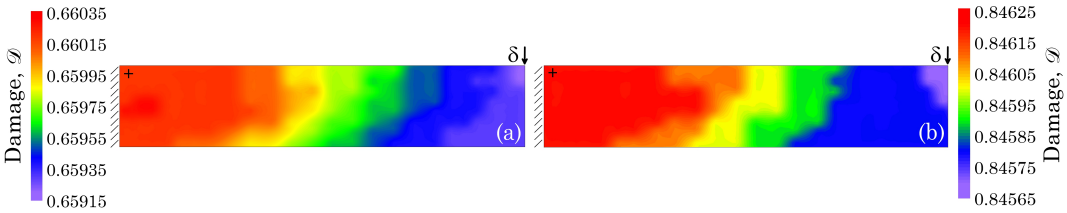

Figure 5.11: *FE parametric test on two beams made of polymers with breakable chains. Contour plot of the damage parameter $\mathscr{D}$ for $\delta = 0.3\,\mathrm{m}$ ($\alpha = 1$ at $t = 1\,\mathrm{s}$, see fig. 5.5): polymer with normalized bond strength $\overline{w}/k_BT = 32.59$ (a) and 32.08 (b).*

5.6 Conclusions

The solution of the boundary value problem in a continuum body made of a responsive material capable of adsorbing a fluid, involves the evaluation, at any time instants, of the displacement and of the strain and stress fields, as well as the solvent concentration and the active fraction of mechanophores in each point of the body.

In the present chapter, a Finite Element formulation implementing the proposed constitutive model, has been presented. The non-linear discretized problem has been numerically solved through the Newton-Raphson approach by using the initial stiffness method. The formulation considers the large deformations theory and takes into account for the geometric the geometric stiffness due to the large displacements assumption. The 3D chains configuration space is discretized (at each FE Gauss point) through a grid of points whose configurational coordinates are defined according to the Gaussian quadrature rule. The evaluation of the stress state (accounting for the presence of dynamic cross-links, damage and chains unfolding) and of the active fraction of mechanophores is numerically evaluated in the discretized configuration space.

Finally, the results of some parametric FE analysis, accounting for the main involved phenomena, are illustrated. The effects induced by the variation of the main physical parameters of the problem have been studied and discussed; the obtained results are clearly consistent with the physics of the problem and outline the reliability of the proposed approach.

CHAPTER 6

FE ANALYSIS PERFORMED WITH THE PROPOSED MODEL

The FE formulation presented in chap. 5 is used henceforth to study, through the proposed constitutive model, real cases involving structural elements. The mechanical behavior of traditional polymers, commonly used in industrial applications, can be simulated by taking into account the main related aspects, such as the time-dependent response, damage and irreversible deformations. Furthermore, the enhanced features of stimuli-responsive polymers can be accounted for through the evaluation of the mechanophores activation triggered by mechanical or chemical stimuli.

In the present chapter, two experimental tests are simulated through the FE formulation implementing the proposed constitutive model: the first considered case is a series of tensile test, performed with different loading rates on thermoplastic polyolefin (TPO) samples, while the second case is a three-point bending test carried on an elastomeric sample enriched with a self-diagnostic molecular probe.

6.1 Tensile tests on a TPO samples

Thermoplastic polyolefins (TPO) are common polymeric materials used in high consumption commodities, for example in the automotive field. They are made of a blend of a thermoplastic polymer (usually an elastomer) and a filler.

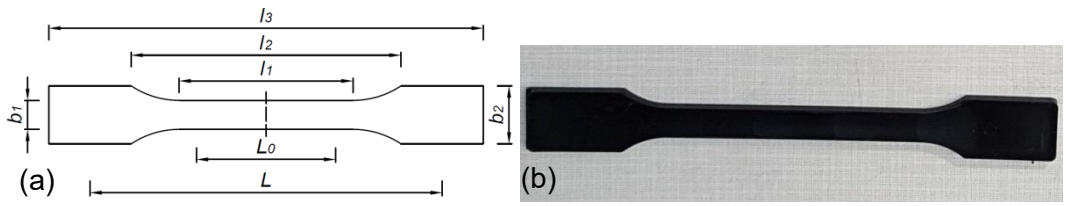

Figure 6.1: *TPO sample. Main dimensions defined in ISO 527 (a) and picture of a sample (b).*

A series of tensile tests has been conducted on TPO specimens in order to investigate the mechanical properties of the material, by taking into account for the strain rate effect. The samples have been manufactured through molding in a dog-bone shape, according to the standards ISO 527 (see fig. 6.1). The tensile tests were performed in the Strength of Materials Laboratory of Polytechnic University of Timisoara by using a Zwick Proline Z005 testing machine, having a maximum load capacity of 5 kN. The strain was measured with an extensometer with length gauge of 30 mm and the elastic modulus has been also experimentally determined. Because of the large deformations reached by the specimens, the extensometer was removed during the tests after a 10 mm elongation, while the tests were continued up to break. The sample's deformation was measured by the crosshead travel, by recording the grip-to-grip separation, starting from the initial length equal to 90 mm. The tests were performed under displacement control at three different loading speeds, i.e. 4, 40 and 400 mm/min; three TPO samples after the tensile test are shown in fig. 6.2 together with an as-built sample. The tests were performed at the room temperature of 294 K.

FE analysis simulating the tensile test are carried out with the code presented in chap. 5. In fig. 6.3 the adopted mesh, composed of 75 four-nodes bilinear elements with 2×2 integration points, is illustrated. The analysis are performed in plane stress condition. The polymer is assumed to be incompressible and made of a single network; the elastic modulus, measured through the test, is equal to 629.2 MPa.

In fig. 6.4(a) the measured Cauchy true stress vs. Hencky true strain (see eq. (2.5)) curves for the three adopted displacement rates are reported. The stress vs. strain relationship show an initial highly stiffness branch trend in the early stage of the deformation, followed by the characteristic J-shape curve. Because of the viscoelastic nature of the material, the stiffness increases with the strain rate.

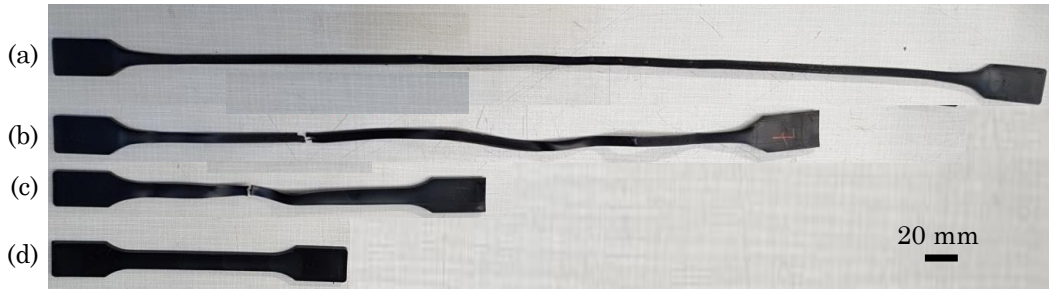

Figure 6.2: *TPO samples after the tensile test. Sample tested with displacement rate equal to 4 mm/min (a), 40 mm/min and 400 mm/min (c) compared to an integer sample (d). The sample (a) did not reach the failure during the test.*

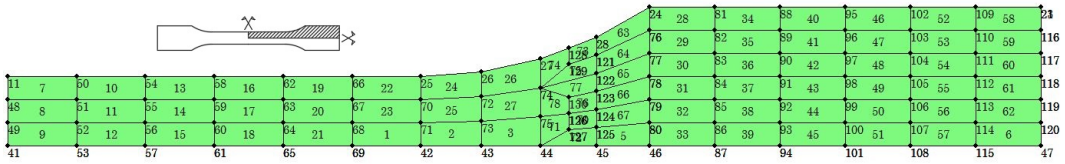

Figure 6.3: *FE mesh of the TPO sample.*

In fig. 6.4(b) the Cauchy stress vs. true strain curves obtained through the FE analysis are reported. The values of the material's parameter adopted to fit the experimental curves are the following: bond strength $\overline{w}/k_BT = 39.901$, number of Kuhn segments per chain $N = 55$, segments length $b = 1\,\text{nm}$. Three different values of the deactivation rate are assumed, i.e. $k_d = 6.022 \cdot 10^{-7}\,\text{Hz}$ for the displacement rate $\dot{\delta} = 400$ mm/min, $k_d = 8.310 \cdot 10^{-5}\,\text{Hz}$ for $\dot{\delta} = 40$ mm/min and $k_d = 8.732 \cdot 10^{-4}\,\text{Hz}$ for $\dot{\delta} = 4$ mm/min.

The FE analysis captures the mechanical response of the TPO samples, in particular the viscoelastic behavior and the damage of the material. The simulations suggest that a dependency of the cross-links deactivation rate on the applied strain rate exists.

6.2 Strain field detection in elastomers with molecular probes

The inclusion of a proper designed molecular probe in the micro-structure of a polymer allows for the visualization of the strain field and the detection of damage due to

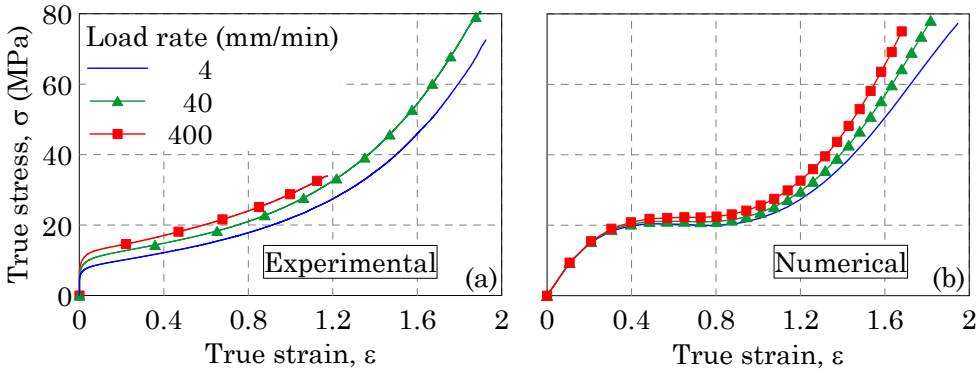

Figure 6.4: *Tensile test on TPO samples. Cauchy stress vs. true strain curves experimentally measured (a) and numerically obtained (b).*

excessive deformations. Mechanophores-based molecular probes are activated by a sufficiently high values of the force in the polymer's chain, which triggers a detectable signal, such as a light emission [14, 40].

In the case reported in [57], we have performed an experimental test in which a fluorescent molecular probe is introduced in a Polydimethylsiloxane (PDMS) elastomer in order to enable the detection of the strain field in the material. Pre-notched samples made of such a self-diagnostic polymer were subjected to a three-point bending test; after the test, the fluorescence field in the elastomer were measured through a special camera under the UV light. The samples' geometry is depicted in fig. 6.5(a); the main dimensions are: span length $L = 110$ mm, height $H = 25$ mm, thickness $t = 2.5$ mm and initial notch's depth $c = 5$ mm. The test was carried out by controlling the displacement δ, which was increased at constant rate equal to 0.05 mm/s. A picture of the sample after the three-point bending test is shown in fig. 6.5(b); a crack starting from the notch is clearly visible.

A FE simulation of the three-point bending test is carried out with the code presented in chap. 5. The analysis is performed in plane stress condition. The adopted mesh is illustrated in fig. 6.6(a); it is composed by 131 four-nodes bilinear elements with 2×2 integration points; the notch (visible in the insert of the figure) has a tip radius of 0.2 mm. The material is assumed to be elastic and incompressible (no damage or strain rate effects are considered), with a shear modulus $\mu = 3$ MPa and $N = 10$

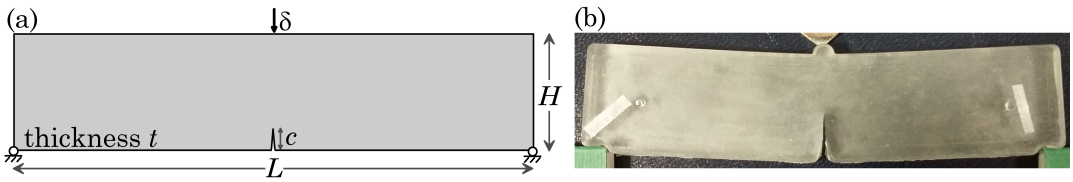

Figure 6.5: *PDMS pre-notched sample. Geometry (a) and picture of a sample taken after the three-point bending test (b). The dimensions indicated in (a) are: span length* $L = 110\,\text{mm}$*, height* $H = 25\,\text{mm}$*, thickness* $t = 2.5\,\text{mm}$*, initial notch's depth* $c = 5\,\text{mm}$.

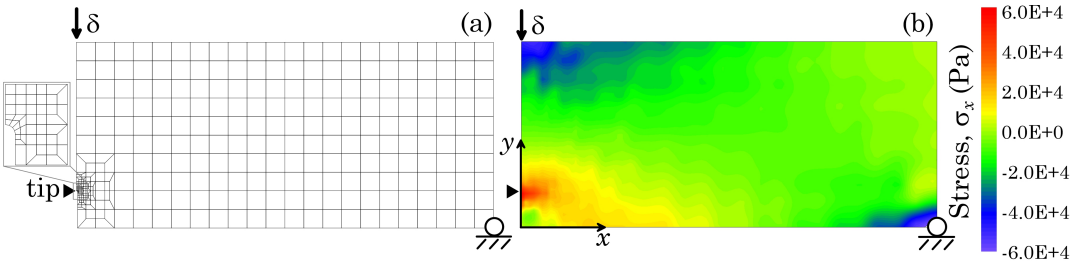

Figure 6.6: *FE simulation of the three-point bending test of a PDMS sample containing molecular probes. Adopted mesh (a) and contour plot of the Cauchy stress* σ_x *for an imposed displacement* $\delta = 5\,\text{mm}$.

Kuhn segments with length b = 1 nm per polymer chain. The temperature is assumed to be T = 300 K and no fluid solvent is present. The mechanophores representing the molecular probe are characterized by the following parameters: size variation upon switching $\delta s_{sw} = 5b$, energy barriers for the activation reaction $\Delta G_{A0} = 4.82 \cdot 10^4$ J/mol and for the deactivation reaction $\Delta G_{D0} = 1.51 \cdot 10^{-1}$ J/mol, activation and deactivation frequencies $C_A = 6.02 \cdot 10^1$ Hz and $C_D = 6.02 \cdot 10^4$ Hz, respectively. The volume fraction of the mechanophore is assumed to be α_{sw} = 2%. In fig. 6.6(b) the contour plot of the Cauchy stress σ_x for δ = 5 mm is shown; the stress concentration near the notch tip is clearly visible.

The contour plot of the fraction $\overline{h}$ of active (i.e. luminescent) mechanophores, evaluated according to the model proposed in chap. 4, is illustrated for two values of the applied displacement δ = 2.5 mm and δ = 5 mm, in fig. 6.7. Since the stress concentration promotes the switching of the mechanophores, the highest value of the active fraction is localized in a small region of the sample near the notch tip; meanwhile, in the rest of the sample far from the tip, the active fraction reaches lower values,

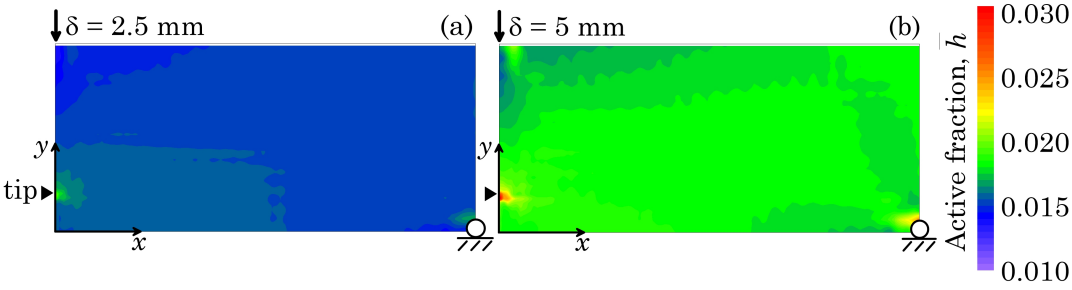

Figure 6.7: *FE simulation of the three-point bending test of a PDMS sample containing molecular probes. Contour plot of the active fraction $\overline{h}$ of mechanophores for an imposed displacement $\delta = 2.5\,\text{mm}$ (a) and $\delta = 5\,\text{mm}$ (b).*

mainly due to the spontaneous activation. The light emission detected in the stress-free material can be seen as a background noise in the fluorescent signal.

The measured fluorescent signal is normalized with respect to the maximum value expected for the given concentration of molecular probes in the elastomer, such that the normalized fluorescence is equal to 1 when all the molecular probes are activated. By assuming that each molecular probe emits the same amount of light, the normalized fluorescence is proportional to the fraction of active molecular probes $\overline{h}$.

In fig. 6.8(a), the normalized fluorescence intensity measured near the notch tip is compared to the active fraction $\overline{h}$ obtained from the FE analysis. The notch tip, observed with a microscope, is approximately circular with radius equal to about 0.2 mm. The fluorescence have been measured with a microscope operating at the UV wavelength; the highest values occurred ahead the notch tip in a region whose extension is 2÷3 times the notch's radius. The region with the highest active fraction $\overline{h}$, evaluated through the FE analysis, has an extension similar to the experimental one. In fig. 6.8(b) the evolution of the active fraction, evaluated with the FE analysis in the Gauss point closest to the notch's tip, is reported vs. the imposed displacement δ. The evolution of $\overline{h}$ appears to be approximately linear with the imposed displacement and starts from a value greater than zero according to the kinetic equilibrium (4.1) (see [19]).

In fig. 6.8(c), a picture of the fluorescent intensity under UV light near to the notch tip has been reported. It is clearly visible, directly ahead to the tip, a white region caused by the high concentration of emitting mechanophores. The extension of such a fluorescent zone can be related to the critical energy release rate of the material,

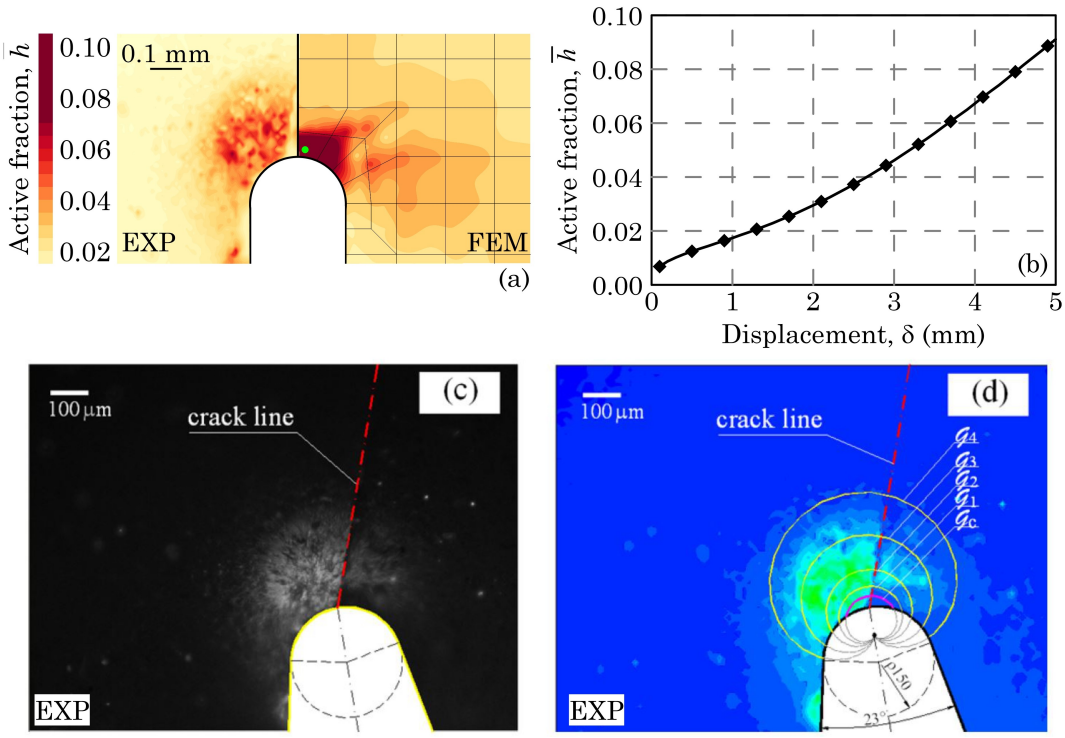

Figure 6.8: *Three-point bending test of a PDMS sample containing molecular probes. Contour plot of the measured fluorescence field near to the notch's tip compared to the active fraction $\bar{h}$ evaluated through a FE analysis (a). Evolution of the active fraction in the Gauss point closest to the notch tip vs. imposed displacement δ (see green dot in (a)) (b). Picture of the fluorescent intensity under UV light near to the notch tip (c). Comparison between the observed fluorescence and the iso-hydrostatic strain curves evaluated for different values of the surface energy: $\mathcal{G}_c$ = 110 N/m (critical energy for material failure), $\mathcal{G}_1$ = 83 N/m, $\mathcal{G}_2$ = 55 N/m, $\mathcal{G}_3$ = 27 N/m and $\mathcal{G}_4$ = 11 N/m (d). The images (c) and (d) are reported from [57].*

as it can be appreciated in fig. 6.8(d), in which the extension of the fluorescent zone is compared to the iso-hydrostatic strain curves evaluated for different values of the surface energy $\mathscr{G}$, i.e. $\mathscr{G}_c$ = 110 N/m (critical energy for material failure), $\mathscr{G}_1$ = 83 N/m, $\mathscr{G}_2$ = 55 N/m, $\mathscr{G}_3$ = 27 N/m and $\mathscr{G}_4$ = 11 N/m) [57].

6.3 Conclusions

In the present chapter, two mechanical tests have been simulated through FE analysis by adopting the proposed physics-based model.

Tensile tests on thermoplastic polyolefin (TPO) loaded at three different displacement rates have been experimentally performed. The tests have been simulated with FE analysis providing the mechanical response of the material in terms of stress vs. stretch curve. Furthermore, a three-point bending test on an elastomeric sample enriched with a self-diagnostic molecular probe have been performed. When activated by the polymer chain forces, the considered molecular probes change their optical properties (within the UV-light wavelength interval), allowing the visualization of the strain field in the material and the detection of localized damage. The mechanical test has been simulated with FE analysis in order to compare the calculated activation level of the molecular probes with the measured UV fluorescence.

The results have shown that the FE approach is able to reproduce the main aspects involved in the mechanical behavior of polymeric materials, such as viscoelasticity and damage, and also to evaluate quantitatively the activation of responsive molecules, sensible to mechanical and/or chemical stimuli, added to a polymer network.

Conclusions

The mechanics of polymers can be usefully adopted to describe the response of a variety of materials, such as elastomers, plastics, soft tissues and biological matters. Several phenomena play a role in the definition of the so-called «entropic elasticity» of polymers: damage, network entanglement, dynamic bond and bond exchange, swelling, etc. A comprehensive constitutive model for such a class of materials is useful for the analysis of polymer-based structural elements and for the design of new polymers.

In the present thesis, a physics-based model has been developed to capture the mechanical response of polymers and polymer-like materials, by accounting for the main physical phenomena involved. The proposed theory is based on a thermodynamic description of the entropic elasticity of the polymer networks, based on the evolution of the network's chains configuration. The time-dependent mechanical response is represented through two different irreversible phenomena that can be encountered in real polymers: through the concept of dynamic cross-links and through the unfolding of the entangled network's chains. The material's damage, due to the failure of the polymer chains, is taken into account by limiting the chains' bond strength.

Furthermore, the study focused on polymers with enhanced features, commonly identified as «*functional*» or «*stimuli-responsive*». The presence in the polymer network of properly designed stimuli-responsive molecules («*mechanophores*») provides detectable effects at the meso-scale level, leading to a so-called «*responsive material*». The proposed constitutive model is enriched by considering the effect of switchable mechanophores whose activation can be triggered by both chemical and/or mechanical actions; since the chemical stimulus generally requires a fluid phase carrying the chemical agent, the fluid uptake and the related swelling phenomenon have been also accounted for.

The theoretical model has been implemented in a in-house Finite Element code formulated by accounting for the large displacements and the large deformation effects typical of this class of materials. Some representative numerical analysis have been

performed with the developed FE code, as well as some simulation of real experimental cases.

The proposed approach have shown the capability to capture the main physical phenomena and reproduce the complex mechanical response of polymeric materials.

Future advances of the proposed theory could be, among others, the introduction of: temperature-driven effects (e.g. glass transition); topological constraints to the chains motions; force-dependence of the dynamic cross-link phenomenon; spatial description of the swelling mechanism and its dependence on temperature, strain rate and mechanophores activation; uncertainties in the distribution of the bond's strength in the polymer; reversibility of the unfolding phenomenon in some networks; development of a theory for electric field-polymer interaction (*Electroactive Polymers*, EAPs) in presence of mechanophores; mechanical model of stimuli-responsive polymers containing active molecules sensible to different stimuli such as magnetic field, light, etc.

BIBLIOGRAPHY

[1] H. ALEXANDER, *A constitutive relation for rubber-like materials*, International Journal of Engineering Science, 6 (1968), pp. 549–563.

[2] S. ARRHENIUS, *Über die dissociationswärme und den einfluss der temperatur auf den dissociationsgrad der elektrolyte*, Zeitschrift für physikalische Chemie, 4 (1889), pp. 96–116.

[3] E. ARRUDA AND M. BOYCE, *A three-dimensional constitutive model for the large stretch behavior of rubber elastic materials*, Journal of the Mechanics and Physics of Solids, 41 (1993), pp. 389–412.

[4] I. BAHAR AND B. ERMAN, *Investigation of local motions in polymers by the dynamic rotational isomeric state model*, Macromolecules, 20 (1987), pp. 1368–1376.

[5] I. BAHAR, B. ERMAN, AND L. MONNERIE, *Kinematics of polymer chains with freely rotating bonds in a restrictive environment. 1. theory*, Macromolecules, 25 (1992), pp. 6309–6314.

[6] J. BALL, *Convexity conditions and existence theorems in nonlinear elasticity*, Archive for rational mechanics and Analysis, 63 (1976), pp. 337–403.

[7] R. BALL, M. DOI, S. EDWARDS, AND M. WARNER, *Elasticity of entangled networks*, Polymer, 22 (1981), pp. 1010–1018.

[8] D. BANORIYA, R. PUROHIT, AND R. DWIVEDI, *Advanced application of polymer based biomaterials*, Materials Today: Proceedings, 4 (2017), pp. 3534–3541.

[9] M. BEATTY, *An average-stretch full-network model for rubber elasticity*, Journal of Elasticity, 70 (2003), pp. 65–86.

[10] J. BEMIS, B. AKHREMITCHEV, AND G. WALKER, *Single polymer chain elongation by atomic force microscopy*, Langmuir, 15 (1999), pp. 2799–2805.

[11] J. BERGSTRÖM AND M. BOYCE, *Constitutive modeling of the large strain time-dependent behavior of elastomers*, Journal of the Mechanics and Physics of Solids, 46 (1998), pp. 931–954.

[12] V. BIDERMAN, *Calculation of rubber parts*, Rascheti na prochnost, 40 (1958).

[13] G. BINNIG, C. QUATE, AND C. GERBER, *Atomic force microscope*, Physical review letters, 56 (1986), p. 930.

[14] A. BLACK, J. LENHARDT, AND S. CRAIG, *From molecular mechanochemistry to stress-responsive materials*, Journal of Materials Chemistry, 21 (2011), pp. 1655–1663.

[15] N. BOUKLAS AND R. HUANG, *Swelling kinetics of polymer gels: comparison of linear and nonlinear theories*, Soft Matter, 8 (2012), pp. 8194–8203.

[16] M. BOYCE AND E. ARRUDA, *Constitutive models of rubber elasticity: a review*, Rubber chemistry and technology, 73 (2000), pp. 504–523.

[17] J. BRANTLEY, K. WIGGINS, AND C. BIELAWSKI, *Polymer mechanochemistry: the design and study of mechanophores*, Polymer International, 62 (2013), pp. 2–12.

[18] R. BRIGHENTI AND F. ARTONI, *A fracture mechanics based model for the analysis of seal effectiveness*, Fatigue & Fracture of Engineering Materials & Structures, 39 (2016), pp. 1445–1460.

[19] R. BRIGHENTI AND F. ARTONI, *Mechanical modelling of self-diagnostic polymers*, Procedia Structural Integrity, 13 (2018), pp. 819–824.

[20] R. BRIGHENTI, F. ARTONI, AND M. COSMA, *Mechanics of active mechanochemical responsive polymers*, in IOP Conference Series: Materials Science and Engineering, vol. 416, IOP Publishing, 2018, p. 012080.

[21] R. BRIGHENTI, F. ARTONI, AND M. COSMA, *Mechanics of active mechanochemical responsive polymers*, in IOP Conference Series: Materials Science and Engineering, vol. 416, IOP Publishing, 2018, p. 012080.

[22] R. BRIGHENTI, F. ARTONI, AND M. COSMA, *Mechanics of materials with embedded unstable molecules*, International Journal of Solids and Structures, (2018).

[23] R. BRIGHENTI, F. ARTONI, F. VERNEREY, M. TORELLI, A. PEDRINI, I. DOMENICHELLI, AND E. DALCANALE, *Mechanics of responsive polymers via conformationally switchable molecules*, Journal of the Mechanics and Physics of Solids, 113 (2018), pp. 65–81.

[24] R. BRIGHENTI, A. CARPINTERI, AND F. ARTONI, *Defect sensitivity to failure of highly deformable polymeric materials*, Theoretical and Applied Fracture Mechanics, 88 (2017), pp. 107–116.

[25] R. BRIGHENTI, A. CARPINTERI, AND F. ARTONI, *Fracture toughness of highly deformable polymeric materials*, Procedia Structural Integrity, 3 (2017), pp. 18–24.

[26] R. BRIGHENTI, A. CARPINTERI, F. ARTONI, AND I. DOMENICHELLI, *Defect sensitivity of highly deformable polymeric materials with different intrinsic qualities at various strain rates*, Fatigue & Fracture of Engineering Materials & Structures, 41 (2018), pp. 806–820.

[27] R. BRIGHENTI, A. SPAGNOLI, A. CARPINTERI, AND F. ARTONI, *Defect tolerance in soft materials*, Procedia Structural Integrity, 2 (2016), pp. 2788–2795.

[28] R. BRIGHENTI, A. SPAGNOLI, A. CARPINTERI, AND F. ARTONI, *Notch effect in highly deformable material sheets*, Thin-Walled Structures, 105 (2016), pp. 90–100.

[29] R. BRIGHENTI, A. SPAGNOLI, A. CARPINTERI, AND F. ARTONI, *Defect tolerance at various strain rates in elastomeric materials: An experimental investigation*, Engineering Fracture Mechanics, 183 (2017), pp. 79–93.

[30] R. BRIGHENTI, F. VERNEREY, AND F. ARTONI, *Rate-dependent failure mechanism of elastomers*, International Journal of Mechanical Sciences, 130 (2017), pp. 448–457.

[31] C. BUSTAMANTE, Y. CHEMLA, N. FORDE, AND D. IZHAKY, *Mechanical processes in biochemistry*, Annual review of biochemistry, 73 (2004), pp. 705–748.

[32] Y. CAO AND H. LI, *Polyprotein of gb1 is an ideal artificial elastomeric protein*, Nature materials, 6 (2007), p. 109.

[33] F. CARAVENNA, *Random walk models and probabilistic techniques for inhomogeneous polymer chains*, PhD thesis, 2005.

[34] A. CARMICHAEL AND H. HOLDAWAY, *Phenomenological elastomechanical behavior of rubbers over wide ranges of strain*, Journal of Applied Physics, 32 (1961), pp. 159–166.

[35] Y. CHAN, R. HAVERKAMP, AND J. HILL, *Force-extension formula for the worm-like chain model from a variational principle*, Journal of theoretical biology, 262 (2010), pp. 498–504.

[36] M. CHAUDHURY, *Rate-dependent fracture at adhesive interface*, The Journal of Physical Chemistry B, 103 (1999), pp. 6562–6566.

[37] M. CHEN, Y. TAN, AND B. WANG, *General invariant representations of the constitutive equations for isotropic nonlinearly elastic materials*, International Journal of Solids and Structures, 49 (2012), pp. 318–327.

[38] M. CHI-SING AND Z. GUO, *A basis-free formula for time rate of hill's strain tensors*, International journal of solids and structures, 30 (1993), pp. 2819–2842.

[39] J. CHUNG, A. KUSHNER, A. WEISMAN, AND Z. GUAN, *Direct correlation of single-molecule properties with bulk mechanical performance for the biomimetic design of polymers*, Nature materials, 13 (2014), p. 1055.

[40] F. CIARDELLI, G. RUGGERI, AND A. PUCCI, *Dye-containing polymers: methods for preparation of mechanochromic materials*, Chemical Society Reviews, 42 (2013), pp. 857–870.

[41] S. COCCO, J. MARKO, R. MONASSON, A. SARKAR, AND J. YAN, *Force-extension behavior of folding polymers*, The European Physical Journal E, 10 (2003), pp. 249–263.

[42] D. CRESSEY, *The plastic ocean*, Nature, 536 (2016), pp. 263–265.

[43] S. DAI, P. RAVI, AND K. TAM, *ph-responsive polymers: synthesis, properties and applications*, Soft Matter, 4 (2008), pp. 435–449.

[44] E. DARABI AND M. ITSKOV, *A simple and accurate approximation of the inverse langevin function*, Rheologica Acta, 54 (2015), pp. 455–459.

[45] P. DE GENNES, *Reptation of a polymer chain in the presence of fixed obstacles*, The journal of chemical physics, 55 (1971), pp. 572–579.

[46] P. DE GENNES AND L. LEGER, *Dynamics of entangled polymer chains*, Annual Review of Physical Chemistry, 33 (1982), pp. 49–61.

[47] M. DOI, *Gel dynamics*, Journal of the Physical Society of Japan, 78 (2009), pp. 052001–052001.

[48] M. DOI, *Soft matter physics*, Oxford University Press, 2013.

[49] S. EDWARDS, *The statistical mechanics of polymers with excluded volume*, Proceedings of the Physical Society, 85 (1965), p. 613.

[50] S. EDWARDS AND T. VILGIS, *The tube model theory of rubber elasticity*, Reports on Progress in Physics, 51 (1988), p. 243.

[51] D. FELDMAN, *Polymer history*, Designed monomers and polymers, 11 (2008), pp. 1–15.

[52] M. FIXMAN, *Excluded volume in polymer chains*, The Journal of Chemical Physics, 23 (1955), pp. 1656–1659.

[53] P. FLORY, *Statistical thermodynamics of random networks*, Proc. R. Soc. Lond. A, 351 (1976), pp. 351–380.

[54] P. FLORY AND B. ERMAN, *Theory of elasticity of polymer networks. 3*, Macromolecules, 15 (1982), pp. 800–806.

[55] P. FLORY AND J. REHNER, *Statistical mechanics of cross-linked polymer networks i. rubberlike elasticity*, The Journal of Chemical Physics, 11 (1943), pp. 512–520.

[56] P. FLORY AND J. REHNER, *Statistical mechanics of cross-linked polymer networks ii. swelling*, The Journal of Chemical Physics, 11 (1943), pp. 521–526.

[57] A. FRÜH, F. ARTONI, R. BRIGHENTI, AND E. DALCANALE, *Strain field self-diagnostic poly (dimethylsiloxane) elastomers*, Chemistry of Materials, 29 (2017), pp. 7450–7457.

[58] A. GENT, *A new constitutive relation for rubber*, Rubber chemistry and technology, 69 (1996), pp. 59–61.

[59] A. GENT AND A. THOMAS, *Forms for the stored (strain) energy function for vulcanized rubber*, Journal of Polymer Science Part A: Polymer Chemistry, 28 (1958), pp. 625–628.

[60] R. GEYER, J. JAMBECK, AND K. LAW, *Production, use, and fate of all plastics ever made*, Science advances, 3 (2017), p. e1700782.

[61] A. GHATAK, K. VORVOLAKOS, H. SHE, D. MALOTKY, AND M. CHAUDHURY, *Interfacial rate processes in adhesion and friction*, The Journal of Physical Chemistry B, 104 (2000), pp. 4018–4030.

[62] J. GONG, Y. KATSUYAMA, T. KUROKAWA, AND Y. OSADA, *Double-network hydrogels with extremely high mechanical strength*, Advanced materials, 15 (2003), pp. 1155–1158.

[63] G. GREST AND K. KREMER, *Statistical properties of random cross-linked rubbers*, Macromolecules, 23 (1990), pp. 4994–5000.

[64] O. GÜLTEKIN, G. SOMMER, AND G. HOLZAPFEL, *An orthotropic viscoelastic model for the passive myocardium: continuum basis and numerical treatment*, Computer methods in biomechanics and biomedical engineering, 19 (2016), pp. 1647–1664.

[65] E. GUTH AND H. MARK, *Zur innermolekularen, statistik, insbesondere bei kettenmolekiilen i*, Monatshefte für Chemie und verwandte Teile anderer Wissenschaften, 65 (1934), pp. 93–121.

[66] P. HÄNGGI, P. TALKNER, AND M. BORKOVEC, *Reaction-rate theory: fifty years after kramers*, Reviews of modern physics, 62 (1990), p. 251.

[67] L. HART-SMITH, *Elasticity parameters for finite deformations of rubber-like materials*, Zeitschrift für angewandte Mathematik und Physik ZAMP, 17 (1966), pp. 608–626.

[68] C. HICKENBOTH, J. MOORE, S. WHITE, N. SOTTOS, J. BAUDRY, AND S. WILSON, *Biasing reaction pathways with mechanical force*, Nature, 446 (2007), p. 423.

[69] R. HILL, *Constitutive inequalities for isotropic elastic solids under finite strain*, Proceedings of the Royal Society of London. Series A, Mathematical and Physical Sciences, (1970), pp. 457–472.

[70] G. HOLZAPFEL, *Nonlinear Solid Mechanics: A Continuum Approach for Engineering*, John Wiley & Sons, Ltd, 2000.

[71] W. HONG, X. ZHAO, J. ZHOU, AND Z. SUO, *A theory of coupled diffusion and large deformation in polymeric gels*, Journal of the Mechanics and Physics of Solids, 56 (2008), pp. 1779–1793.

[72] C. HUI, T. TANG, Y. LIN, AND M. CHAUDHURY, *Failure of elastomeric polymers due to rate dependent bond rupture*, Langmuir, 20 (2004), pp. 6052–6064.

[73] A. ISIHARA, N. HASHITSUME, AND M. TATIBANA, *Statistical theory of rubber-like elasticity. iv.(two-dimensional stretching)*, The Journal of Chemical Physics, 19 (1951), pp. 1508–1512.

[74] M. ITSKOV AND A. KNYAZEVA, *A rubber elasticity and softening model based on chain length statistics*, International Journal of Solids and Structures, 80 (2016), pp. 512–519.

[75] A. JAMES, A. GREEN, AND G. SIMPSON, *Strain energy functions of rubber. i. characterization of gum vulcanizates*, Journal of Applied Polymer Science, 19 (1975), pp. 2033–2058.

[76] H. JAMES AND E. GUTH, *Theory of the elastic properties of rubber*, The Journal of Chemical Physics, 11 (1943), pp. 455–481.

[77] R. JEDYNAK, *Approximation of the inverse langevin function revisited*, Rheologica Acta, 54 (2015), pp. 29–39.

[78] F. JOCHUM AND P. THEATO, *Temperature-and light-responsive smart polymer materials*, Chemical Society Reviews, 42 (2013), pp. 7468–7483.

[79] M. KALISKE AND G. HEINRICH, *An extended tube-model for rubber elasticity: statistical-mechanical theory and finite element implementation*, Rubber Chemistry and Technology, 72 (1999), pp. 602–632.

[80] H. KHAJEHSAEID, J. ARGHAVANI, R. NAGHDABADI, AND S. SOHRABPOUR, *A visco-hyperelastic constitutive model for rubber-like materials: a rate-dependent relaxation time scheme*, International Journal of Engineering Science, 79 (2014), pp. 44–58.

[81] H. KILIAN, *Equation of state of real networks*, Polymer, 22 (1981), pp. 209–217.

[82] H. KIM, W. GODDARD III, S. JANG, W. DICHTEL, J. HEATH, AND J. STODDART, *Free energy barrier for molecular motions in bistable [2] rotaxane molecular electronic devices*, The Journal of Physical Chemistry A, 113 (2009), pp. 2136–2143.

[83] T. KIM, L. ZHU, R. AL-KAYSI, AND C. BARDEEN, *Organic photomechanical materials*, ChemPhysChem, 15 (2014), pp. 400–414.

[84] W. KLINGBELL AND R. SHIELD, *Some numerical investigations on empirical strain energy functions in the large axi-symmetric extensions of rubber membranes*, Zeitschrift für angewandte Mathematik und Physik ZAMP, 15 (1964), pp. 608–629.

[85] O. KRATKY AND G. POROD, *Röntgenuntersuchung gelöster fadenmoleküle*, Recueil des Travaux Chimiques des Pays-Bas, 68 (1949), pp. 1106–1122.

[86] W. KUHN, *Die bedeutung der nebenvalenzkräfte für die elastischen eigenschaften hochmolekularer stoffe*, Angewandte Chemie, 51 (1938), pp. 640–647.

[87] W. KUHN AND F. GRÜN, *Beziehungen zwischen elastischen konstanten und dehnungsdoppelbrechung hochelastischer stoffe*, Colloid & Polymer Science, 101 (1942), pp. 248–271.

[88] W. KUHN AND H. KUHN, *Statistische und energieelastische rückstellkraft bei stark auf dehnung beanspruchten fadenmolekeln*, Helvetica Chimica Acta, 29 (1946), pp. 1095–1115.

[89] F. LAGUGNÉ-LABARTHET, Y. AN, T. YU, Y. SHEN, E. DALCANALE, AND D. SHENOY, *Proton driven vase-to-kite conformational change in cavitands at an air- water interface monitored by surface shg*, Langmuir, 21 (2005), pp. 7066–7070.

[90] G. LAKE, A. THOMAS, AND D. TABOR, *The strength of highly elastic materials*, Proceedings of the Royal Society of London. Series A. Mathematical and Physical Sciences, 300 (1967).

[91] P. LANG AND E. FREY, *Disentangling entanglements in biopolymer solutions*, Nature communications, 9 (2018), p. 494.

[92] M. LARSEN AND A. BOYDSTON, *"flex-activated" mechanophores: Using polymer mechanochemistry to direct bond bending activation*, Journal of the American Chemical Society, 135 (2013), pp. 8189–8192.

[93] S. LAVOIE, R. LONG, AND T. TANG, *A rate-dependent damage model for elastomers at large strain*, Extreme Mechanics Letters, 8 (2016), pp. 114–124.

[94] J. LENHARDT, M. ONG, R. CHOE, C. EVENHUIS, T. MARTINEZ, AND S. CRAIG, *Trapping a diradical transition state by mechanochemical polymer extension*, Science, 329 (2010), pp. 1057–1060.

[95] J. LI, Y. HU, J. VLASSAK, AND Z. SUO, *Experimental determination of equations of state for ideal elastomeric gels*, Soft Matter, 8 (2012), pp. 8121–8128.

[96] J. LI, C. NAGAMANI, AND J. MOORE, *Polymer mechanochemistry: from destructive to productive*, Accounts of chemical research, 48 (2015), pp. 2181–2190.

[97] J. LIPHARDT, B. ONOA, S. SMITH, I. TINOCO, AND C. BUSTAMANTE, *Reversible unfolding of single rna molecules by mechanical force*, Science, 292 (2001), pp. 733–737.

[98] R. LONG AND C.-Y. HUI, *Crack tip fields in soft elastic solids subjected to large quasi-static deformation — a review*, Extreme Mechanics Letters, 4 (2015), pp. 131–155.

[99] T. MANOURAS AND M. VAMVAKAKI, *Field responsive materials: photo-, electro-, magnetic-and ultrasound-sensitive polymers*, Polymer Chemistry, 8 (2017), pp. 74–96.

[100] M. MANRIQUE-JUAREZ, S. RAT, L. SALMON, G. MOLNÁR, C. QUINTERO, L. NICU, H. SHEPHERD, AND A. BOUSSEKSOU, *Switchable molecule-based materials for micro-and nanoscale actuating applications: Achievements and prospects*, Coordination Chemistry Reviews, 308 (2016), pp. 395–408.

[101] Y. MAO AND L. ANAND, *A theory for fracture of polymeric gels*, Journal of the Mechanics and Physics of Solids, 115 (2018), pp. 30–53.

[102] Y. MAO, B. TALAMINI, AND L. ANAND, *Rupture of polymers by chain scission*, Extreme Mechanics Letters, 13 (2017), pp. 17–24.

[103] G. MARCKMANN AND E. VERRON, *Comparison of hyperelastic models for rubber-like materials*, Rubber chemistry and technology, 79 (2006), pp. 835–858.

[104] R. MARCOMBE, S. CAI, W. HONG, X. ZHAO, Y. LAPUSTA, AND Z. SUO, *A theory of constrained swelling of a ph-sensitive hydrogel*, Soft Matter, 6 (2010), pp. 784–793.

[105] J. MARK, *Elastomers with multimodal distributions of network chain lengths*, in Macromolecular Symposia, vol. 191, Wiley Online Library, 2003, pp. 121–130.

[106] P. MARSZALEK, H. LU, H. LI, M. CARRION-VAZQUEZ, A. OBERHAUSER, K. SCHULTEN, AND J. FERNANDEZ, *Mechanical unfolding intermediates in titin modules*, Nature, 402 (1999), p. 100.

[107] C. MIEHE, S. GÖKTEPE, AND F. LULEI, *A micro-macro approach to rubber-like materials—part i: the non-affine micro-sphere model of rubber elasticity*, Journal of the Mechanics and Physics of Solids, 52 (2004), pp. 2617–2660.

[108] M. MOONEY, *A theory of large elastic deformation*, Journal of applied physics, 11 (1940), pp. 582–592.

[109] J. MORAN, J. ERICSON, E. DALCANALE, J. BRYANT, C. KNOBLER, AND D. CRAM, *Vases and kites as cavitands*, Journal of the American Chemical Society, 113 (1991), pp. 5707–5714.

[110] E. MUNIZ AND G. GEUSKENS, *Compressive elastic modulus of polyacrylamide hydrogels and semi-ipns with poly (n-isopropylacrylamide)*, Macromolecules, 34 (2001), pp. 4480–4484.

[111] S. MÜNSTER, L. JAWERTH, B. LESLIE, J. WEITZ, B. FABRY, AND D. WEITZ, *Strain history dependence of the nonlinear stress response of fibrin and collagen networks*, Proceedings of the National Academy of Sciences, 110 (2013), pp. 12197–12202.

[112] A. NATANSOHN AND P. ROCHON, *Photoinduced motions in azo-containing polymers*, Chemical reviews, 102 (2002), pp. 4139–4176.

[113] R. OGDEN, *Large deformation isotropic elasticity–on the correlation of theory and experiment for incompressible rubberlike solids*, in Proc. R. Soc. Lond. A, vol. 326, The Royal Society, 1972, pp. 565–584.

[114] C. ORTIZ AND G. HADZIIOANNOU, *Entropic elasticity of single polymer chains of poly (methacrylic acid) measured by atomic force microscopy*, Macromolecules, 32 (1999), pp. 780–787.

[115] W. PAUL, K. BINDER, D. HEERMANN, AND K. KREMER, *Dynamics of polymer solutions and melts. reptation predictions and scaling of relaxation times*, The Journal of chemical physics, 95 (1991), pp. 7726–7740.

[116] M. PEPLOW, *The plastics revolution: how chemists are pushing polymers to new limits*, Nature, 536 (2016).

[117] H. PETRI, N. SCHULD, AND B. WOLF, *Hitherto ignored effects of chain length on the flory-huggins interaction parameters in concentrated polymer solutions*, Macromolecules, 28 (1995), pp. 4975–4980.

[118] A. PIERMATTEI, S. KARTHIKEYAN, AND R. SIJBESMA, *Activating catalysts with mechanical force*, Nature chemistry, 1 (2009), pp. 133–137.

[119] A. PRIIMAGI, C. BARRETT, AND A. SHISHIDO, *Recent twists in photoactuation and photoalignment control*, Journal of Materials Chemistry C, 2 (2014), pp. 7155–7162.

[120] A. PUCCI, F. DI CUIA, F. SIGNORI, AND G. RUGGERI, *Bis (benzoxazolyl) stilbene excimers as temperature and deformation sensors for biodegradable poly (1, 4-butylene succinate) films*, Journal of Materials Chemistry, 17 (2007), pp. 783–790.

[121] M. PUSO, *Mechanistic constitutive models for rubber elasticity and viscoelasticity*, tech. rep., Lawrence Livermore National Lab., CA (US), 2003.

[122] S. RICKABY AND N. SCOTT, *A comparison of limited-stretch models of rubber elasticity*, International Journal of Non-Linear Mechanics, 68 (2015), pp. 71–86.

[123] M. RIEF, M. GAUTEL, F. OESTERHELT, J. FERNANDEZ, AND H. GAUB, *Reversible unfolding of individual titin immunoglobulin domains by afm*, science, 276 (1997), pp. 1109–1112.

[124] R. RIVLIN, *A note on the torsion of an incompressible highly-elastic cylinder*, in Mathematical Proceedings of the Cambridge Philosophical Society, vol. 45, Cambridge University Press, 1949, pp. 485–487.

[125] R. RIVLIN AND J. ERICKSEN, *Stress-deformation relations for isotropic materials*, Journal of Rational Mechanics and Analysis, 4 (1955), pp. 323–425.

[126] R. RIVLIN AND D. SAUNDERS, *Large elastic deformations of isotropic materials vii. experiments on the deformation of rubber*, Phil. Trans. R. Soc. Lond. A, 243 (1951), pp. 251–288.

[127] D. RUS AND M. TOLLEY, *Design, fabrication and control of soft robots*, Nature, 521 (2015), p. 467.

[128] A. SCHALLAMACH, *A theory of dynamic rubber friction*, Wear, 6 (1963), pp. 375–382.

[129] B. SETH, *Generalized strain measure with applications to physical problems*, tech. rep., Wisconsin Univ. - Madison Mathematics Research Center, 1961.

[130] G. SEWELL, *Stability, equilibrium and metastability in statistical mechanics*, Physics Reports, 57 (1980), pp. 307–342.

[131] M. SHARIFF, *Strain energy function for filled and unfilled rubberlike material*, Rubber chemistry and technology, 73 (2000), pp. 1–18.

[132] M. SILBERSTEIN, K. MIN, L. CREMAR, C. DEGEN, T. MARTINEZ, N. ALURU, S. WHITE, AND N. SOTTOS, *Modeling mechanophore activation within a crosslinked glassy matrix*, Journal of Applied Physics, 114 (2013), p. 023504.

[133] A. SPAGNOLI, R. BRIGHENTI, M. TERZANO, F. ARTONI, AND P. STÅHLE, *Cutting resistance of polymeric materials: experimental and theoretical investigation*, Procedia Structural Integrity, 13 (2018), pp. 137–142.

[134] A. SPAGNOLI, M. TERZANO, R. BRIGHENTI, F. ARTONI, AND P. STÅHLE, *The fracture mechanics in cutting: A comparative study on hard and soft polymeric materials*, International Journal of Mechanical Sciences, 148 (2018), pp. 554–564.

[135] G. STAHL, *A short history of polymer science*, ACS Publications, 1981.

[136] T. TANAKA AND D. FILLMORE, *Kinetics of swelling of gels*, The Journal of Chemical Physics, 70 (1979), pp. 1214–1218.

[137] M. TEHRANI AND A. SARVESTANI, *Effect of chain length distribution on mechanical behavior of polymeric networks*, European Polymer Journal, 87 (2017), pp. 136–146.

[138] A. THOMAS, *The departures from the statistical theory of rubber elasticity*, Transactions of the Faraday Society, 51 (1955), pp. 569–582.

[139] K. TOBISCH, *A three-parameter strain energy density function for filled and unfilled elastomers*, Rubber Chemistry and Technology, 54 (1981), pp. 930–939.

[140] A. TOBOLSKY, *Measurement of random scission by stress relaxation*, Journal of Polymer Science Part C: Polymer Letters, 2 (1964), pp. 637–641.

[141] M. TORELLI, *Molecular Strategies for Functional Materials: Soft Mechanochemistry and Surface Functionalization*, PhD thesis, Università di Parma. Dipartimento di Scienze Chimiche, della Vita e della Sostenibilità Ambientale, 2018.

[142] M. TORELLI, I. DOMENICHELLI, A. PEDRINI, F. GUAGNINI, R. PINALLI, F. TERENZIANI, F. ARTONI, R. BRIGHENTI, AND E. DALCANALE, *ph-driven conformational switching of quinoxaline cavitands in polymer matrices*, Synlett, 29 (2018), pp. 2503–2508.

[143] L. TRELOAR, *The elasticity of a network of long-chain molecules—ii*, Transactions of the Faraday Society, 39 (1943), pp. 241–246.

[144] L. TRELOAR, *The elasticity and related properties of rubbers*, Reports on progress in physics, 36 (1973), p. 755.

[145] L. TRELOAR, *The physics of rubber elasticity*, Oxford University Press, USA, 1975.

[146] L. TRELOAR AND G. RIDING, *A non-gaussian theory for rubber in biaxial strain. i. mechanical properties*, in Proceedings of the Royal Society of London A: Mathematical, Physical and Engineering Sciences, vol. 369, The Royal Society, 1979, pp. 261–280.

[147] K. VALANIS AND R. LANDEL, *The strain-energy function of a hyperelastic material in terms of the extension ratios*, Journal of Applied Physics, 38 (1967), pp. 2997–3002.

[148] F. VERNEREY, R. BRIGHENTI, R. LONG, AND T. SHEN, *Statistical damage mechanics of polymer networks*, Macromolecules, 51 (2018), pp. 6609–6622.

[149] F. VERNEREY, R. LONG, AND R. BRIGHENTI, *A statistically-based continuum theory for polymers with transient networks*, Journal of the Mechanics and Physics of Solids, 107 (2017), pp. 1–20.

[150] E. VERRON AND A. GROS, *An equal force theory for network models of soft materials with arbitrary molecular weight distribution*, Journal of the Mechanics and Physics of Solids, (2017).

[151] M. WANG AND E. GUTH, *Statistical theory of networks of non-gaussian flexible chains*, The Journal of Chemical Physics, 20 (1952), pp. 1144–1157.

[152] Q. WANG, G. R. GOSSWEILER, S. L. CRAIG, AND X. ZHAO, *Mechanics of mechanochemically responsive elastomers*, Journal of the Mechanics and Physics of Solids, 82 (2015), pp. 320–344.

[153] X. WANG AND W. HONG, *Pseudo-elasticity of a double network gel*, Soft Matter, 7 (2011), pp. 8576–8581.

[154] M. WEI, Y. GAO, X. LI, AND M. SERPE, *Stimuli-responsive polymers and their applications*, Polymer Chemistry, 8 (2017), pp. 127–143.

[155] A. WINEMAN, *Nonlinear viscoelastic solids—a review*, Mathematics and Mechanics of Solids, 14 (2009), pp. 300–366.

[156] P. WU AND E. VAN DER GIESSEN, *On improved network models for rubber elasticity and their applications to orientation hardening in glassy polymers*, Journal of the Mechanics and Physics of Solids, 41 (1993), pp. 427–456.

[157] O. YEOH, *Some forms of the strain energy function for rubber*, Rubber Chemistry and technology, 66 (1993), pp. 754–771.

[158] O. YEOH AND P. FLEMING, *A new attempt to reconcile the statistical and phenomenological theories of rubber elasticity*, Journal of Polymer Science Part B: Polymer Physics, 35 (1997), pp. 1919–1931.

[159] J. ZHANG, L. YUE, P. HU, Z. LIU, B. QIN, B. ZHANG, Q. WANG, G. DING, C. ZHANG, X. ZHOU, ET AL., *Taichi-inspired rigid-flexible coupling cellulose-supported solid polymer electrolyte for high-performance lithium batteries*, Scientific reports, 4 (2014), p. 6272.